REMOTE SENSING ASSESSMENT OF THE IMPACT OF THE 2018 AND 2019 DROUGHTS ON THE FORESTS IN THE NETHERLANDS

ELSE LINDA BOOGAARD
September 2021

SUPERVISORS:
Dr. C. van der Tol
Dr. T.A. Groen

REMOTE SENSING ASSESSMENT OF THE IMPACT OF THE 2018 AND 2019 DROUGHTS ON THE FORESTS IN THE NETHERLANDS

ELSE LINDA BOOGAARD
Enschede, The Netherlands, September 2021

Thesis submitted to the Faculty of Geo-Information Science and Earth Observation of the University of Twente in partial fulfilment of the requirements for the degree of Master of Science in Spatial Engineering

SUPERVISORS:
Dr. C. van der Tol
Dr. T.A. Groen

THESIS ASSESSMENT BOARD:
Dr. B. Su (Chair)
Dr. M. Schelhaas (External Examiner, Wageningen University & Research)

ABSTRACT

Forests play an essential role for human society by providing provisioning, regulating and cultural services. Drought is one of the most damaging natural disasters that can cause huge losses to the forest ecosystem and society. Satellite imagery has been used in many countries in boreal and Mediterranean areas for assessing drought impact on forests, but so far not in oceanic climates. In this study, Landsat 8 and Sentinel-2 time series are used for deriving various vegetation indices to evaluate their ability in measuring impacts of droughts on forests in the Netherlands. Six vegetation indices (NDVI, EVI, RVI, DVI, NDMI, and SAVI) were compared on their correlation with droughts (Standardized Precipitation Index) using 170 forest points categorised by three forest types (broadleaved, coniferous, and mixed). NDMI and NVDI were found to be the vegetation indices that correlate strongest to periods of drought.

An analysis of the full dataset showed an overall decrease in NDMI and NDVI during the summer of drought-year 2018, but on a yearly scale this difference is not visible. An analysis of the variation between the forest types was inconclusive: while the forest types were found to have different yearly cycles, neither of the forest types had significantly different NDMI or NDVI values than the other forest types in 2018. Similarly, the analysis of the variation between soil types was also inconclusive, partly as a consequence of lack of available data to do an unbiased analysis to separate the forest type and soil type factor.

This study shows that remotely sensed vegetation index analysis is currently not a feasible method for assessing drought impact on forests in the Netherlands, as the results are inconclusive and do not confirm the ground-based findings. Future research will require larger time series or will need to combine datasets to create a dataset of sufficient temporal and spatial resolution to understand how Dutch forest respond to periods of drought, which are predicted to increase in the coming decade as a result of climate change.

Keywords: NDMI, NDVI, drought, vegetation index, time series, remote sensing, forest drought resilience

SAMENVATTING

Bossen spelen een essentiële rol binnen de samenleving door het verstrekken van producerende, regulerende, ondersteunende en culturele diensten, zoals houtoogst en ruimte voor biodiversiteit en recreatie. Droogte is een van de meest schadelijke natuurrampen dat enorme schade kan veroorzaken aan bossen en daarmee aan de samenleving. Satellietbeelden zijn in veel landen in boreale en mediterrane gebieden gebruikt om de gevolgen van droogte voor bossen vanuit de lucht op grote schaal te beoordelen, maar tot nu toe niet in oceanische klimaten. In deze studie worden Landsat 8 en Sentinel-2-tijdreeksen gebruikt voor het afleiden van verschillende vegetatie-indexen om hun vermogen te evalueren om de effecten van droogte op bossen in Nederland te meten. Zes vegetatie-indexen (NDVI, EVI, RVI, DVI, NDMI en SAVI) werden vergeleken op hun correlatie met droogte (Standardized Precipitation Index) met behulp van 170 bospunten, gecategoriseerd door drie bostypes (loofbos, naaldbos en gemengd). NDMI en NVDI bleken de vegetatie-indexen te zijn die het sterkst correleren met perioden van droogte.

Een analyse van de volledige dataset toonde een gering lagere NDMI en NDVI tijdens de zomermaanden (juni, juli en augustus) van het droogtejaar 2018 dan in andere jaren. Echter, op jaarschaal is dit verschil niet zichtbaar. Een analyse van de variatie tussen de bostypen gaf geen uitsluitsel: hoewel de bostypen wel significant verschillende jaarcycli bleken te hebben, had geen van de bostypen significant grotere afwijking in NDMI- of NDVI-waarden dan de andere bostypen in 2018. De analyse van de variatie tussen bodemtypes gaf ook geen duidelijk resultaat, deels als gevolg van een gebrek aan beschikbare data om een objectieve analyse uit te voeren om de factor bostype en bodemtype te scheiden.

Deze studie laat zien dat remote-sensing vegetatie-indexanalyse momenteel geen geschikte methode is om de impact van droogte op bossen in Nederland te beoordelen, omdat de huidige hoeveelheden van droogte schade aan bossen te klein is om met de huidige beschikbare data op te vangen en ze dus de bevindingen op de grond niet kunnen bevestigen. Toekomstig onderzoek zal langere tijdreeksen vereisen of zal datasets moeten combineren om een dataset met voldoende temporele en ruimtelijke resolutie te creëren om te begrijpen hoe Nederlandse bossen reageren op perioden van droogte, die naar verwachting in het komende decennium zullen toenemen als gevolg van klimaatverandering. Met de groei van beschikbare hogere resolutie data en de verwachting van meer extreme droogtes in de toekomst is het aannemelijk dat deze methode in de toekomst wel op de Nederlandse bossen kan worden toegepast om de droogte-impact te monitoren.

ACKNOWLEDGEMENTS

A would like to acknowledge all the people to helped me to get to this point where I can present my Master thesis. First, I would like to thank my supervisors, Thomas Groen and Christiaan van der Tol, for their guidance during the thesis period of my study. I am grateful for their support, critical questions, and opportunities to further my research and to improve my research skills.

I also want to thank my teachers and my classmates during my studies of spatial engineering, because they are to thank for how much I have grown in the past two years with all the learning opportunities I have gotten. My classmates have been a positive motivation and a support even during this covid-times where it was sometimes a challenge to stay sane.

I would also like to thank Suhaib, he has been my support this whole time and I could not have done it without him.

TABLE OF CONTENTS

LIST OF FIGURES

LIST OF TABLES

1. INTRODUCTION

This study focuses on the detection of drought impact in forests in the Netherlands using vegetation indices derived from satellite imagery time series.

1.1. Importance of Forests

Forests play an important part in society, as they provide various services. Forests contribute to the welfare of people in three ways: (1) they produce wood resources; (2) they provide regulating services such as facilitating biodiversity and mitigating climate change; and (3) they provide recreation and health benefits.
As for the wood resources (1), forests produce timber, paper, fuel, and other purposes. The sales of wood is a major source of income for forest management organizations such as Staatsbosbeheer, and therefore necessary to retrieve the financial resources to maintain and revitalize forests(Staatsbosbeheer, 2020). The forest and wood industry makes an important contribution to our economy by producing and providing a circular resource (Thomassen et al., 2020). Therefore, it is essential to ensure the sustainability of forests in the future. Besides the production of wood, forests have a natural function of filtering water, and play a significant role in clean drinking water supply. This way, forests also produce filtered water as a service that is used by society.
Secondly, forests provide many maintenance and regulating services, such as biodiversity and climate mitigation. The 227 million hectares of forests in Europe absorb 155 million tonnes of carbon each year, which is 10% of the greenhouse gas emissions of Europe each year and therefore these forests play a significant role in the fight against climate change (FOREST EUROPE, 2020). Forests provide a habitat for a wide range of organisms, who in itself are able to provide ecosystem services such as: more efficient use of nutrients and water, sometimes higher productivity (and CO2 sequestration), pollination and greater resilience to storm, fire, invasive exotic species (e.g. black cherry), and pests (e.g. oak processionary caterpillar) (Thomassen et al., 2020). In addition, forests provide other regulating services such as carbon sequestration, particulates filtering, water purification, water purification, and erosion prevention.
Lastly, forests and their biodiversity provide important cultural ecosystems such as aesthetics and health benefits. Forests contribute to "well-being and public health, a pleasant living environment, a welcome place for rest and recreation" (Thomassen et al., 2020). Dutch forests are visited 150 million times per year for recreational purposes (Staatsbosbeheer, 2019). Forests also contribute to the health of people, they provide spiritual meaning, contribute to the quality of the landscape and increase living enjoyment (Thomassen et al., 2020). This cultural value of forests leads to additional economic value through the sales of park tickets and overnight stays.

1.2. Vulnerability of Forests to Droughts

As forests are of great importance to our society and wellbeing through various services as stated above, it is important to ensure the future sustainability of the forests. Forests depend on water availability and certain climatic conditions to be able to grow and survive. What these specific water and climatic needs are, differs per tree species and therefore, species are climate dependent.
Changing climate can have an immense impact on forests as it causes an increase in weather extremes such as extremely wet and dry periods (droughts). According to the fifth assessment report of the IPCC (2014), climate changes put a lot of stress on forests globally and they expect that it will lead to changes in the structure and composition of forests, as models are showing significant increases in forest dieback. Forest dieback is the phenomenon of forests dying or losing health without an direct cause (Allen, 2009). Losing health may include

falling of discoloration of leaves of needles, thinning of tree crowns, or damage to the roots of the trees. This forest dieback can be caused by pathogens, parasites or conditions like acid rain and periods of drought, which are expected to happen more frequent as a result of climate change (Allen, 2009). The IPCC states that fast adaptation is important as a response to this (Sohngen et al., 2016).

An example of an extreme weather event (in this case an unusually sunny spring and dry summer) that impacted forests are the meteorological droughts of 2018 in Europe (Bastos et al., 2020). A meteorological drought is a prolonged period of time with less than average rainfall and great evaporation (influenced by high temperatures), as defined by the KNMI (KNMI, 2021a). In 2018, the Netherlands experienced extremely high temperatures and little rain, calling 2018 "the record breaking drought of 2018 in Europe" (Buitink et al., 2020). The year 2018 was with a rainfall deficit of 309 mm (average = 90 mm) the fifth severest meteorological drought ever measured in the Netherlands since the beginning of the measurements in 1901 (KNMI, 2021a). On average, the Netherlands has about 2-5 tropical days per year (days of 30 °C or higher), whereas 2018 had 8 tropical days (KNMI, 2021b).

In 2019, another extreme weather event occurred. That year was only slightly drier than average, but with record breaking temperatures reaching well over 40 °C (KNMI, 2020), the increased evaporation resulted in a precipitation deficit of 160 mm. There were in total 11 tropical days in 2019, which it the most tropical days ever recorded in one summer in the Netherlands (KNMI, 2021b). The KNMI defines the top 5% of droughts as extreme drought, for which the benchmark is 260 mm of rainfall deficit at the end of September.

These droughts (caused by lack of rainfall or increased evaporation) have an impact on the forests. Even though there has not been large-scale research on this, this impact is observed by local foresters: for example, forester Laurens Jansen discusses how the combination of drought and the bark beetle pests makes larches and Norway spruces the true drought victims (Koopman, 2020), and forest ecologist Bart Nyssen calls the drought damage in the forests a silent disaster (Reijman and Prooijen, 2020). Researchers from Wageningen used field measurement of tree rings to determine the impact of droughts on the tree species in the Netherlands (Thomassen et al., 2020). They compared the growth of sixteen trees between 2015-2017 with 2018 and concluded that pine trees and Douglas firs were more affected by the drought than oak and beech trees. Other examples of drought impact of forests in various European countries are found in literature (Buras et al., 2020; Khoury and Coomes, 2020; Pichler and Oberhuber, 2007; Vicente-Serrano, 2007). Due to global warming, these extreme droughts are only expected to become more severe and more frequent (Diermanse et al., 2018).

1.3. Monitoring Forests from Space

As mentioned, ground observations have been used to monitor damage to forests after droughts. However, a more large-scale method using objective data is the use of remotely sensed indices.

Various researchers have studied the effects of droughts on forest by means of often freely accessible satellite imagery using vegetation indices to derive the state of forests. For instance, Buras et al. (2020) compared the 2003 and 2018 across Europe, Vicente-Serrano (2007) studied droughts in the Iberian peninsula, and Assal et al. (2016) compared the effectivity of different vegetation indices in the detection of drought impact on forests. All these studies found satellite-derived vegetation index analysis to be an effective method of studying drought impact, and they found that long periods of drought have a negative effect on forests on forests, although the size of the impact varies per study. The spatial resolution that is used varies from 30x30 m up to 1x1 km, and time comparison varies from comparing one drought year with several non-drought years to comparing every year over several decades. Most studies have taken place on a large scale (such as entire Europe or south of Europe) and in more southern or Mediterranean climates. However, the method of satellite-derived vegetation index analysis has not yet been used on the forests in Central West Europe in low forest density areas like the Netherlands, the United Kingdom and Ireland, that have generally high forest fragmentation. Therefore, it is unknown if countries of a Central West Europe (oceanic) climate are affected differently than countries with a Mediterranean climate. As dry summers are less common in oceanic climates than in Mediterranean or continental climates, it is plausible that forests in Central West Europe are less adapted to dry conditions than forests in Southern and Eastern Europe. In these countries with a lot of forest fragmentation, high resolution imagery is needed to assess and monitor the forests and their changes.

1.4. Forest Management and Planning For The Future

The responsibility for the management and planning of forests is at the owners of forests. In the Netherlands, 48% of the forests are owned by the government, 19% by private conservation organisations, and 32% by other private owners (Probos, 2019). In order to sustain forests for the future climatic conditions, forest management organisations need to account for the changing climate in their planting of new forests trees, as well as in rejuvenation of existing forests; to ensure sufficient forest coverage in the coming decades. However, this is a complex process, in which the forest management organisations face a variety of knowledge and social challenges that impact the strategies they adopt. In this section, the knowledge challenges and social challenges are discussed to demonstrate the wickedness of forest management.

1.4.1. Knowledge Challenges

As for the knowledge challenges, it is important to know which types of forests are least impacted by drought in the Central West European climate. In July 2020, the Unie van Bosgroepen published in collaboration with Staatsbosbeheer and Stichting Probos a report on revitalizing the Dutch forests (Thomassen et al., 2020). This report proposes a set of recommended actions for revitalizing the Dutch forests. One of the actions the writers recommend is research into climate resilient tree species and the planting of these species, as they found that there is currently a lack of knowledge about this. According to Forest Europe (2020), about 67% of the European forests is mixed forests and 33% of the forests contains one singe tree species (either monocultures or naturally homogenous). They found that forests composed of mixed forest types (broadleaved and coniferous) are often more resilient and richer in biodiversity. However, no direct link is discussed on the connection between forest types and drought resilience.

Similarly, there are studies that suggest that a soils type on which a forest is located can play a role in the amount of drought impact on the forest. For example, a study of Jiang et al. (2020) suggests that Chinese forests on sandy soil are more drought resilient than forests on clay soil, and Agaba et al. (2010) found similar results in their experiment with sandy and clay soils. However, there is paucity of research around conducting such studies for the context of the Netherlands.

1.4.2. Social Challenges

Forest management organisations deal with legislation as well as opinion of the public. An example is Staatsbosbeheer, the Dutch public forest management organisation, which owns 26% of the forests in the Netherlands. They state that their strategy towards more climate resilient forests is to plant and develop forests with a wide variety of species together (Hekhuis, n.d.). In the process of managing their forests, besides maintaining the forests, they are aiming for nature and biodiversity restoration (as agreed upon in the Natura 2000 Habitats Directive) and forestation (UN, 2015). These two international agreements are sometimes conflicting, as nature restoration in some cases requires a forest landscape to be returned into another type of habitat to increase biodiversity. An example of such a landscape is the sand drifts in the nature reserve the Veluwe, that were reintroduced in the landscape by removing the (planted) forests in designated areas of the park. Sand drifts are a European protected habitat type and serve as habitat for specific species of interest, however, the active removal of trees required for this type of landscape conflicts with the goal of increasing forest area.

Forest management policy has been regularly a topic of conflict, and forest owners such as Staatsbosbeheer and Natuurmonumenten have been heavily criticized by the public for their actions. Regularly citizens protest against the cutting of trees. In 2019, this even led to Natuurmonumenten temporarily stopping with the clearing of any trees after a wave of criticism of their members (NOS, 2019a), and Staatsbosbeheer calling for a better forest management strategy of the ministry (NOS, 2019b) after more protests and even punctured tires of some of the foresters (NOS, 2018). Not only the forest management organisations receive such criticism, also the government is targeted and criticised to not have their priorities right. For example, currently there are protests against the cutting of forests in Amelisweerd to make room for broadening the highway (NOS, 2021). This highway has been the cause for protests in the past, because between 1978 and 1982 there were protests against the initial construction of the highway, leading to strong conflicts between the protesters and the police, also known as "The Battle of Amelisweerd" (NOS, 2021).

Besides the various forest management organisations, the government, and citizens, there are more parties that have conflicting opinions and stakes in the policies surrounding forests and nature conservation, such as water boards and farmers. For instance, farmers typically prefer a lower groundwater level to protect their crops. There can be many other similar conflicting opinions surrounding the field of forest and nature management policy and practice. In 2019, the German government invested 800 million euros into generating drought resilient forests, which puts pressure on the Netherlands to take action as well (Stroo, 2019).

1.4.3. Decision Making

As the previous paragraphs demonstrate, the decision-making process for forest management and planning is complex, and the forest owners have to take into account a variety of perspectives and uncertainties. Large scale objective data about how drought (and therefore the expected future climatic conditions) impact forests would help with making decisions for future planning of climate resilient forests. For example, if the independent data from remote sensing could show the need to switch to more drought resilient forests, that would give a certain amount of justification for such actions.

1.5. Research Gap

To ensure future sustainability of forests, there is a dire need to have forests that are resilient to future climatic conditions. To do this, knowledge is required to identify the climate resilient forest types in order to plant or maintain these types of forests and design a suitable management strategy. As the climate becomes more extreme, we need such foresight in order to have forests live on years from now, since it takes time for seedlings to grow into forests. Required to start this process is the knowledge which current forest types are most sensitive to the future climatic conditions that includes droughts and high temperatures, and which forest types are least sensitive to those conditions.

This research aims to fill this gap by studying the drought impacts of the 2018 and 2019 droughts on the various types of forest in the Netherlands using a remote sensing approach. Satellite imagery is widely available and has been used in many countries in boreal and Mediterranean areas for this purpose, but so far not in oceanic climates. Using this technique in the Netherlands would give new insights in the drought resilience of the Dutch forest and identify forests and forest locations that are more vulnerable to extreme droughts, which ultimately contributes towards planning future forests that are more climate resilient.

1.6. Research Objectives and Research Questions

Based on the identified research gap, this research aims to fill this gap by reaching the following research objective:

- To evaluate with satellite data what impact the meteorological droughts of 2018 and 2019 had on the forests in the Netherlands.

The remotely sensed drought impact is measured using vegetation indices derived from spectral bands as measured by an instrument on a satellite platform. These bands can be combined to construct a variety of vegetation indices that highlight various properties of vegetation and its changes. Periods of drought are quantified using the rainfall deficit, and drought impact is any significant change that can be observed using satellite images and their derived vegetation indices. This can be greenness, early loss of leaves, reduced moisture content, or something similar.
In order to reach the research objective, the vegetation index or indices that are most suitable to detect drought impact need to be found. Therefore, the first research question is:

1. Which satellite-derived vegetation indices respond best to drought impact on forests?

The objective of this first research question is to find out to which vegetation index or indices respond strongest to drought impact, and to what extent the drought impact on forests in the Netherlands can be observed using these satellite indices.

2. Does drought impact, as detected with remote sensing, vary among forest types in the Netherlands?

The objective of this research question is to find patterns in the measured drought impact based on forest type. The forest drought impact is already established in research question 1, and this research question builds up on that splitting the results into three categories of forest types and analysing the difference between them. Based on observations of foresters (Hekhuis, n.d.) and studies from other countries in Europe (Khoury and Coomes, 2020), the expected outcome is to observe the biggest drought impact on pine trees and the least effect on deciduous and mixed forests.

3. Does drought impact on forests vary between soil types on which a particular forest is located?

The report of Revitalizing Dutch Forests (Thomassen et al., 2020) indicated that forests on sand were stronger affected by the drought than forests on other soil types, like clay. Therefore, the expected outcome is to observe the biggest drought impact on that are located on sandy soils.

Figure 1 shows an overview of the research questions and the steps that were taken during this research.

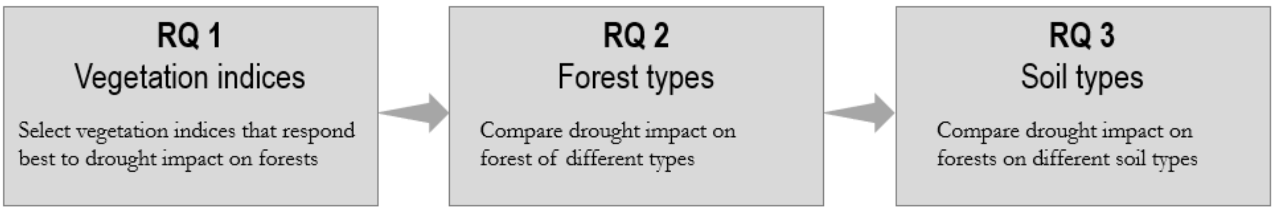

Figure 1: Overview of the research questions.

2. THEORETICAL BACKGROUND

This section gives the theoretical background on which this research is based. The first part describes previous studies that have been done that have similarities to this research, and the main outcomes and differences with this research are described. In the second section, there is a summary and a description of vegetation indices that have been used in the previous studies for the purpose of drought impact detection on forests.

2.1. Previous Studies in Other Climates

Various researchers have studied the effects of droughts on forest by means of remote sensing. To start with a prominent one, Lobo et al. (2010) used satellite imagery to investigate the impact of heatwaves and droughts on forests in South-West Europe (mainly Spain). They used temperature, precipitation, and potential evapotranspiration data of June, July, and August 2003 to calculate rainfall deficit and correlate this to the NDVI from satellite data from drought year 2003 and 1960 as reference years. Whilst they do differentiate between herbaceous vegetation and deciduous forests, their study does not make any differentiation between different tree species. They conclude that the drought of 2003 had a strong impact on the vegetation on South-West Europe, although the herbaceous vegetation had a stronger decrease in NDVI than the deciduous forests. Along similar lines, Vicente-Serrano's work (2007) assesses the relation between drought and seasons (in which season a drought has the biggest impact), as well as between drought and land-cover types on the Iberian Peninsula. This work also uses NDVI and the drought index Standardised Precipitation Index (SPI) to determine what counts as a drought. The project concludes that more arid regions (with low annual rainfall, about 320 mm per year) are more affected by drought than humid regions (600 mm per year). They also found that coniferous forests have a stronger negative response to long droughts (12 months) than broadleaved forests.

Yoshida et al. (2015) also looked at the impact of a drought in 2010 on vegetation in Russia. They also utilized NDVI, besides solar-induced chlorophyll fluorescence (SIF). Their results pointed towards NDVI being more effective than the SIF measurements for forests if detecting drought damage, unlike cropland and grassland areas. A similar but more recent study is the one of Buras et al. (2020), using climate data, land use data, and satellite imagery to do a statistical analysis on the 2018 drought compared to the 2003 drought. They used MODIS vegetation indices NDVI and Enhanced Vegetation Index (EVI) for large, forested areas in the whole of Europe, with a spatial resolution of 231x231 m; concluding that the 2018 drought is a yet unpreceded event impacting pastures, arable land, and forests. They found that the results of EVI generally confirmed the results of NDVI and showed that coniferous forests were generally more affected than mixed forests and broadleaved forests. They found that 130.000 km2 of coniferous forests and 30.000 km2 of deciduous trees had an extremely low NDVI in 2018 due to the drought throughout Europe, which was for the deciduous trees likely related to early leaf shedding. In this study, no specific results were found for the Netherlands, as the spatial resolution was too coarse to capture significant amounts of forests in the Netherlands.

All aforementioned studies used one vegetation index to determine drought impact. However, Assal et al. (2016) compared for their forest drought impact research in western North America four different vegetation indices: NDVI, EVI, NDMI (Normalized Difference Moisture Index), and SAVI (Soil Adjusted Vegetation Index). They used vegetation indices derived from Landsat data from 1985 to 2012 to find the most appropriate index for temporal trend analysis. They found that NDMI was the most accurate index as it had the strongest correlation with the field measures, closely followed by NDVI, and that coniferous forest more often had a decline in NDMI than deciduous forests. Choubin et al. (2019) also compared four MODIS-derived vegetation indices (NDVI, EVI, DVI (difference vegetation index), and RVI (ratio vegetation index)) for vegetative cover in general and compared them to two different drought indices, in which they discovered that NDVI and SPI had the strongest correlation. Gu et al. (2008) also compared the indices NDVI and NDMI, for vegetation drought monitoring, and they concluded that, even though NDVI is more commonly used, it was found to have no additional benefit over NDMI.

By making differentiation between types of forest vegetation in the NDVI data, properties such as drought resilience can be established that can lead to knowledge about climate change resilience. There is a study that combines species specific analysis with the remote sensing approach that is mentioned previously. The research of Khoury and Coomes (2020) investigates how drought resilience varies amongst ten different forest types of the Spanish forests. They used eighteen years of MODIS multispectral reflectance data from the NASA database to extract monthly NDVI estimates that represent the greenness of the forests. Besides NDVI to study the greenness of the forests, they also studied the impact of canopy density using leaf area index (LAI) that was also calculated from the MODIS imagery. They found that dense canopies are most sensitive to droughts and that chestnut trees are quite resilient to droughts, while pines were relatively sensitive.

Some studies have also looked at the role soil plays in the impact of a drought on forests. Jiang et al. (2020) studied the responses of vegetation growth to droughts under different soil textures in pastoral areas of China. They found that soil types play an important role in a plant's water uptake, and therefore affect the response of vegetation to drought. Their results showed that vegetation located on soil with a high sand percentage had relatively small deviation during drought, as opposed to clay soil, which had the opposite effect. Agaba et al. (2010) found similar results in their experiment in which they simulated drought conditions with hydrogel to study the effect of different soils of the survival of trees under drought conditions. In their experiment, the survival rate of trees was highest on sandy soil, and significantly lower on (loamy and clay) soils under drought conditions.

All these studies show, firstly, that the use of remotely sensed vegetation indices is an effective method of capturing this impact in data; and, secondly, that there is a need for and viable possibilities for assessing the impact of droughts on vegetation. This shows that it is possible to combine the (vegetation)species specific analysis with the accuracy and scalability of remotely sensed data, and this method needs to be brought to the Netherlands to learn more about the state of the Dutch forests and identify which types of forests are more drought resilient. Earlier this year, foresters sounded the alarm (Koopman, 2020) after another year of drought and they stated to be eagerly looking for trees that will thrive in the "new reality". As Khoury and Coomes (2020) stated: "Understanding differences in the resilience of forest types is key to improving resilience to drought". The method proposed in this document can provide the needed answers and contribute towards a strategy for more drought resilient forests.

2.2. Vegetation Indices

To assess forest health using remote sensing, vegetation indices (VI's) are often used to indicate levels of leaf pigments, carbon, or water concentration (Qi et al., 2017). A vegetation index is composed of two or more spectral bands reflectance values. The sections below describe the characteristics of the vegetation indices that are used in the aforementioned studies. Table 1 provides an overview of the indices.

Vegetation Index	General description
Normalized difference vegetation index (NDVI)	(NearInfraRed–Red) / (NearInfraRed+Red)
Enhanced vegetation index (EVI)	G((NearInfraRed–Red) / (L+ NearInfraRed +C1*Red–C2*Blue))
Ratio vegetation index (RVI)	NearInfraRed / Red
Difference vegetation index (DVI)	NearInfraRed–Red
Normalized difference moisture index (NDMI/NDWI)	(NearInfraRed–ShortWaveInfraRed) / (NearInfraRed +ShortWaveInfraRed)
Soil adjusted vegetation index (SAVI)	(1+L)(NearInfraRed–Red) / (NearInfraRed +Red+L)

Table 1: Overview of vegetation indices evaluated in this study.

2.2.1. Normalized Difference Vegetation Index

The Normalized difference vegetation index (NDVI) is one of the most well known and used vegetation indices, which uses the red spectral band and the near-infrared spectral band reflectance. It is one of the oldest widely used vegetation indices, as it was proposed in 1974 by Rouse and his team (Rouse et al., 1974; Xue and Su, 2017). It is used for monitoring vegetation on local scales and on global scales (Vrieling et al., 2013). NDVI is calculated as:

NDVI = (NearInfraRed–Red)/(NearInfraRed+Red).

The value of NDVI ranges between -1 and 1, in which the higher values generally mean a higher greenness of vegetation, and values below 0 are no vegetation, such as water, ice, snow, bare earth, or clouds (Choubin et al., 2019).

NDVI is a successful index to compare seasonal and interannual changes in vegetation growth and activity. Since NDVI is a ratio, many forms of multiplicative noise that are present in multiple bands (such as cloud shadows, illumination differences, atmospheric attenuation) are reduced (Huete et al., 2002). NDVI is often used for regional and global vegetation assessment and relates to canopy photosynthesis and Leaf area Index (LAI)(Xue and Su, 2017). However, there are also certain disadvantages tied to a ratio-based index such as NDVI, such as the inherent nonlinearity and the influence of additive ground noise effects (Huete, 1988). NDVI also had the problem of saturation over high biomass conditions (e.g. mature forests) and responds strongly to canopy background variations, such as soil changes (Huete, 1988). According to Buras et al. (2020), NDVI is often used for drought monitoring and assessing impact of drought on ecosystems on large scales.

2.2.2. Enhanced Vegetation Index

Enhanced vegetation index (EVI) is similar to the NDVI, with the addition of some coefficients and the blue band. Just like NDVI, the values for EVI range between -1 and 1, with the values for vegetation usually between 0.2 and 0.8 (Choubin et al., 2019). The formula for EVI is:

EVI = G((NearInfraRed–Red)/(L+NearInfraRed+C1*Red–C2*Blue))

The values that are used for the coefficients in this research are the standard values that are found back in the literature (Choubin et al., 2019; Huete et al., 2002): Canopy background adjustment (L) is 1, the gain factor (G) is equal to 2.5, the coefficients of aerosol resistance (C1 and C2) are equal to 6 and 6.5 respectively.

EVI was developed to simultaneously reduce atmospheric noise and canopy background noise, as in most previously adopted indices a decrease in one of these effects resulted in an increase in the other due to the interaction of the soils and atmosphere (Xue and Su, 2017). The main difference between NDVI and EVI is that EVI is more sensitive to structural variations of the canopy, while NDVI is more sensitive to chlorophyll (Huete et al., 2002). Therefore, EVI is more likely to reflect leaf shedding, while NDVI better reflects changes in leaf coloration (which can be a result of early aging due to drought) (Buras et al., 2020). In addition, EVI does not saturate as fast as NDVI in dense forests with a high LAI (Huete et al., 2002).

2.2.3. Ratio Vegetation Index

The Ratio vegetation index (RVI) was one of the first vegetation indices introduced in 1969 by Carl Jordan as a ratio to derive Leaf Area Index (Jordan, 1969). RVI is calculated as the Near Infrared band divided by the Red band:

RVI = NearInfraRed/Red

RVI is based on the principle that leaves absorb more red light than infrared light (Xue and Su, 2017). RVI uses the same two bands as NDVI, however, the RVI can range from 0 to infinity (Huete et al., 2002). RVI is widely used for green biomass estimation for dense forests or vegetation types, but with low density vegetation (less than 50%), the RVI is affected too much by atmospheric noise to give a reliable representation (Xue and Su, 2017). Choubin et al. used RVI as one of the indices to detect drought impact on forests in their research in 2019.

2.2.4. Difference Vegetation Index

Difference vegetation index (DVI) was proposed several years later in 1977 by Richardson and Weigand and is one of the simplest vegetation indices (Richardson and Wiegand, 1977). DVI is calculated as

DVI = NearInfrared–Red

The DVI is a small number close to zero. DVI distinguishes well between soil and vegetation, where soil, water, and rock are small numbers close to zero, and green vegetation are relatively high numbers (Choubin et al., 2019). However, it does not deal with atmospheric effects like NDVI and EVI (Xue and Su, 2017) and is therefore more suited for comparisons within one satellite scene than for satellite time series. Choubin et al. used DVI as one of the indices to detect drought impact on forests in their research in 2019, although it showed a smaller correlation to drought than NDVI, EVI, and RVI.

2.2.5. Normalized Difference Moisture Index

Normalized Difference Moisture Index (NDMI) is the only index in this research that does not use the Red band, but instead the Short-Wave InfraRed band. The NDMI is computed using:

NDMI = (NearInfraRed– ShortWaveInfraRed) / (NIR+ShortWaveInfraRed)

NDMI is also sometimes called NDWI (Normalized Difference Water Index), however, NDWI is in other instances defined by different band combinations. The NDMI was proposed by Gao in 1995 to detect moisture in vegetation and changes in this. In 1983, Hardisky et al. already used the same band combinations as NDMI for an index they called the Normalized Difference Infrared Index (NDII) (Assal et al., 2016).
As NDMI is computed using the SWIR, is sensitive to changes in liquid water content of vegetation canopies. NDMI is less sensitive to the greenness of vegetation, as the chlorophyll content that the Red band response is not included in this index (Gao, 1996). According to Gao (1996), the canopy background effects is similar to NDVI, however, the NDMI is less sensitive to atmospheric effects, as there is little aerosol scattering in the bands NIR and SWIR. Assal et al. (2016) compared NDVI, NDMI, EVI, and SAVI with field measured drought effects in a heterogeneous semi-arid area, and found that NDMI had the strongest relation to the field measured drought impact (Gu et al., 2008) found that NDVI and NDMI respond similarly to vegetation drought conditions.

2.2.6. Soil Adjusted Vegetation Index

The Soil Adjusted Vegetation Index (SAVI) was developed to overcome the sensitivity of NDVI on canopy background effects by including a canopy background adjustment constant (L) (Huete, 1988). The NDMI is computed using:

SAVI = (1+L)(NearInfraRed–Red) / (NearInfraRed+Red+L)

The canopy background adjustment constant L is a value between 0 and 1, with a value close to 1 for high background vegetation coverage and a low LAI of the canopy (Xue and Su, 2017). When the value for L is 0, the value SAVI is equal to NDVI. Therefore, in this research, the highest possible value for L is used. This value is 1 and is chosen to maximize the contrast between NDVI and SAVI. This enables clear comparison between the different vegetation indices.

3. STUDY AREA

In this study, the Netherlands is used as study area. The Netherlands has 373.480 ha of forests, which is about 11.1% of the surface area of the Netherlands (CBS, 2014; Probos, 2019). With this percentage, the Netherlands is one of the least forested countries of Europe, according to Forest Europe (2020), with an average forest cover of 32% over the whole continent. The rest of this section will go into detail about the history and composition of Dutch forests, and will compare them to European forests in general.

3.1. A Short History

For many centuries the influence of man on land and forest has been great, and is still decisive today in determining where and how forests grow (van Goor, 1993). The cause of the low percentage of forests in the Netherlands is that in the past centuries, forests have been cut down for various purposes benefitting the Dutch economy. A strong driver has been the high population density the Netherlands has had over the centuries, which created a need for land for agriculture, houses, and industry. Forests were also cut down to use as product, such as fuel, furniture, and construction material for ships. Around 1750 the Dutch forests were at an all time low, reaching only 100,000 ha (3%) of forest land in the whole country (Boosten, 2016). Throughout the 19th century, the interest and perceived value of forests slowly increased and new forests were planted. However, around 1870 the last ancient forest of the Netherlands was again cut down to make room for agricultural practices (Boosten, 2016). Nevertheless, there are also many forests planted, for production and for reforesting heath and sandy areas. Mainly oak and European red pine are popular, but after WOII larch, Douglas fir, and the Norway spruce were planted in large quantities.

3.2. Composition of Dutch Forests

With the economy as a driver for much of the deforestation and reforestation in the Netherlands, the current forests are mostly planted and a carefully chosen species composition. In 2013, 51% of the trees in the Netherlands were coniferous trees, and 49% broadleaf trees. In 2015 this ratio was 54% over 46%, which shows that the share of broadleaf trees is decreasing (Oldenburger, 2019). Scots pine (36%), native oak (17%) and Douglas fir (11%) are the three tree species with the largest area shares within the Dutch forest. Figure 2 shows that 51% is mixed coniferous forest and broadleaf forest, while 46% is only coniferous forest (26%) or broadleaf forest (20%). This is a large increase in mixed forests, as in 1983 23% was mixed, 47% was coniferous forest, and 23% was broadleaf forest (Oldenburger, 2019).

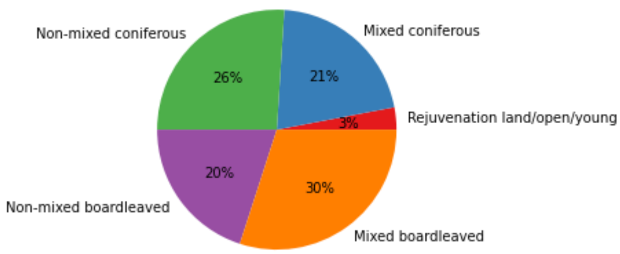

Figure 2: Composition of the Dutch forests. (source: Forest Europe, 2020)

3.3. Comparison to Other Countries in Central-West Europe

The percentage of forest cover in central-West Europe is 27.9% (FOREST EUROPE, 2020). The Netherlands has one of the lowest percentages of forest area of these countries, particularly lower than Austria (50%), Luxembourg (36%), Germany (33%), Switzerland (33%), France (31%), and Belgium (23%). Ireland (11%) and the United Kingdom (10%) have about the same percentage of forested area.

3.4. Comparison of Central-West Europe to Rest of Europe

Previous studies already have used remote sensing methods to monitor drought impact on forests in the South of Europe and have a Mediterranean climate. Central-West-European countries have an oceanic climate (Cfb in the Köppen classification) and therefore it is possible that the impact of drought is also different.

Many characteristics make Central-West European forests different from the forests in the rest of Europe. For instance, a recent study of by Forest Europe (2020) shows that Central-West European forests are smaller and more fragmented throughout the land, have small percentages of coniferous forests and high percentages of mixed forests, and have a higher percentages of planted forests than in other parts of Europe.

Regarding European forests, Central-West Europe is the least densely covered area (27.9%) together with Central-East Europe (27.3%). The North of Europe is most densely forested with 53.8% of the land area covered with forest. Central-West Europe has the largest share of their forests available for wood supply with 91.9%. South-East Europe on the other hand has the least of their forests available for wood supply (53.2%) (FOREST EUROPE, 2020).

4. DATA

4.1. Forest Data

The data of the forests was retrieved from the Sixth Dutch Forest Inventory (Nederlandse Bosinventarisatie - NBI6). This inventory was executed by Alterra Wageningen UR in 2012 and 2013, with the results published in 2014 (Schelhaas et al., 2014). The inventory was commissioned by the Ministry of Economic Affairs in the context of the policy-supporting research theme "Nature and Regional Biodiversity terrestrial". In the NBI6, measurements were carried out at 3190 forest sample points (see figure 3). Out of these, 1235 points were a re-recording of measurements of the previous forest inventory in 2005.

In this study, a subset of the NBI6 is used with a mixture of broadleaved, coniferous, and mixed forests. Forests are defined as areas with trees larger than 0.5 hectare. Broadleaved forests are forests with at least 80% of broadleaved tree species, while coniferous forests are forests with at least 80% of coniferous tree species. Mixed forests have at least 20% of both broadleaved and coniferous tree species. These definitions are based on the definitions of the Dutch Forest Inventory (Schelhaas et al., 2014), as that is where the data comes from.

Figure 3: Overview of the 3190 forest sample points of the NBI6.

4.2. Satellite Time series

The vegetation indices are calculated from satellite time series data from both Sentinel-2 and Landsat 8 imagery as described in this section. Both time series datasets were analysed separately to look for a drought related pattern.

Sentinel-2 imagery is suitable for this research as it has a high spatial resolution of 20x20 m, and therefore is able to sense small or narrow forests patches with minimal noise of surrounding land covers. Sentinel-2 also has a high revisit time of on average 5 days (ESA, n.d.), so that there are few gaps in time series after removing cloud covered pixels. However, the disadvantage of this dataset is the lack of historical data, as the atmospherically corrected data is only available from March 2017 onwards. This might lead to a lack of data to establish a meaningful pre-drought baseline (Wolf, 2020).

Landsat 8 does not have this problem of a lack of historical data, as the available surface reflectance data starts in July 2013. However, the spatial resolution is lower (30x30 m), which can lead to more noise from surrounding land covers. The temporal resolution is also significantly lower with a revisit time of 16 days, which can lead to gaps in the time series as a result of applying a could cover filter (Saleem and Awange, 2019).
The Sentinel-2 and Landsat 8 imagery surface reflectance time series were retrieved from Google Earth Engine (GEE). As the clouded imagery does not accurately reflect the surface reflectance values, these images are filtered out using a cloud filter in the algorithm. As the number of cloudy images differs per year, the total amount of useful data per year differs as well as demonstrated by the example in figure 4, which demonstrated the total number of recordings per year in the Sentinel-2 time series dataset for all locations.

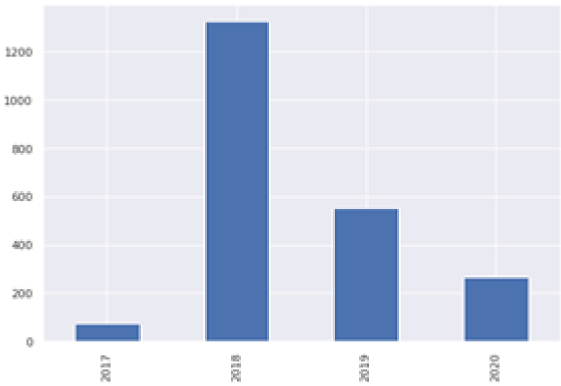

Figure 4: Total number of recordings per year in the Sentinel-2 time series dataset for all forest locations.

4.3. Method Validation Data

Points with ground truth point information were obtained to validate the method. A dataset was used containing 12 locations of dead spruce forests plots and 5 locations with healthy forests plots at the recorded date of sampling. This dataset of locations is based on dieback that occurs as a result of bark beetle outbreaks in spruce forests. Every one of these samples contained relevant information about the location coordinates, percentage of living trees, and date of sampling among other details.
The data was provided by researcher Harold Hauzeur from Wageningen University and the full dataset is provided in appendix A.

4.4. Reproducibility

This study is fully reproducible, as all the data is online openly available, and the methods are fully discussed the method section. When the methods and data retrieval are repeated exactly as stated, this should lead to the same results. Data extraction codes from Google Earth Engine and data processing codes performed in Python are provided in appendix B.

5. METHODS

In this section, several steps are described to reach the research objective and answer the research questions. First, a selection of forest locations is selected and the satellite time series data of these locations is retrieved. This data is cleaned to decrease the chance of extreme outliers.

As for the vegetation index selection, six indices were selected from literature and calculated for the time series dataset. The standard precipitation index was calculated for the Netherlands, and this was correlated to the vegetation indices to find the vegetation index that most strongly corresponds with drought impact. After that, method validation was done on a sample set with known ground truth values in order to test the performance of the method. Finally, the selected vegetation indices are used for exploratory and statistical analysis of drought impact on all forests.

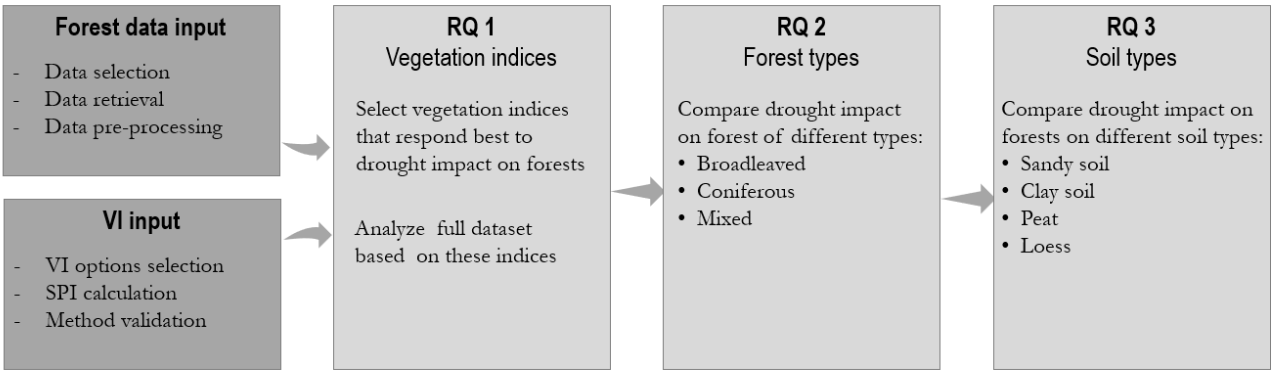

Figure 5: Main steps of this research.

5.1. Data Selection and Retrieval

This section consists of two main parts: the selection of locations from the NBI6 database and the retrieval of time series data for these locations.

The forests of the NBI6 were sorted by size and forest density. From the largest and densest forests of the database, the ones were selected with forest types of >80% coniferous trees, >80% broadleaf trees, and 40%-60% of each tree type. Forests with other compositions of tree types were discarded, in order to make a clear distinction between the forest types. Of this selection, a selection was made of ten largest forests of each different soil type (poor sand, rich sand, limeless clay, calcareous clay, loess, peat, calcareous sand) from all three different forest types (broadleaf, coniferous, mixed). This came down to 84 plots, as not every forest type had five forests on every soil type. After iterating through the process, 114 plot locations were added based on the same criteria to increase the total to 198 points, as the subset of 84 points showed to be a rather small sample set (see figure 6).

After selecting the locations, the time series of the 198 points was retrieved using Google Earth Engine. For each of the 198 points, the spectral band values were downloaded of the Sentinel-2 Surface Reflectance from April 2017 till September 2020, which is the entirety of the data that is available on Google Earth Engine for Sentinel-2 Surface Reflectance. In addition, the spectral band values of Landsat 8 Surface Reflectance were downloaded from July 2013 till September 2020, which is all the data that is available on Google Earth Engine for Landsat 8 Surface Reflectance.

The code used to retrieve the satellite time series data from Google Earth Engine is provided is Appendix B.

Figure 6: overview of all the 198 samples of the subset of the NBI6 used in this research. Red is broadleaved, blue is coniferous, and green is mixed forest.

5.2. Data Pre-processing

All 198 points were manually verified for correctness (whether they are located in a forest) using Sentinel-2 real-colour images of September 2020. This was done because the source that was used (the Dutch Forest Inventory) is seven years old, and it is possible that some forests have been cut down in the last seven years. In total 28 points were taken out, as they were not located on a place that is currently covered by forest or they were located close (<20m) to the edge of a forest.

Of the remaining 170, individual recordings that had an NDVI below 0 or above 1 were removed, as these are impossible values for forest NDVI, and this indicates a faulty recording. In addition, extreme outliers were manually checked by looking at the satellite image and checking for clouds on the specific date and location, and these measurements were also removed.

5.3. Vegetation Indices Selection

To answer which satellite-derived vegetation indices respond best to drought impact on forests, six indices (derived from literature) were compared with the Standardised Precipitation Index (SPI) of July of different years. The indices with the strongest correlation to SPI were selected as vegetation indices that most clearly represent drought impact on forests. This method using SPI to compare various vegetation indices was inspired by the paper of Choubin et al. (2019). First the SPI needs to be calculated based on rainfall data before it is correlated to the vegetation indices. All the vegetation indices used in this research are found through their previous application for similar studies in literature, and therefore the selection of the vegetation indices is next to the Landsat 8 time series supported by literature.

5.3.1. Calculating Drought Index

Standardised Precipitation Index (SPI) is a commonly used drought index to quantify the severity of droughts. In essence, SPI is a standardized measure for precipitation deficit, calculated using only rainfall data (Huang et al., 2020). SPI values are calculated using the equation (Bak and Labedzki, 2002):

$$SPI = (f(P) - \mu) / \delta$$

where: f(P) = transformed sum of precipitation, μ = mean value of the normalised precipitation sequence, and δ = standard deviation of the normalised precipitation sequence.

The flexibility and simplicity of the index make it so popular, as it can be used for any time scale, and it only needs precipitation as input. SPI can be calculated over various timespans. For example, the SPI3 is the precipitation deficit over a timespan of three months. According to (Santos et al., 2013), the general agreement is that times scales up to 6 months are associated with meteorological and agricultural droughts, while time scales between 9 and 12 months are used for the assessment of hydrological droughts that impact streams and water reservoirs. Time scales longer than that are used for long term droughts that impact the more resilient aquifers. As this research is investigating the impact of a meteorological drought on forests, SPI values of 6 months and lower are used. In this research, national rainfall data is used and therefore their spatial variety is not taken into account in the process of vegetation indices selection.

The SPI of 1, 2, 3, and 6 month were calculated using monthly precipitation data from the (KNMI, 2021c). The SPI values were calculated using R (for code see appendix B.3). The month with the lowest SPI value was selected and used for the vegetation index selection.

5.3.2. Compare Drought Index to Vegetation Index

Six vegetation indices that are used for drought impact assessment were selected from the literature and they were calculated for all recordings of the Sentinel-2 and Landsat 8 time series dataset. The bands that were used to calculate the indices are found in table 2.

VI	General description	Sentinel-2	Landsat 8	Parameters used
NDVI	(NIR-Red) / (NIR+Red)	(B08 – B04) / (B08 + B04)	(B05 – B04) / (B05 + B04)	
EVI	G((NIR-Red) / (L+NIR+C1Red-C2Blue))	G(B08 – B04) / (L+B08 + C1B04-C2B02)	G(B05 – B04) / (L+B05 + C1B04-C2B02)	L = 1, G = 2.5, C1 = 6, C2 = 6.5
RVI	NIR / Red	B08 / B04	B05 / B04	
DVI	NIR-Red	B08 – B04	B05 – B04	
NDMI (NDWI)	(NIR-SWIR) / (NIR+SWIR)	(B08 - B11) / (B08 + B11)	(B05 – B06) / (B05 + B06)	
SAVI	(1+L)(NIR-Red) / (NIR+Red+L)	(B08 – B04) / (B08 + B04)	(B05 – B04) / (B05 + B04)	L = 1

Table 2: Vegetation indices and their bands and parameters for Sentinel-2 and Landsat 8.

Correlation analysis was done between the vegetation indices series (average per month) and the SPI1, SPI2, SPI3, and SPI6 for the month of July (of each year), as this month showed the strongest indication of drought in the SPI values and therefore is expected to display the strongest results. The vegetation index with the best correlation with the SPI was selected for further analysis. For the correlation analysis, only the time series of Landsat 8 were used, as Sentinel-2 does only have 4 years of data. Four years means four times the month of July, which is not enough for correlation analysis. Landsat 8 is with eight times the month of July a significantly larger sample set, and therefore Landsat 8 was used for the correlation analysis.

5.4. Method Validation

Method validation was done on a small dataset of which there are ground measurements. This is a dataset of which through ground measurements and aerial photos it is known that these forests have died as a result of bark beetle infestations. Therefore, using the method on this dataset can verify whether the method can detect the difference between dead and living trees (regardless of the cause of death). Drought impact may be a much smaller effect than the differences in this dataset, however, validating this method can help identifying whether a potential lack of significant drought impact findings is caused by shortcomings of the method or if there is actually no drought impact.

The vegetation indices were calculated for the locations using the same method as described in the previous section. There are 12 plots with confirmed dead forest plots (although it is not known when they died), and 5 alive forest plots. For the dead forests, it is not known what year the forests died, but it is known that they were dead in 2020 during the sampling date. One plot was excluded from the analysis as it showed a strong broadleaved vegetation pattern, which suggests that the background noise was significantly stronger than the forest signal, as spruces are coniferous trees and should not give a broadleaf vegetation signal (a year pattern with strong seasonal differences).

5.5. Data Analysis

To answer the three research questions and establish if there is a measurable difference in the vegetation indices values between drought years and non-drought years, an analysis was done to compare the indices per year. As this is a new case study, in an area that has not yet been studied with these techniques, broader exploratory questions need to be answered before deeper models can be constructed. Hence, most of the data analysis is of exploratory nature.

For each of the research questions, an exploratory data analysis and a confirmatory statistical analysis was done. Exploratory data analysis is a type of analysis that revolves around the substantive understanding of data and is characterized by data visualisations (Behrens, 1997). The goal of this exploratory data analysis is to find patterns in the data and to discover the "story" of the data, rather than only the statistical significance of data (Behrens, 1997). Exploratory data analysis focuses on questions like which data features should be focused on, what kind of outliers exist, or what the general "shape" of the dataset is.

These are exploratory questions that address the early and messy stages of data analysis that statistical data analysis does not capture (Behrens, 1997). Data visualisations are able to capture all relevant information, while avoiding large parts of non-relevant information (Larkin and Simon, 1987). In addition, data visualizations can show details (such as patterns) that other analysis techniques do not reveal (such as summary descriptive statistics) (Cleveland, 1994). Moreover, a similar study from Buras et al. (2020) also used data visualizations as an analysis technique to compare vegetation index values of drought years.

After the exploratory data analysis, a statistical analysis was done to see whether there was a clear difference in the vegetation index values between drought and non-drought years. For this, a mixed model ANOVA was done. To do this, the monthly average per point was taken for each year, in order to have consistent repeated measures. As vegetation indices have a seasonal pattern, the average vegetation index values vary greatly per month. This means that different months cannot be compared to each other. Therefore, the difference in vegetation indices between the drought years 2018 and 2019 and preceding years for the months in which the highest rainfall deficit as expressed by the SPI was observed were tested.

These two types of analyses were done for all the research questions. For the first research question, the whole dataset was used and studied whether there were significant differences between the drought years and the non-drought years. For the second research question, the data was separated into forest types, to use the two analysis methods to see if there is a difference in drought impact between the forest types. Finally, for the third research question, the soil types are categorized in four main texture types, and a visual and statistical analyses are done to see if there is a significant difference between the soil types of how much drought impact there is.

6. RESULTS

6.1. Vegetation Indices Selection

The calculated SPI values show that the month July has the largest precipitation deficit in the growing season of the drought year 2018, and therefore the largest meteorological drought (see table 3). As 2018 is the year with the strongest drought within the timespan of available data, this means that July is the month with the largest range of SPI values. Therefore, this month appears to be a suitable candidate for the vegetation indices selection, as a larger range of SPI values can enable a more meaningful regression.

Year	Month	SPI1	SPI2	SPI3	SPI6
2018	May	-0.56872	0.60232	0.56442	1.05207
2018	June	-1.89615	-2.02078	-0.65133	-1.1274
2018	July	-3.24728	-3.36606	-3.1036	-2.38648
2018	August	-0.27915	-1.85469	-2.70543	-1.88167
2018	September	-0.60447	-0.87472	-1.91174	-2.17845

Table 3: Calculated SPI values during the drought summer of 2018.

Linear regression was done of vegetation indices versus SPI with both the Sentinel-2 time series dataset and the Landsat 8 time series dataset. However, as Sentinel-2 only has 3.5 years of surface reflectance available (covering four times the month of July), this time is too short for a pre-drought baseline. Therefore, this analysis was not used for the selection of vegetation indices. For completeness, the Sentinel-2 drought and vegetation index analysis can be found in appendix C. Landsat 8 has measurements for 8 months of July. This is, although it is a small dataset, the only available high spatial resolution satellite data with acceptable revisit time.

Pearson correlation was done to identify the vegetation index or indices that respond strongest to drought (quantified in the drought index SPI). Pearson correlation analysis shows that all the correlations between natural vegetation reflectance indices and precipitation deficit are positive. As outlined in figure 7, the best correlation occurred between NDMI and SPI1 (r=0.64) and between NDMI and SPI2 (r=0.59) for all forests from the Landsat 8 time series. The vegetation index that has the second-best correlation with SPI is NDVI, correlating strongest to SPI2 (r=0.46) and SPI6 (r=0.45). EVI, RVI, DVI, and SAVI have significantly weaker correlations (with range of r of 0.095-0.38, 0.092-0.37, 0.073-0.32, and 0.12-0.32 respectively). For the different timespans of the SPI, the SPI2 shows the strongest correlation to the vegetation indices (average R2 = 0.1493). Out of the vegetation indices, NDMI and NDVI were selected for further analysis, as they showed the best correlation with the drought index.

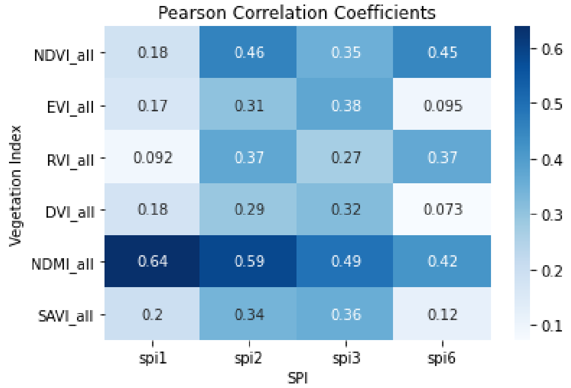

Figure 7: Pearson correlation coefficients of the regression analysis of the vegetation indices and the SPI values.

In figure 8, examples are given for the Pearson correlation analysis that is done for all vegetation indices with SPI1, SPI2, SPI3, and SPI6. The graphs show NDMI and EVI values of July of each year, which are an example of a vegetation index with a strong correlation to the SPI values and one with a weak correlation. An overview with visualizations of all correlations and the determination coefficients (R2) is found in appendix C.

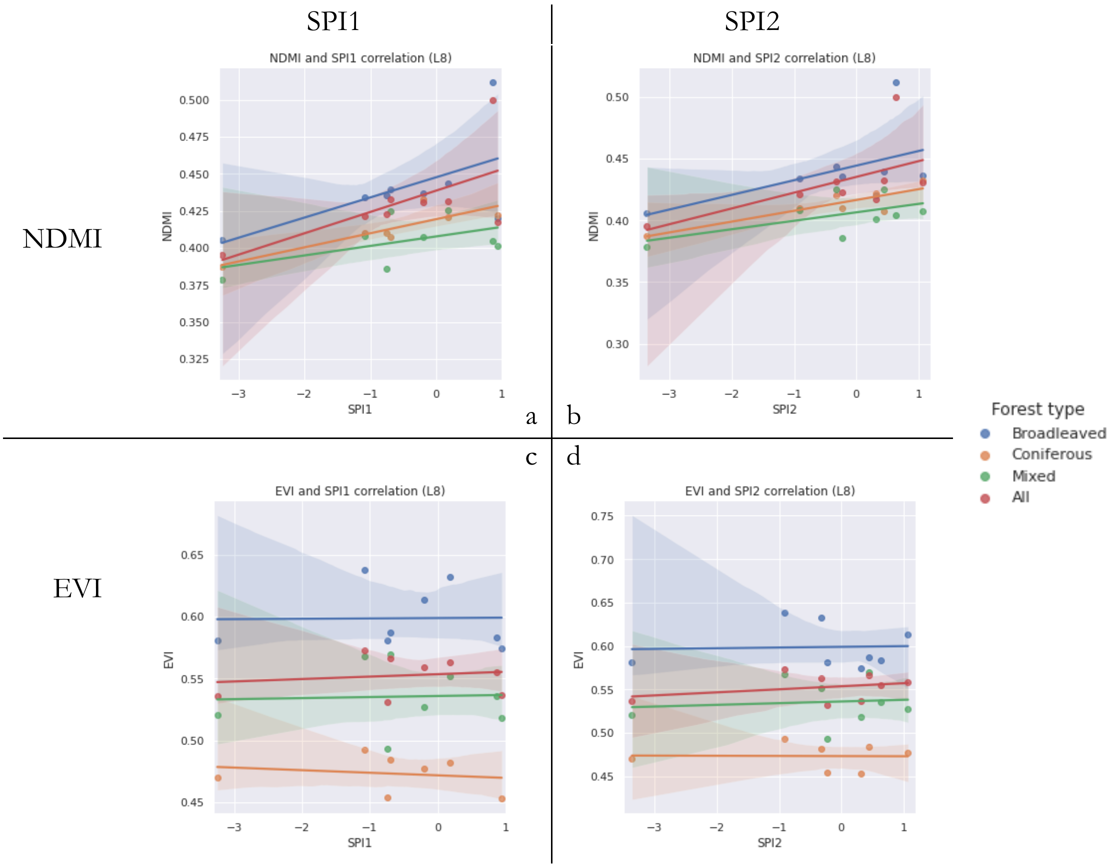

Figure 8a-d: Four examples of the correlation analysis. Precipitation deficits in the month July (2013-2020) are correlated to the various vegetation indices of that month. (a) and (b) are examples of strong correlations and (c) and (d) are examples of weak correlations.

6.2. Method Validation

In the validation dataset of spruce forests, a decrease in NDMI and NDVI was found for all plots marked as dead. The difference between dying spruce forests and healthy spruce forests is demonstrated in figure 9. For the dead spruce plots, an average decrease in NDMI of 0.323 was found between 2017 (0.352) and 2020 (0.029), while for the healthy spruce forest a decrease of only 0.097 was found over the same time period (0.385 and 0.288 respectively) (see figure 9a). Similarly, an average decrease in NDVI of 0.208 was found between 2017 (0.747) and 2020 (0.539) for the dead spruce forest plots, while for the healthy spruce forest a decrease of only 0.077 in NDVI was found over the same time period (0.823 and 0.756 respectively) (see figure 9b).

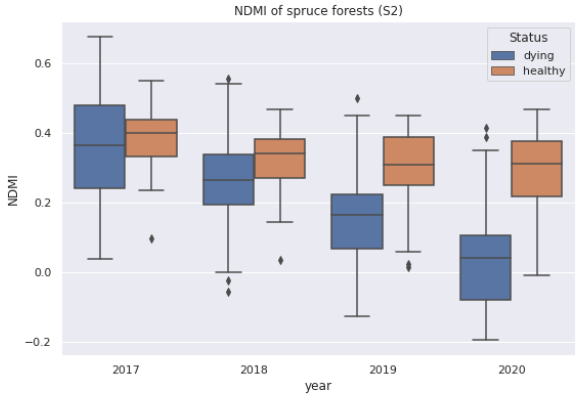

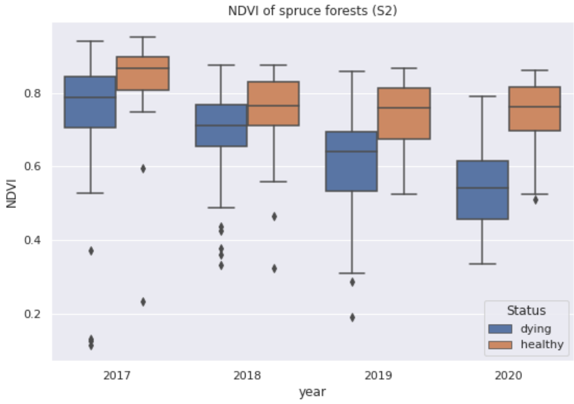

Figure 9: NDMI and NDVI values of the spruce forests. The graphs show a gradual decrease in NDMI and NDVI in the dying forests, while the healthy forests show relatively stable VI values.

Figure 10 is a demonstrative example of the NDMI values of one of the plots marked as dead trees and one of the plots as marked with healthy trees. Figure 10a clearly shows a gradual decrease in NDMI over the 4 years of data of a spruce forest that is dying, while the forest plot that is healthy (figure 10b) shows a rather stable NDMI.

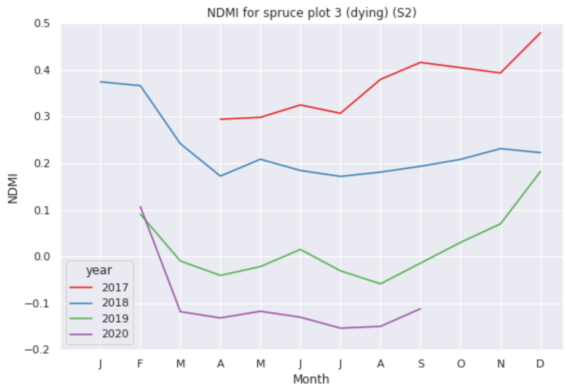

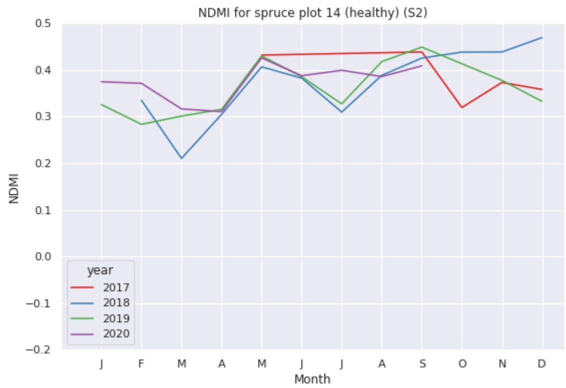

Figure 10: Two examples of monthly NDVI values of the spruce forests. Point 3 (left) is an example of a dying spruce forest and point 14 (right) is an example of a healthy spruce forest. The graph demonstrates well how the NDVI decreases each year while the forest is dying.

6.3. Data Analysis

This section describes the results of the assessment of the vegetation index responses to the drought year indices, and therefore answering the three research questions. This section consists of three parts: (1) All forests, related to the application of research question 1 ("*Which satellite-derived vegetation indices respond best to drought impact on forests?*"); (2) forest types, related to research question 2 ("*Does drought impact, as detected with remote sensing, vary among forest types in the Netherlands?*"); and (3) soil types, related to research question 3 ("*Does drought impact on forests vary between soil type s on which a particular forest is located?*").
This section focusses on the results that provide the clearest information to answer the research questions. Additional analyses and visualizations that were less informative are included in appendix D.

6.3.1. All Forests

This section contains the results that are related to research question 1 ("*Which satellite-derived vegetation indices respond best to drought impact on forests?*").

6.3.1.1. Descriptive Statistics

For the overall dataset, a total of 21,450 time series measurements were retrieved from Sentinel-2 after the pre-processing of the 170 forest locations over the period of three years and seven months. The Landsat 8 time series dataset contains 9,226 measurements for the period of seven years and seven months. Detailed descriptive statistics for the datasets can be found in appendix E.

The statistical analysis is done for the overall (all year) dataset and for the summer months only (June, July, and August) to study the drought impact specifically in the period of greatest drought. For the summer months in the Sentinel-2 dataset, a total of 5754 measurements were retrieved, ranging between 320 in 2017 and 2233 in 2018. It should be taken into account that 2017 has significantly less measurements than the other years, and therefore show a different statistical distribution. For the Landsat 8 time series, there is a total of 2369 measurements of the summer, ranging from 197 in 2017 to 473 in 2018.

6.3.1.2. Exploratory Analysis

The NDMI and NDVI results for both Sentinel-2 and Landsat 8 have a distinct annual cycle as can be seen in figure 11. Both curves show a dip around March for each year and a peak between May and October for NDMI as well as for NDVI with both sensors. As 2018 and 2019 are the drought and heat years, the hypothesis is to have lower values for these two years have for NDMI and NDVI than the other years. In the graphs of the Sentinel-2 vegetation indices, however, the years 2018 (yellow line) and 2019 (green line) do not stand out from the other years. As for the Landsat, the NDVI values between June and September of 2018 are lower than in other years, which is in line with the hypothesis. However, the values of 2018 are well within the margins of the standard deviation of the other years, which means that the difference between 2018 and the other years might be negligible. The NDMI and NDVI values of Landsat 8 for 2019 do not visually appear to stand out.

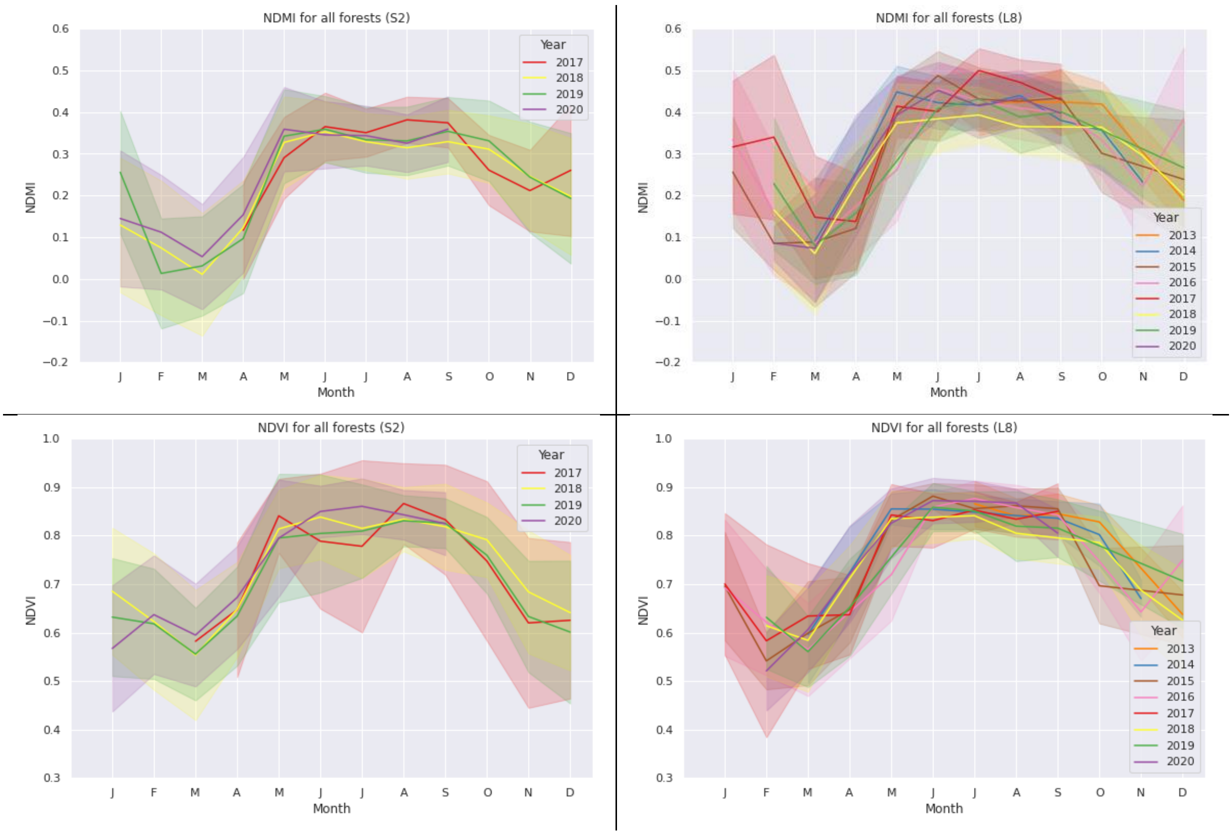

Figure 11a-d: Monthly NDMI and NDVI values for all types of forests in the Sentinel-2 dataset and the Landsat 8 dataset. The shading in the figure is the standard deviation.

6.3.1.3. Statistical Analysis

Pairwise comparison was done for the complete dataset of the Sentinel-2 data. The NDMI and NDVI values of each year (2017-2020) were significantly different ($p<0.05$) from each other, with the exception of the NDVI values for 2017 and 2018, which are not significantly different (see also figure 12). This means that there is not a significant difference between the NDVI and NDMI values of the drought years (2018 and 2019) and the non-drought years (2017 and 2020) in the Sentinel-2 dataset.

In the Landsat 8 dataset, the results of analysis of the yearly average VI values of the 170 locations varied. There is not a significant difference found between the NDVI values of the drought years (2018 and 2019) and the non-drought years (2013-2017 and 2020) in the Landsat 8 dataset. For NDMI, four out of six non-drought years are statistically not different from each other ($p<0.05$), however, this is also the case for a drought year and a non-drought year. Therefore, NDMI also does not give conclusive results of a significant difference between drought and non-drought years.

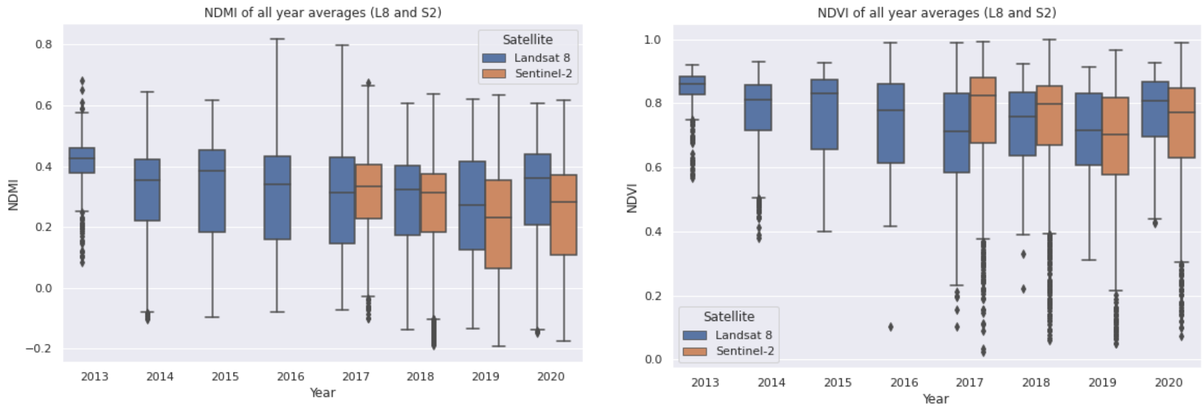

Figure 12a-b: Yearly NDMI and NDVI averages for all forests.

The same analysis was done for the summer months (June, July, August) only. In the analysis of these NDMI and NDVI values, there was some variation in the results (see also figure 13).

For the Sentinel-2 dataset, the NDMI values are statistically significantly lower in the years 2018 (0.343) and 2019 (0.348) than in the years 2017 (0.377) and 2020 (0.357) ($p<0.005$). The drought years (2018 and 2019) do not significantly differ from each other, and the non-drought years also do not significantly differ from each other. As for the NDVI values, they show a similar pattern with 2018 and 2019 relatively low (0.827 and 0.818) and 2020 significantly higher (0.854)) ($p<0.005$) , however, with the exception that 2017 is relatively lower (0.831), similar to the value of 2018.

The analysis of the Landsat 8 dataset of the summer months shows a similar pattern that is extended in the years before (see figure 13). The NDMI values for this dataset are statistically significantly lower in 2018 (0.360) than in all the other years (with values between 0.399 and 0.411). The other years are not significantly different from each other. The only exception in this is 2016, in which the NDMI was 0.399, which is not significantly different from 2018 ($p=0.057$). The NDVI values of the same data show a similar pattern, although there is more variation in the non-drought years. With an NDVI value of 0.825, 2018 is significantly lower than all the other years except for 2014 (0.848, $p=0.092$). The years 2020, 2016 and 2013 have relatively high NDVI values (0.860, 0.861 and 0.870 respectively), although 2013 and 2016 are not significantly higher than 2015, 2017 and 2019 (0.849, 0.842, and 0.847).

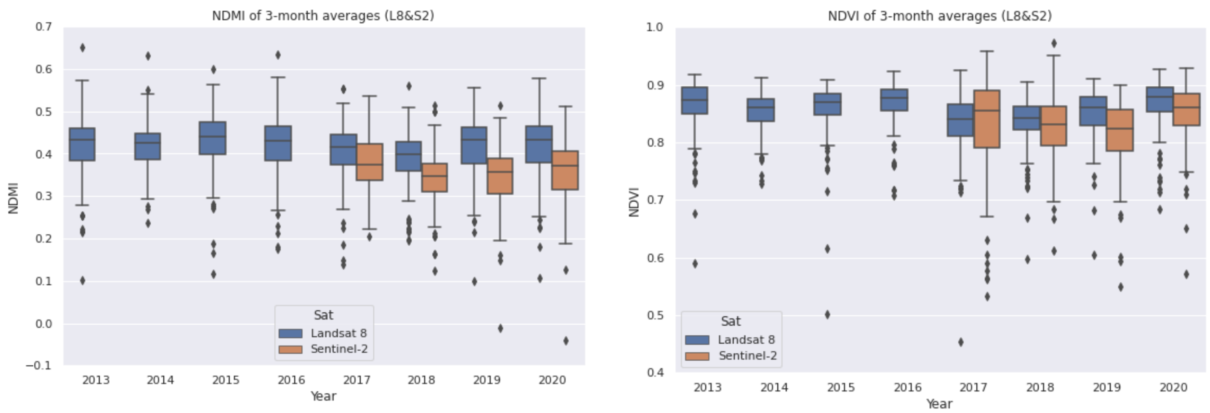

Figure 13a-b: Average NDMI and NDVI values for the summer months (June, July, August) of each year for all forests.

6.3.2. Per Forest Type

This section contains the results that are related to research question 2 ("*Does drought impact, as detected with remote sensing, vary among forest types in the Netherlands?*").

6.3.2.1. Descriptive Statistics

The time series of the 170 forest locations consist of 74 broadleaved forest, 45 coniferous forests, and 51 mixed forests. Of 21,450 time series measurements that were retrieved from Sentinel-2 (after the pre-processing), 7,955 measurements were from broadleaved forests, 6,342 were from coniferous forests, and 7.150 were from mixed forests. The Landsat 8 time series dataset contains 9,226 measurements, of which 4,353 from broadleaved forests, 2,314 from coniferous forests, and 2,560 from mixed forests. Detailed descriptive statistics for the datasets are found in appendix E.

6.3.2.2. Exploratory Analysis

Just as for the previous section, a distinctive yearly pattern is seen in all tree types (as shown in figure 11). All curves show a dip in the curve around March for each year and a peak between May and October for NDMI as well as for NDVI with both sensors. This pattern is stronger present for broadleaves than conifers (see figure 14 and 15) as a consequence of broadleaved trees are deciduous and therefore lose their leaves in the winter as opposed to conifers, which are generally evergreen. As the hypothesis is that coniferous forests are more affected by drought, the NDMI and NDVI of coniferous forests is expected to have a larger deviation in the drought years than the values of broadleaved and mixed forests. However, this is not apparent in the visual analysis of the Sentinel-2 dataset (see figure 14) in which there do not appear to be large differences between the NDMI and NDVI values of the different years for any of the forest types.

The visualisations of the Landsat 8 time series (figure 15) reveal that the coniferous forests vary a lot over the years, while broadleaved and mixed forests are relatively constant. The standard deviation margins also appear to be larger for the coniferous forests. For all forest types, the NDMI values between June and September of 2018 (blue line) are lower than in other years. The difference in NDMI between 2018 and the other years is largest for the coniferous forests, which is in line with the hypothesis.

As for NDVI, the values between July and September of 2018 are also lower than in other years, however, the timeframe of this decrease is shorter, and the difference is smaller than that of the NDMI. Mixed forests do not show this trend at all, as the NDVI values of multiple other years are lower than the values of 2018. The NDMI and NDVI values of Landsat 8 for 2019 do not visually appear to stand out for any of the tree types.

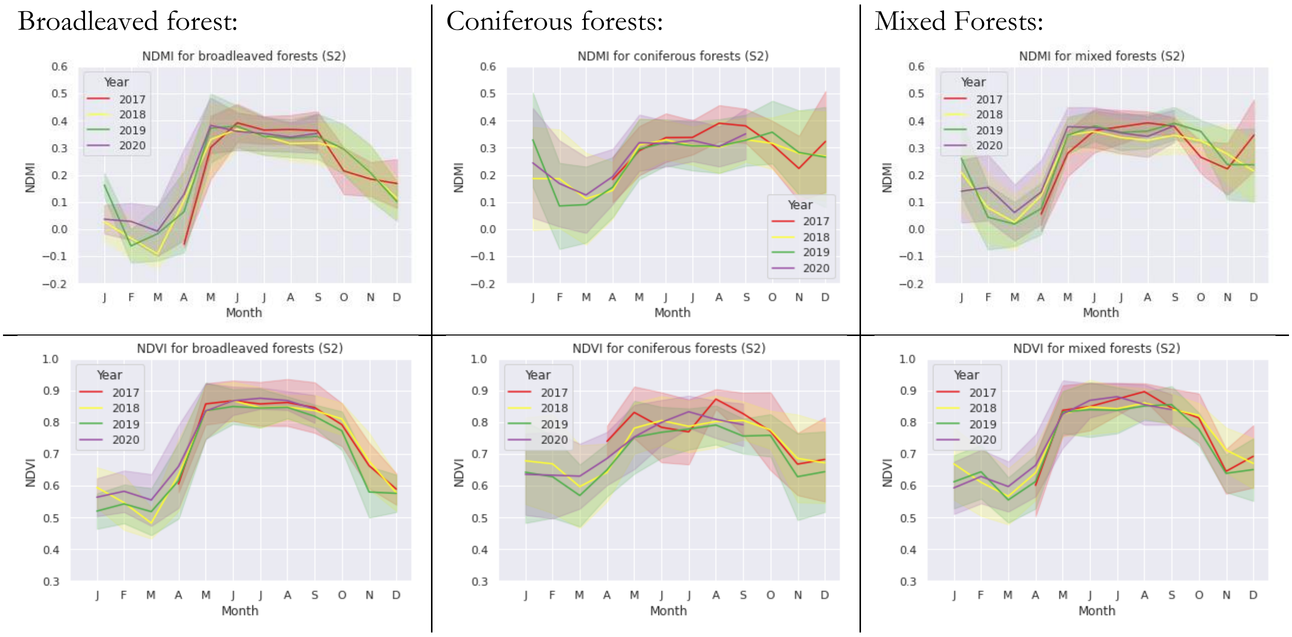

Figure 14a-f: Monthly NDMI (a-c) and NDVI (d-f) values for the various forest types in the Sentinel-2 dataset.

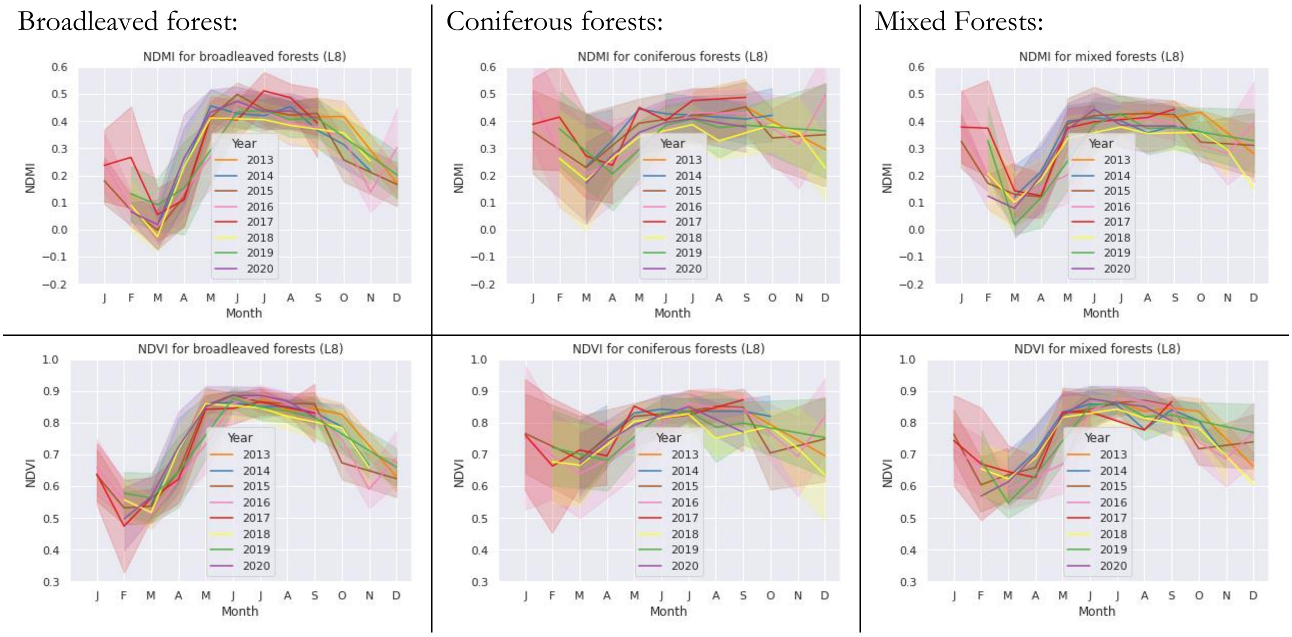

Figure 15a-f: Monthly NDMI (a-c) and NDVI (d-f) values for the various forest types in the Landsat 8 dataset.

6.3.2.3. Statistical Analysis

An ANOVA statistical analysis was done for both the Sentinel-2 and the Landsat 8 datasets on year-level.
As for Sentinel-2, the statistical analysis shows that there are significant differences between the NDMI values of the different forest types within the dataset (see also figure 16). Coniferous forests and broadleaved forests are significantly different from each other ($p<0.001$), as are mixed forests and coniferous forests ($p=0.024$). Broadleaved forests and mixed forests do not meet the benchmark of $p>0.05$ for this, but are very close ($p=0.056$). In contrast, the NDVI values of this dataset do not have significant differences between the forest types ($p>0.05$) as seen in figure 16.
This does not mean, however, that the trends over time (over the years) are significantly different from each other between the forest types. A Mauchly's test of sphericity showed that the variances between all different years are not equal, and hence we are not meeting a key assumption for repeated measures ANOVA. Therefore,

the Huynh-Feldt test is used for the test of within-subjects effects, because the Huynh-Feldt test corrects for this lack of sphericity (Girden, 1992). This test showed that the forest types do not have a significantly different trend over time ("year*foresttype") both for NDMI (F=0.581, p=0.680) and for NDVI (F=0.738, p=0.552) within the Sentinel-2 dataset. This means that there is no significant difference in the changes in NDMI and NDVI over the years between the forest types.

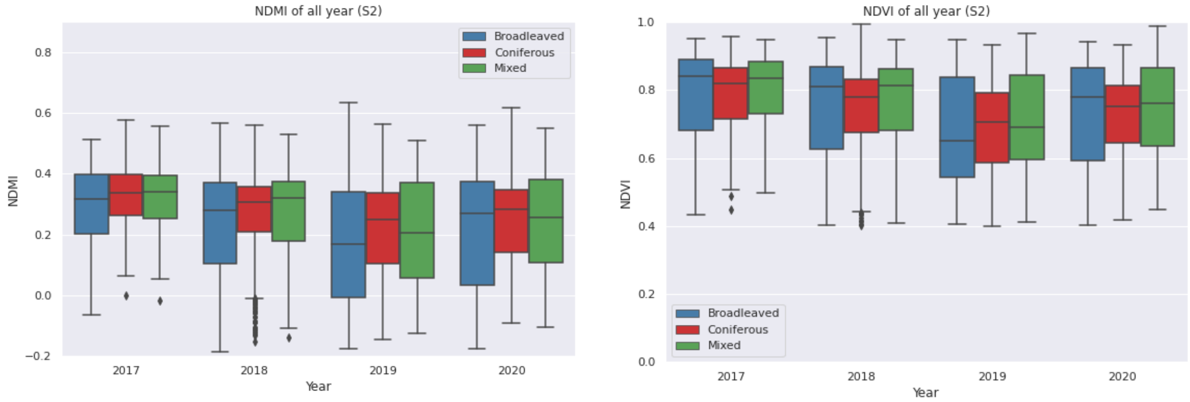

Figure 16a-b: Yearly NDMI and NDVI averages for the different forest types for Sentinel-2.

The statistical analysis of the Landsat 8 dataset shows results similar to the NDMI of the Sentinel dataset. It shows that there are significant differences between the NDMI values of the different forest types. Coniferous forests and broadleaved forests are significantly different from each other (p<0.001), as are mixed forests and coniferous forests (p=0.013). Broadleaved forests and mixed forests do not meet the benchmark of 0.05 for this, but are close (p=0.081). Similarly, the NDVI patterns differ significantly between coniferous and broadleaved forests (p<0.001) and mixed and coniferous forests, but not between broadleaved and mixed forests (0.216). This means that the NDMI and NDVI patterns differ greatly between most forest types.
In contrast to the results of the Sentinel dataset, there is a statistically significant difference in the trend over the years (2013-2020) between the forest types (for both NDMI and NDVI) for the Landsat dataset (F=3.642, p<0.01 and F=4.983, p<0.01 respectively in the Huynh-Feldt test) as can be seen in figure 17.

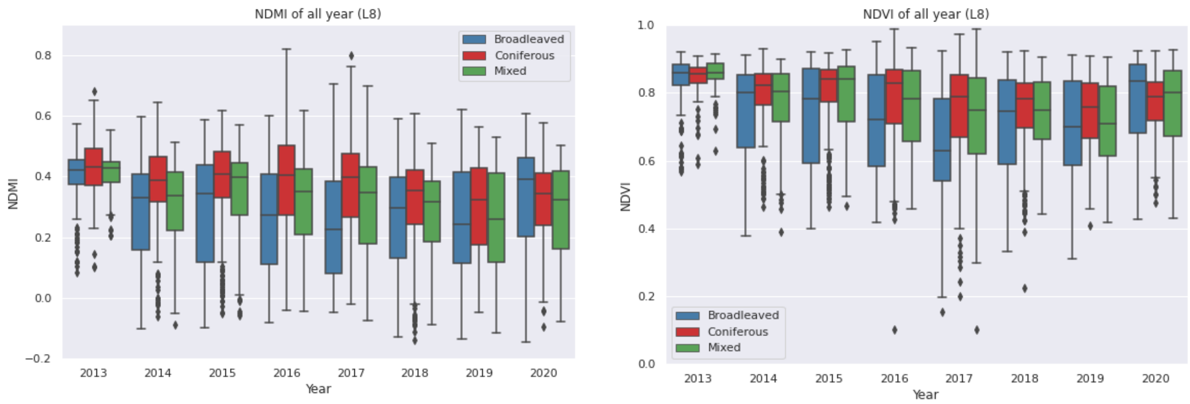

Figure 17a-b: Yearly NDMI and NDVI averages for the different forest types for Sentinel-2.

An ANOVA statistical analysis was also done for both the Sentinel-2 and the Landsat 8 datasets on a summer level, containing only the months June, July, and August.
As for Sentinel-2, the statistical analysis shows that there are no significant differences between the NDMI values or between the NDVI values of the different forest types within the dataset (p>0.05) (see also figure 18a and 18c). The Huynh-Feldt test showed that the forest types do not have a significantly different trend over time

("year*foresttype") both for NDMI (F=0.616, p=0.632) and for NDVI (F=0.530, p=0.764) within the Sentinel-2 dataset. This means that there is no significant difference in the changes in NDMI and NDVI over the years between the forest types.
The statistical analysis of the Landsat 8 dataset shows results similar to the Sentinel-2 dataset. It shows that there are significant differences between the NDMI values of the different forest types (see also figure 18b and 18d). None of the forest types are significantly different from each other in both NDMI and NDVI values in the pairwise comparisons (p>0.05 for all pairs). There is also no significant difference in the changes in NDMI and NDVI over the years between the forest types (Huynh-Feldt test: F=0.721, p=0.727 and F=0.237, p=0.992 respectively).

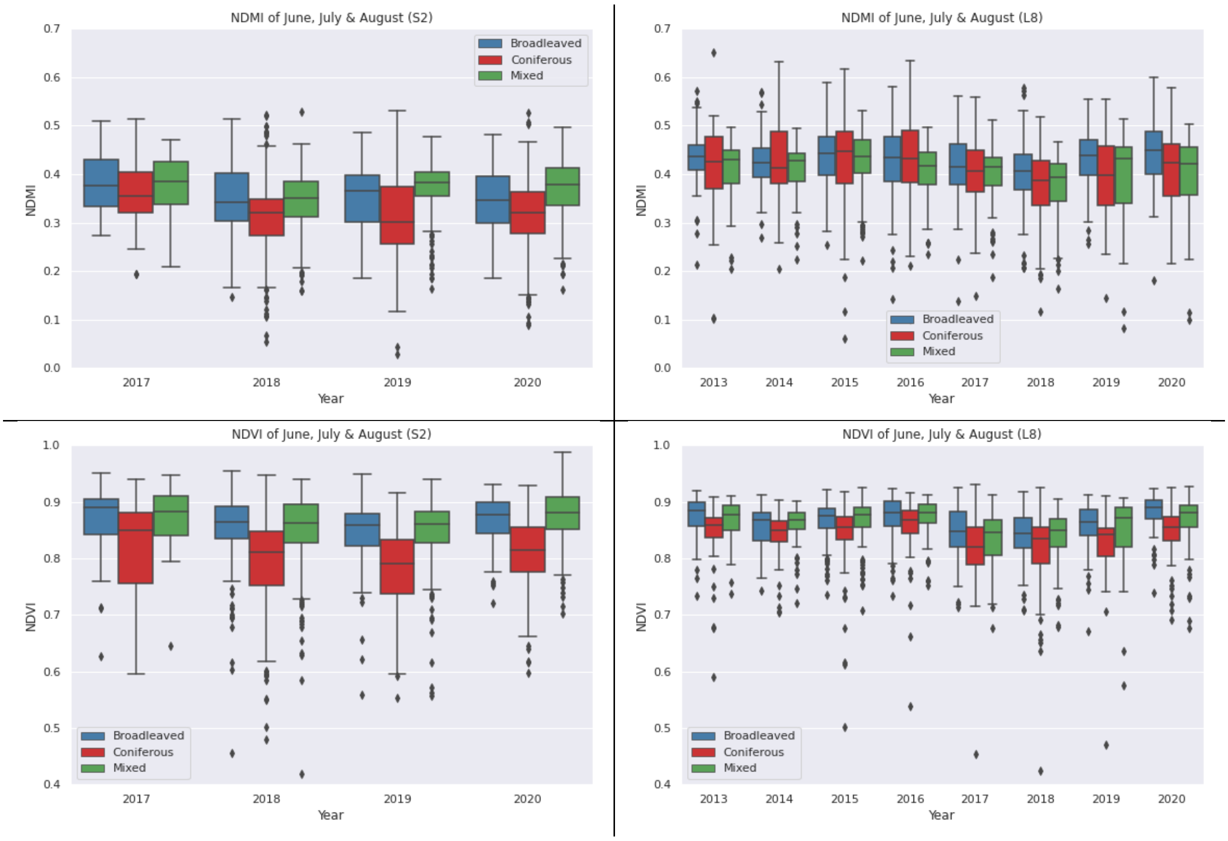

Figure 18a-d: Average NDMI and NDVI values for the summer months (June, July, August) of each year for the different forest types (Sentinel-2 and Landsat 8).

6.3.3. Per Soil Type

This section contains the results that are related to research question 3 ("*Does drought impact on forests vary between soil types on which a particular forest is located?*"). To answer this research question, the soil types of the forests from the NBI6 data subset are categorized into three main texture types: sand, clay, peat, and loess.

6.3.3.1. Descriptive Statistics

Out of the 170 forests studied in this research, 97 forests are located on sandy soil, 33 on clay soil, 31 on peat, and 9 on loess according to data of the NBI6. Out of the forests on sandy soil, 31 are broadleaved forests, 30 are coniferous forests, and 36 are mixed forests. For more detailed descriptive statistics, see appendix E. As demonstrated in figure 19, the percentages of forest types for each soil type vary strongly, which means there is a bias that should not be overlooked. Therefore, an analysis was done for VI differences between soil types in broadleaved forests only, to avoid this bias. Note that the total numbers of forests get small by taking subsets of soil types. Therefore, the data was analysed at yearly level (instead of monthly level), as otherwise the sample size at individual months would be too small.

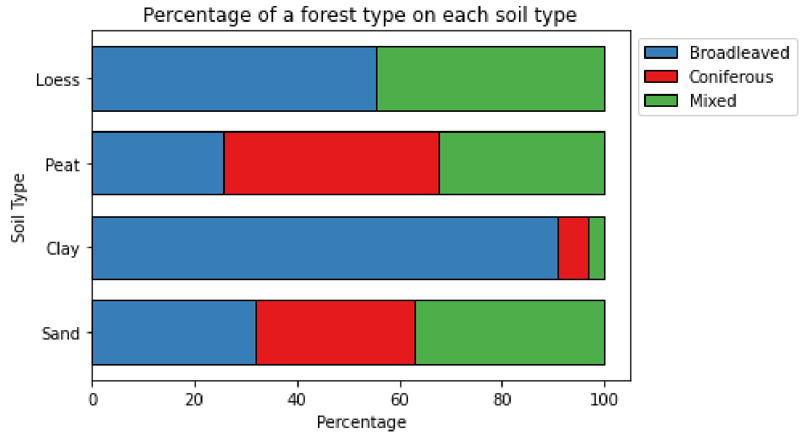

Figure 19: The distribution of different forest types on each soil types within the dataset of this study.

6.3.3.2. Exploratory Analysis

The graphs below show (figure 20) the trend over time of NDMI and NDVI for all forests together. Noticeably, the year 2019 is visibly lower than the other years for almost all soil types. The NDVI values of the Landsat dataset are also lower than the 2018 values for all soil types, however, this is not the case in the Sentinel dataset. Clay for Landsat 8 also stands out, as it is the only one that has a lower NDMI in 2018 than in 2019, and it has an outstanding dip in 2017 for NDVI. However, as the descriptive statistics show, about 90% of the forests plots on clay soil are broadleaved forests, which is a lot more than for the other soil types. This strong relationship between forest types and soil types may influence the results.

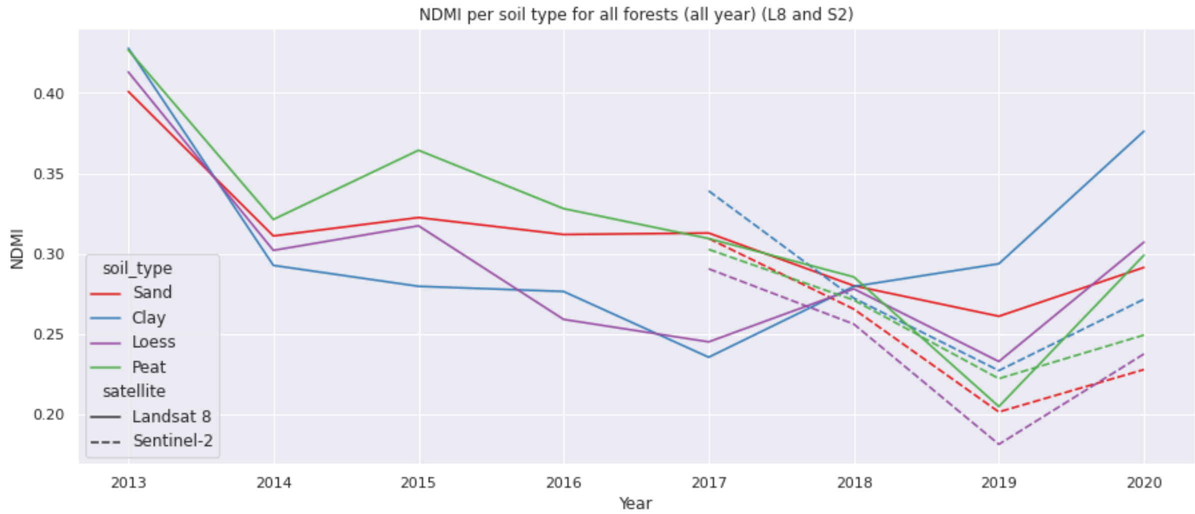

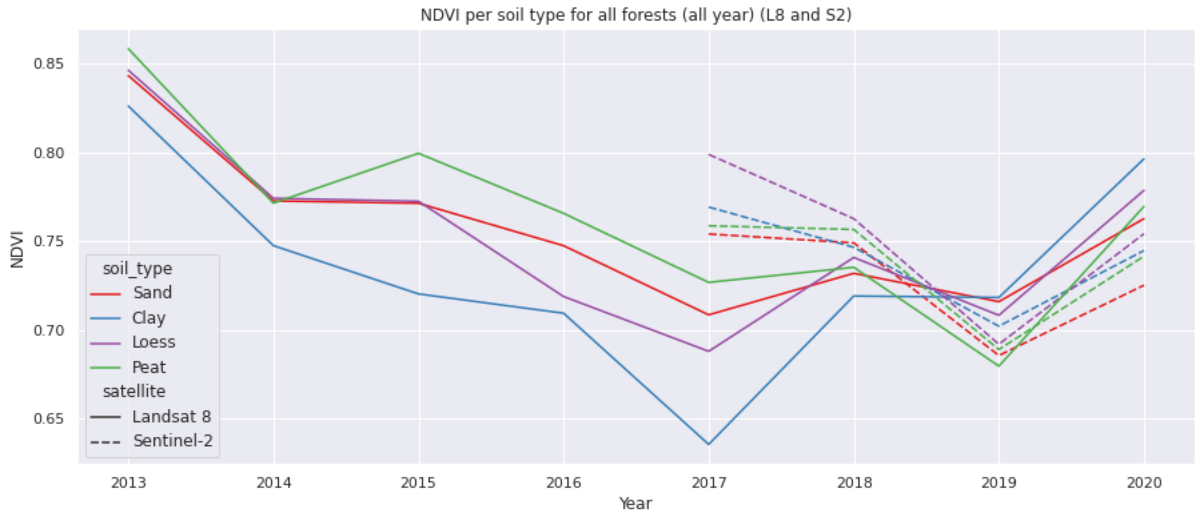

Figure 20a-b: NDMI and NDMI values of the forests per soil type: sandy soil (98 forests), clay (33 forests), peat soil (31 forests), and loess soil (9 forests). Note that 2020 and 2013 of Landsat 8 and 2017 of Sentinel-2 are inaccurate, as they do not contain the whole year.

To reduce the forest type influence on the exploratory analysis of the influence of soil types, the subset of broadleaved forest was used for further analysis (as shown in figure 21). This analysis was done on broadleaved forests as broadleaved is the largest forest type and has the best spread across different (soil types as seen in the descriptive statistics). Figure 21 shows that even within one forest type, there is still variation between the soil types in NDMI and NDVI values. The NDVI and NDMI values of forests on clay soil are relatively high in comparison to other soil types in 2018 and 2019, and unlike other soil types, the Landsat 8 dataset does not have a downward trend between 2018 and 2019.

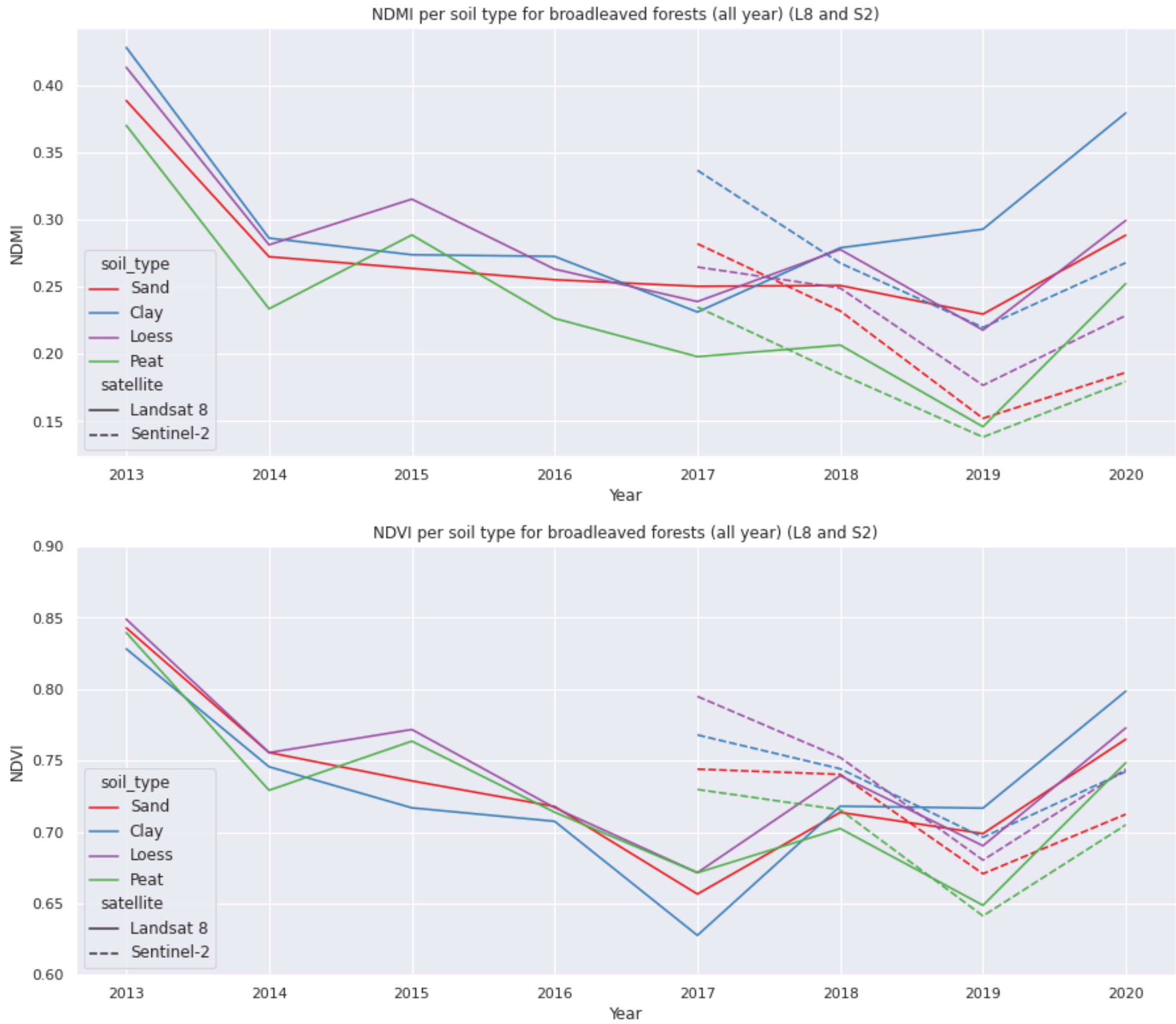

Figure 21a-b: NDMI and NDMI values of the broadleaved forests per soil type: sandy soil (31 forests), clay (30 forests), peat soil (8 forests), and loess soil (5 forests). Note that 2020 and 2013 of Landsat 8 and 2017 of Sentinel-2 are inaccurate, as they do not contain the whole year.

6.3.3.3. Statistical Analysis

An ANOVA statistical analysis was done for both the Sentinel-2 and the Landsat 8 datasets on year-level to assess the impact of different soil types (see also figure 22).

The Huynh-Feldt test for within-subject factors showed that the soil types have a significantly different trend over time both (year*soil type) for NDMI ($F=3.231$, $p<0.01$) and for NDVI ($F=3.028$, $p<0.01$) in the Landsat 8 dataset. However, this same test on the Sentinel-2 dataset does not detect a significantly different trend over time between the soil types for both NDMI ($F=1.649$, $p=0.143$) and for NDVI ($F=0.675$, $p=0.661$). However, when comparing the trends over time of the different types of forests for different soil types (year*forest type*soil type), this test indicates no significant differences for NDMI or NDVI for both the Landsat 8 and Sentinel-2 datasets ($p=0.520$-0.889). The pairwise comparisons also do not show significant differences between soil types.

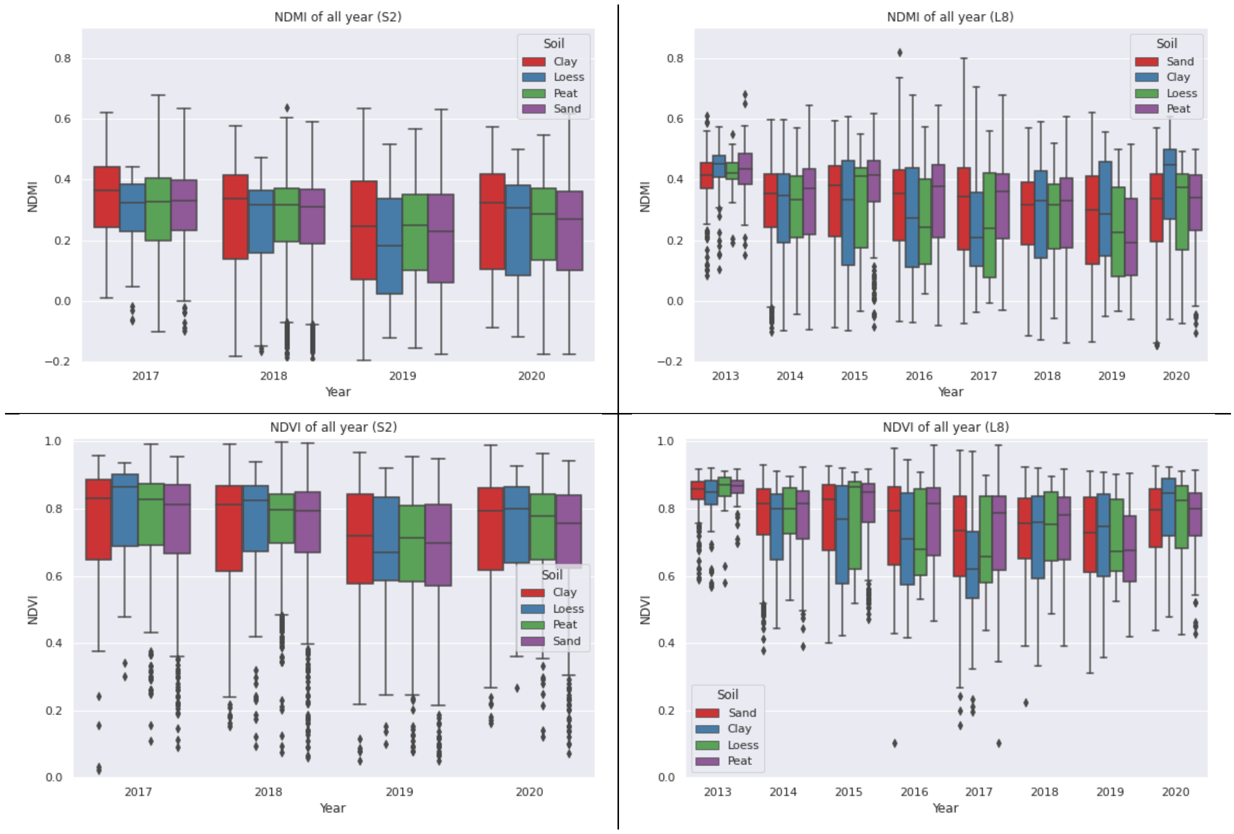

Figure 22a-d: Yearly NDMI and NDVI averages for the different soil types for all forests (Sentinel-2 and Landsat 8).

To account for the forest type – soil type bias, an additional ANOVA was done for the broadleaved forests only (shown in figure 23). The results of this analysis were inconclusive, as they vary strongly per dataset. As for the Landsat and Sentinel NDVI datasets, no significant differences were bound between the soil types in the pairwise comparisons or the within-subjects' effects (Huynh-Feldt) test ($p>0.05$). Landsat and Sentinel NDMI datasets showed more differences, however minimal. See Appendix F for the full results of the ANOVA. Therefore, the data was analysed at yearly level (instead of monthly level), as otherwise the sample size at individual months would be too small.

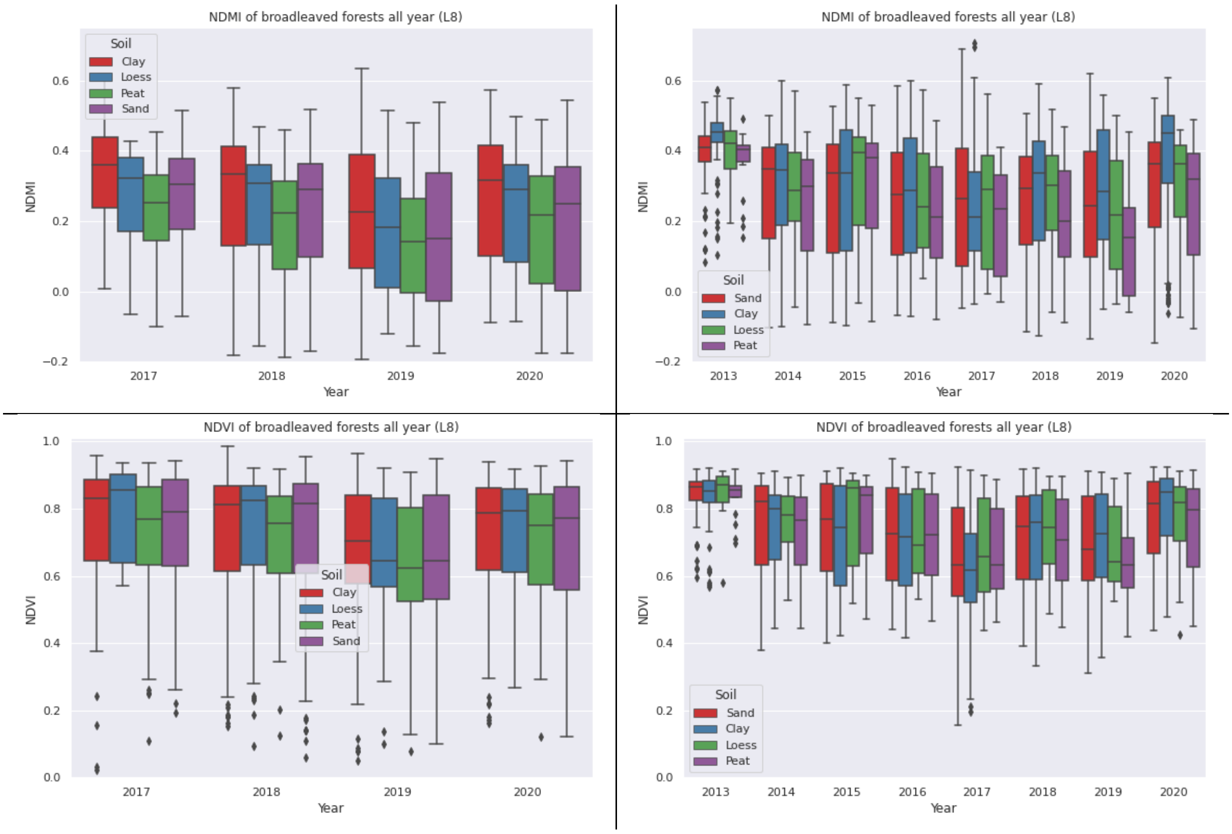

Figure 23a-d: Yearly NDMI and NDVI averages for the different soil types for broadleaved forests (Sentinel-2 and Landsat 8).

7. DISCUSSION

7.1. Detecting Drought Impact on Forests

The results of the analysis vary strongly between the vegetation indices, sensor datasets, and timescales. While there was no significant difference in the VI values of the overall dataset for Sentinel-2, in the Landsat 8 dataset the summer months, 2018 and 2019 were found to be significantly lower than the other years for both NDVI and NDMI. Exceptions for this are 2016 for the NDMI dataset and 2014 for the NDVI set, which were both in their respective datasets statistically similar to 2018 and 2019. These results align with previous research as discussed in chapter 2, including vegetation index analyses of Europe (Buitink et al., 2020; Buras et al., 2020), reports form Dutch foresters (Koopman, 2020; Reijman and Prooijen, 2020), and ground measurements by Wageningen Environmental Research in the Netherlands (Lerink et al., 2019).
Likewise, the results of the forest type differences are also inconclusive. Exploratory analysis revealed some differences in standard deviation, which can be a result of a different in drought impact, but it is also possible that it is caused by the difference in sample size. While the ANOVA shows that NDMI and NDVI values of the forest types are significantly different from each other in the Landsat 8 dataset, for the Sentinel-2 dataset this difference is only found in NDMI. However, neither of the datasets contained a significantly different trend over the years between the forest types. Based on previous research as discussed in chapter 2, coniferous forests were expected to be more affected than broadleaved or mixed forests, as this was the case in all previous studies discussed in chapter 2 where different forest types were compared (Assal et al., 2016; Buras et al., 2020; Vicente-Serrano, 2007). This was supported by the ground measurements in the Netherlands (Lerink et al., 2019). However, this research does not confirm this hypothesis as the results are inconclusive.
As for the influence of the soil types on the forests, no significant difference could be determined between NDVI and NDMI values of forests on different soil types, neither for any differences in their trend over time. However, as the distribution of forest types is strongly linked to the soil types, these two factors were hard to separate. The ANOVA on only the broadleaved forest also shows inconclusive results: while there is some variation between the soil types in NDMI values, the NDVI values do not differ significantly between the soil types. Both Sentinel-2 and Landsat 8 show a significant trend over time, however, these trends differ strongly between NDVI and NDMI especially in 2017 and 2019. No conclusion can be drawn from this. As discussed in chapter 2, literature suggests that forests on sandy soil have the smallest short-term drought impact (Agaba et al., 2010; Jiang et al., 2020), however, this cannot be confirmed in this research.

7.2. Critical Reflection on Inconclusive Results

There could be two possible explanations for the overall inconclusive results: limited drought impact and limitations of the method. To elaborate on the first one: It is possible that there is no or very limited drought damage. Some foresters have stated to observe drought impact from the 2018 and 2019 drought on their forests, so it is unlikely that there is no drought damage at all. The study of tree diameters by the Wageningen Environmental Research showed that particularly the growth of the Douglas fir and the Scots pine stagnated in 2018 as a consequence of the drought (Lerink et al., 2019). However, it is possible that the change in greenness and drought damage is too minimal to detect with this method using large scale objective remotely sensed data. Vicente-Serrano (2007) was using a similar method on multiple areas, and he found that humid areas (600 mm/year) are less affected than arid areas (320 mm/year). As the Netherlands (790 mm/year) is even more humid than the areas Vicente-Serrano used for his study, is plausible that the Netherlands has too little drought impact to be detectable with this method.

The other explanation for the results is that the method is not suitable for drought impact detection in the Netherlands. The tests with the validation dataset showed that the method is able to detect large changes in forest that are dying, but more subtle changes such as drought impact requires more accuracy. The approach of drought impact detection with satellite VI has a number of limitations, as for a thorough analysis of fluctuations, time series of significant length and temporal resolution are required. First of all, the available data has a clear trade-off between spatial resolution and temporal resolution (length of time series). For a region like the Netherlands with a lot of fragmentation of the forests, a high spatial resolution is required to capture the forests without any surrounding landscape. Therefore, imagery of the relatively young Sentinel-2 satellite was used with the highest available resolution of 20mx20m. However, the downside of such a young satellite is that the time series only go back 3.5 years. Satellites that were launched earlier (such as Landsat 8) have longer time series, but have a smaller spatial and temporal resolution that are not as accurate in sensing small or fragmented forests and have significant gaps in the time series due to cloud filters and the lower temporal resolution. That explains why the previous studies as described in chapter 2 only use large, forested study areas, such that lower spatial resolution can be used and time series over many years, to deal with the described temporal-spatial resolution trade-off.

7.3. Selecting the Appropriate Satellite

Besides the age and the resolution of the satellite, the sensor properties also impact the results. Overall, the Sentinel-2 values were lower for all the measurements, which might be a result of the difference in range of the wavelengths of the spectral bands. The range of the bands (in nanometres) is slightly different, which can cause them to define the vegetation indices slightly differently and therefore also the vegetation properties. A study of Arekhi et al. (2019) compared vegetation indices for Landsat 8 and Sentinel-2 and found Pearson's coefficients of 0.92 and 0.89 for NDVI and NDMI respectively, which they consider similar enough to use the data of the two satellites in combination for larger datasets for forestry monitoring.

Overall, the Landsat 8 time series dataset captures the drought impact better than the Sentinel-2 time series dataset, as there are more significant differences or patterns found in the data. The main reason for this is that the dataset is longer, as the Sentinel-2 dataset has insufficient data to set a baseline for non-drought years, which appears to be a stronger weighing factor than the higher spatial resolution. However, the low temporal resolution of Landsat 8 resulted in rather large gaps in the time series, and this limited the analysis that could be done on month-level.

7.4. Selecting the Appropriate Vegetation Indices

Another limitation of this method is that it is very limited in what it can measure. In the vegetation index selection process, NDVI and NDMI were found to respond strongest to droughts, as they measure the wavelengths that represent greenness and moisture content. However, other impacts from droughts, such as smaller increase in diameter, cannot be reflected in these vegetation indices. NDVI is also known to have saturation problems (particularly in dense forests), which decreases the degree to which it can show drought impact. So, while using VI from satellite imagery has the advantage of using large scale objective data, these are some significant drawbacks.

It is noteworthy that the two vegetation indices used in this research, NDMI and NDVI varied slightly in results. This difference between NDMI and NDVI became especially clear in the pairwise comparisons of the soil analysis of coniferous forests. The NDVI datasets did not contain any significant differences between the NDVI values of the different soil types, while for the NDMI dataset, some of them did have significant differences. Even though NDVI is one of the most used VI for this type of research in current literature, NDMI showed more often a significant effect between the drought-years and the non-drought years. A potential explanation that NDMI and NDVI differ is that one includes a short wavelength infrared band that responds to moisture content while the other one includes the red band. Therefore, NDMI represents moisture content levels, while NDVI represents the greenness of vegetation. It is possible that moisture content changes quicker than greenness during times of drought and therefore the NDMI shows a stronger relation to short-term drought impact. A study of Gu et al. (2008) concluded also that NDMI was more sensitive to drought conditions than NDVI, and that this was most likely because NDMI is influenced by both desiccation and wilting (while NDVI is not as much affected by desiccation, as it measures greenness).

7.5. Further Limitations of the Approach

Another limitation that was found during the data preparation was the filtering of the data for cloudy pixels. A filter was used within the Google Earth Engine code to ensure to only extract time series with non-cloudy moments of the locations, but this filter that detects clouds is not entirely accurate. This is not a large problem for arid areas where it is only clouded a small part of the year, but in more humid areas like the Netherlands, the overall number of clouds that are not filtered out will increase and pollute the time series. Cloudiness is in general a larger problem in time series of humid climates, as there will be fewer good measurements and the time series dataset is left with significant gaps due to cloudy months. Months or years with more clouds, which are generally the more wet years (such as 2017), are underrepresented in the datasets relative to the dry years (such as 2018). Such underrepresentation of non-drought years can lead to an artificially high sampling of drought years within filtered data, which could give the impression of more drought impact in the forests than there actually is. Similarly, an inconsistency was found in the sample sizes of the different forest types: coniferous forests have about half as many recordings in the time series data than broadleaved forests. This might explain the difference in standard deviation and can lead to a stronger deviation caused by extreme outliers.

Not only consistency in the time series in a challenge, also imbalances in the distribution of forests of different types on the different soil types is an issue when analysing the effect of soil types. As the forest types are unequally distributed over the soil types, an additional analysis was done with only the broadleaved forests dataset. However, this raises other issues of limited data, as only a third of the dataset can be used that way. When comparing the three forest types (as done in section 6.3.2), the influence of soil types is not considered for two reasons: the sample size would be too small if the forests within only one soil type were analysed; and all discussed literature that studied differences between forest types did not account for soil type differences, and therefore it was assumed the impact would be small.

This research is focussed on short term drought effects. Long-term effects of droughts are not analysed, as this is complex and requires more advanced research methods. As the year-average NDMI and NDMI values were lower for 2019 than 2018, while 2018 was the year with the severest drought, there is most likely a long-term effect or an effect of having multiple drought years in a row. However, this effect was not studied, as this does not fit in the scope of this research, and the satellite time series available are too short for such an analysis.

7.6. Future Outlook

Forest adaptation for climate change is a wicked problem. By increasing the knowledge about local drought impact and vulnerability of forest types and species, we can work towards finding solutions for planning vital and sustainable forests in the future. These possible solutions can go various directions, such as water management, selective species planting, or letting forests naturally adapt to droughts through natural selection.

This research has demonstrated that this method has potential to be used for drought impact analysis of the Dutch forests. However, to harness the full potential, more data is needed for a detailed and accurate drought impact analysis of the Dutch forests in which forest types and soil types can accurately be compared. As the currently available high-resolution data is of too short time timespan for such an analysis, additional data can be achieved over time as the time series datasets grow. As these datasets are growing and predictions of foresters and studies in other countries (as discussed in chapter 1) are that extreme droughts will occur more frequently in the future, it is likely that in several years this method will be effective. This means that as the problem becomes more severe and acute, the available high quality data increases and this approach will be a valuable standard to compare to. Other methods of expanding the data can also be further explored, such as triangulation of multiple datasets including airborne and ground measurements, or combining multiple satellite imagery datasets. There are recent studies such as (Arekhi et al., 2019) that combine Landsat 8 and Sentinel-2 datasets for time series analysis. This however will raise new challenges, such as dealing with differences in sensitivity to atmospheric effects (Arekhi et al., 2019) before these methods can be applied.

8. CONCLUSION

This study focused on the suitability of spaceborne vegetation indices for drought impact assessment in the Dutch forests. NDMI and NDVI have been found to be the most suitable vegetation indices for this assessment, as they responded strongest to drought. The NDMI and NDVI datasets from Sentinel-2 and Landsat 8 indicate some drought impact in the year 2018, however, no significant differences of drought impact are found between different forest types or different soil types on which forests are located.
This research has shown that currently there is not enough high spatial and temporal resolution satellite data available for a detailed drought impact analysis on forests in areas with highly fragmented forests and low forest density such as the Netherlands. The results illustrate the importance of the length of time series for the drought impact analysis, as the time series dataset of Landsat 8 of eight years captures the drought impact of 2018 on the forests more than the Sentinel-2 time series dataset of four years. The results also demonstrated that NDMI is better at capturing drought impact than NDVI. However, both indices are sensitive to ground noise, and further research is required to establish their differences in accuracy on this front.
This study contributes to the forest monitoring research and the development of forest management strategies in low forest density areas. Future research can include the combining of data sources to create a large dataset of high resolution time series, such as combinations of Landsat 8 and Sentinel-2 data or ground measurements.

LIST OF REFERENCES

Agaba, H., Orikiriza, L.J.B., Esegu, J.F.O., Obua, J., Kabasa, J.D., Hüttermann, A., 2010. Effects of hydrogel amendment to different soils on plant available water and survival of trees under drought conditions. Clean - Soil, Air, Water 38, 328–335. https://doi.org/10.1002/clen.200900245

Allen, C.D., 2009. Climate-induced forest dieback: An escalating global phenomenon? Unasylva 60, 43–49.

Arekhi, M., Goksel, C., Sanli, F.B., Senel, G., 2019. Comparative evaluation of the spectral and spatial consistency of Sentinel-2 and Landsat-8 OLI data for Igneada longos forest. ISPRS Int. J. Geo-Information 8. https://doi.org/10.3390/ijgi8020056

Assal, T.J., Anderson, P.J., Sibold, J., 2016. Spatial and temporal trends of drought effects in a heterogeneous semi-arid forest ecosystem. For. Ecol. Manage. 365, 137–151. https://doi.org/10.1016/j.foreco.2016.01.017

Bak, B., Labedzki, L., 2002. Assessing drought severity with the relative precipitation index (RPI) and the standardised precipitation index (SPI). J. Water L. Dev. 29–49.

Bastos, A., Ciais, P., Friedlingstein, P., Sitch, S., Pongratz, J., Fan, L., Wigneron, J.P., Weber, U., Reichstein, M., Fu, Z., Anthoni, P., Arneth, A., Haverd, V., Jain, A.K., Joetzjer, E., Knauer, J., Lienert, S., Loughran, T., McGuire, P.C., Tian, H., Viovy, N., Zaehle, S., 2020. Direct and seasonal legacy effects of the 2018 heat wave and drought on European ecosystem productivity. Sci. Adv. 6, 1–14. https://doi.org/10.1126/sciadv.aba2724

Behrens, J.T., 1997. Principles and Procedures of Exploratory Data Analysis. Psychol. Methods 2, 131–160. https://doi.org/10.1037/1082-989X.2.2.131

Boosten, M. (Stichting P., 2016. Nederlands bos(beheer): al 250 jaar in ontwikkeling. Vakbl. Nat. bos Landsch. 13, 12–14.

Buitink, J., Swank, A.M., van der Ploeg, M., Smith, N.E., Benninga, H.-J.F., van der Bolt, F., Carranza, C.D.U., Koren, G., van der Velde, R., Teuling, A.J., 2020. Anatomy of the 2018 agricultural drought in The Netherlands using in situ soil moisture and canopy nearinfrared reflectance satellite imagery. Hydrol. Earth Syst. Sci. 1–17.

Buras, A., Rammig, A., S. Zang, C., 2020. Quantifying impacts of the 2018 drought on European ecosystems in comparison to 2003. Biogeosciences 17, 1655–1672. https://doi.org/10.5194/bg-17-1655-2020

CBS, 2014. Centraal Bureau voor de Statistiek: Bos en open natuur [WWW Document]. URL https://www.cbs.nl/nl-nl/maatschappij/natuur-en-milieu/groene-groei/natuurlijke-hulpbronnen/indicatoren/bos-en-open-natuur (accessed 12.15.20).

Choubin, B., Soleimani, F., Pirnia, A., Sajedi-Hosseini, F., Alilou, H., Rahmati, O., Melesse, A.M., Singh, V.P., Shahabi, H., 2019. Effects of drought on vegetative cover changes: Investigating spatiotemporal patterns, Extreme Hydrology and Climate Variability: Monitoring, Modelling, Adaptation and Mitigation. Elsevier Inc. https://doi.org/10.1016/B978-0-12-815998-9.00017-8

Cleveland, W.S., 1994. The elements of graphing data., Revised ed. ed. Hobart Press, Summit, New Jersey.

Diermanse, F., Mens, M., Macian-Sorribes, H., Schasfoort, F., 2018. A stochastic model for drought risk analysis in The Netherlands. Hydrol. Earth Syst. Sci. Discuss. 1–20. https://doi.org/10.5194/hess-2018-45

ESA, n.d. THE EUROPEAN SPACE AGENCY: Missions: Sentinel-2 [WWW Document]. URL https://sentinel.esa.int/web/sentinel/missions/sentinel-2 (accessed 9.14.21).

FOREST EUROPE, 2020. State of Europe's Forests 2020 394.

Gao, B.-C., 1996. NDWI A Normalized Difference Water Index for Remote Sensing of Vegetation Liquid Water From Space. Remore Sens. Environ. 58, 257–266. https://doi.org/10.24059/olj.v23i3.1546

Girden, E.R., 1992. ANOVA: Repeated measures (No. 84). Sage.

Gu, Y., Hunt, E., Wardlow, B., Basara, J.B., Brown, J.F., Verdin, J.P., 2008. Evaluation of MODIS NDVI and NDWI for vegetation drought monitoring using Oklahoma Mesonet soil moisture data. Geophys. Res. Lett. 35, 1–5. https://doi.org/10.1029/2008GL035772

Hardisky, M., Klemas, V., Smart, M., 1983. The influence of soil salinity, growth form, and leaf moisture on the spectral radiance. Spartina alterniflora 49, 77–83.

Hekhuis, H. (Staatsbosbeheer), n.d. Klimaat en natuur in de praktijk [WWW Document]. Klimaat, bos en Nat. URL https://www.staatsbosbeheer.nl/over-staatsbosbeheer/dossiers/klimaat-en-natuur/klimaat-en-natuur-in-de-praktijk

Huang, J., Zhuo, W., Li, Y., Huang, R., Sedano, F., Su, W., Dong, J., Tian, L., Huang, Y., Zhu, D., Zhang, X., 2020. Comparison of three remotely sensed drought indices for assessing the impact of drought on winter

wheat yield. Int. J. Digit. Earth 13, 504–526. https://doi.org/10.1080/17538947.2018.1542040
Huete, A., Didan, K., Miura, T., Rodriguez, E.P., Gao, X., Ferreira, L.G., 2002. Overview of the radiometric and biophysical performance of the MODIS vegetation indices. Remote Sens. Environ. 83, 195–213. https://doi.org/10.1016/S0034-4257(02)00096-2
Huete, A.R., 1988. A Soil-Adjusted Vegetation Index (SAVI). Remote Sens. Environ. 25, 295–309.
IPCC, 2014. AR5 Synthesis Report: Climate Change 2014.
Jiang, P., Ding, W., Yuan, Y., Ye, W., 2020. Diverse response of vegetation growth to multi-time-scale drought under different soil textures in China's pastoral areas. J. Environ. Manage. 274, 110992. https://doi.org/10.1016/j.jenvman.2020.110992
Jordan, C., 1969. Derivation of Leaf-Area Index from Quality of Light on the Forest Floor. Ecology 50, 663–666. https://doi.org/10.1155/2012/651039
Khoury, S., Coomes, D.A., 2020. Resilience of Spanish forests to recent droughts and climate change. Glob. Chang. Biol. 1–20. https://doi.org/10.1111/gcb.15268
KNMI, 2021a. Droogte [WWW Document]. URL https://www.knmi.nl/kennis-en-datacentrum/uitleg/droogte (accessed 12.12.20).
KNMI, 2021b. Tropische Dagen [WWW Document]. URL https://www.knmi.nl/kennis-en-datacentrum/uitleg/tropische-dagen (accessed 2.4.21).
KNMI, 2021c. Dagwaarden neerslagstations.
KNMI, 2020. Hittegolven [WWW Document]. URL https://www.knmi.nl/nederland-nu/klimatologie/lijsten/hittegolven
Koopman, O., 2020. Droogte slaat diepe wonden in Veluwse bossen: zijn onze naaldbomen straks verdwenen? De Stentor.
Larkin, J.., Simon, H.A., 1987. Why a Diagram Is (Sometimes) Worth 10000 Words. Cogn. Sci. 11, 65–99.
Lerink, B., Toor, M. van, Konig, L., Nabuurs, G.-J., 2019. Heeft het bos stilgestaan in 2018? Wageningen Environ. Res.
Lobo, A., Maisongrande, P., Coret, L., 2010. The impact of the heat wave of summer 2003 in SW Europe as observed from satellite imagery. Phys. Chem. Earth 35, 19–24. https://doi.org/10.1016/j.pce.2010.03.041
NOS, 2021. Opnieuw protest tegen verbreding A27 in bos Amelisweerd [WWW Document]. URL https://nos.nl/artikel/2373369-opnieuw-protest-tegen-verbreding-a27-in-bos-amelisweerd.html (accessed 5.10.21).
NOS, 2019a. Natuurmonumenten stopt voorlopig met bomen kappen [WWW Document]. URL https://nos.nl/artikel/2279878-natuurmonumenten-stopt-voorlopig-met-bomen-kappen (accessed 5.10.21).
NOS, 2019b. Staatsbosbeheer wil duidelijker bosbeleid van minister [WWW Document].
NOS, 2018. Protest tegen bomenkap, banden boswachters lek gestoken [WWW Document]. URL https://nos.nl/artikel/2255920-protest-tegen-bomenkap-banden-boswachters-lek-gestoken.html (accessed 5.10.21).
Oldenburger, J., 2019. Stand van zaken bos in Nederland 3–33.
Pichler, P., Oberhuber, W., 2007. Radial growth response of coniferous forest trees in an inner Alpine environment to heat-wave in 2003. For. Ecol. Manage. 242, 688–699. https://doi.org/10.1016/j.foreco.2007.02.007
Probos, 2019. Bos en Houtcijfers - Houtverbruik [WWW Document]. URL http://www.bosenhoutcijfers.nl/de-houtmarkt/houtverbruik/
Qi, J., Chen, J., Lafortezza, R., Lin, Z., 2017. Remote sensing for ecosystem sustainability. Compr. Remote Sens. 1–9, 186–201. https://doi.org/10.1016/B978-0-12-409548-9.10428-2
Reijman, J., Prooijen, E. van, 2020. De bossen staan op omvallen door aanhoudende droogte: "We moeten nu al andere bomen naar Nederland halen." eenvandaag.avrotros.
Richardson, A.J., Wiegand, C., 1977. Distinguishing Vegetation from Soil Background Information. Photogramm. Eng. Remote Sensing 43, 1541–1552.
Rouse, J.W., Haas, R.H., Schell, J.A., Deering, D.W., 1974. Monitoring vegetation systems in the Great Plains with ERTS. NASA Spec. Publ. 351 309.
Saleem, A., Awange, J.L., 2019. Coastline shift analysis in data deficient regions: Exploiting the high spatio-temporal resolution Sentinel-2 products. Catena 179, 6–19. https://doi.org/10.1016/j.catena.2019.03.023
Santos, J.F., Portela, M.M., Naghettini, M., Matos, J.P., Silva, A.T., 2013. Precipitation thresholds for drought recognition: A further use of the standardized precipitation index, SPI. WIT Trans. Ecol. Environ. 172, 3–14. https://doi.org/10.2495/RBM130011
Schelhaas, M.J., Clerkx, A.P.P.M., Daamen, W.P., Oldenburger, J.F., Velema, G., Schnitger, P., Schoonderwoerd,

H., Kramer, H., 2014. Zesde Nederlandse bosinventarisatie : methoden en basisresultaten.
Sohngen, B., Tian, X., Kim, J., Ohrel, S., Cole, J., 2016. Global climate change impacts on forests and markets. For. Policy Econ. 72, 18–26. https://doi.org/10.1016/j.forpol.2016.06.011
Staatsbosbeheer, 2020. Jaarverslag 2020.
Staatsbosbeheer, 2019. Staatsbosbeheer - Feiten en cijfers [WWW Document]. URL https://www.staatsbosbeheer.nl/over-staatsbosbeheer/feiten-en-cijfers
Stroo, L., 2019. 800 miljoen moet stervende bossen redden [WWW Document]. URL https://duitslandinstituut.nl/artikel/33529/800-miljoen-moet-stervende-bossen-redden (accessed 5.10.21).
Thomassen, E., Wijdeven, S., Boosten, M., Delforterie, W., Nyssen, B., 2020. Revitalisering Nederlandse bossen.
UN, 2015. The Paris Agreement.
van Goor, C.P., 1993. De geschiedenis van het Nederlandse bos (I). Bos en Hout Ber. 27–30.
Vicente-Serrano, S.M., 2007. Evaluating the impact of drought using remote sensing in a Mediterranean, Semi-arid Region. Nat. Hazards 40, 173–208. https://doi.org/10.1007/s11069-006-0009-7
Vrieling, A., De Leeuw, J., Said, M.Y., 2013. Length of growing period over africa: Variability and trends from 30 years of NDVI time series. Remote Sens. 5, 982–1000. https://doi.org/10.3390/rs5020982
Xue, J., Su, B., 2017. Significant remote sensing vegetation indices: A review of developments and applications. J. Sensors 2017. https://doi.org/10.1155/2017/1353691
Yoshida, Y., Joiner, J., Tucker, C., Berry, J., Lee, J.E., Walker, G., Reichle, R., Koster, R., Lyapustin, A., Wang, Y., 2015. The 2010 Russian drought impact on satellite measurements of solar-induced chlorophyll fluorescence: Insights from modeling and comparisons with parameters derived from satellite reflectances. Remote Sens. Environ. 166, 163–177. https://doi.org/10.1016/j.rse.2015.06.008

APPENDIX A: VALIDATION DATA SPRUCE FORESTS

This is the method validation data as discussed in section 4.3 and 5.4, and 6.2.

Plot number	% of live trees	Sampling date	Aerial image date	Zone	Easting	Northing
1	Close to 0%	/	May-20	32U	325477.86 m E	5846107.97 m N
2	Close to 0%	/	May-20	32U	325294.05 m E	5845998.11 m N
3	Close to 0%	/	May-20	32U	324845.47 m E	5847352.04 m N
4	Close to 0%	/	April-20	31U	665565.63 m E	5689279.97 m N
5	Close to 0%	/	April-20	31U	652835.58 m E	5784082.61 m N
6	Close to 0%	/	March-20	31U	671253.39 m E	5765589.14 m N
7	Close to 0%	/	March-20	31U	671655.81 m E	5766089.61 m N
8	Close to 0%	/	April-20	31U	697074.16 m E	5784684.43 m N
9	Close to 0%	February-21	July-19	31U	702071.35 m E	5684278.69 m N
10	Close to 0%	/	July-19	31U	702574.20 m E	5684840.47 m N
50122	14.29%	July-20	April-20	31U	665585.69 m E	5689343.83 m N
90019	2.56%	September-19	July-19	31U	705324.39 m E	5685791.74 m N

Plot number	% of live trees	Sampling date	Aerial image date	Zone	Easting	Northing
34006	80.77%	September-19	April-19	31U	611881.01 m E	5822040.41 m N
43986	64.52%	May-18	August-18	31U	645732.70 m E	5727757.50 m N
45284	69.56%	October-17	May-16	31U	649345.82 m E	5726030.38 m N
45988	84.61%	October-19	August-19	31U	649964.65 m E	5779632.17 m N
46639	100.00%	October-18	August-18	31U	651933.48 m E	5781344.13 m N

APPENDIX B.1: CODES FOR DATA RETRIEVAL FROM GEE

This is the code used for the time series data retrieval from Google Earth Engine as discussed in section 4.4.

Sentinel-2

```
// cloud masking
function maskS2clouds(image) {
 var qa = image.select('QA60');

// Bits 10 and 11 are clouds and cirrus, respectively.
 var cloudBitMask = 1 << 10;
 var cirrusBitMask = 1 << 11;
// Both flags should be set to zero, indicating clear conditions.
 var mask = qa.bitwiseAnd(cloudBitMask).eq(0)
   .and(qa.bitwiseAnd(cirrusBitMask).eq(0));
 return image.updateMask(mask);
}

var addNDVI = function(image) {
 var ndvi = image.normalizedDifference(['B8', 'B4']).rename('NDVI');
 return image
   .addBands(ndvi);
}

var divideBands = function(image) {
 return image.select('B.*').multiply(0.0001);
}

//choose a location
//var point = ee.Geometry.Point([4.61395, 52.34041])// eerste coordinaat

//all 114 points
var points_list = [ee.Geometry.Point([4.61395, 52.34041]), ee.Geometry.Point([5.79381, 52.02879]), ee.Geometry.Point([5.79522, 52.02469]), ee.Geometry.Point([5.80385, 52.28531]),
ee.Geometry.Point([5.86515, 52.17844]), ee.Geometry.Point([4.69705, 52.44832]), ee.Geometry.Point([4.97238, 52.47084]), ee.Geometry.Point([5.94128, 51.27739]),
ee.Geometry.Point([5.95525, 51.21725]), ee.Geometry.Point([5.68496, 51.30292]), ee.Geometry.Point([4.737042446, 53.05529504]), ee.Geometry.Point([5.154530615, 52.36642171]),
ee.Geometry.Point([5.6700879, 52.66399851]), ee.Geometry.Point([4.91549998, 52.79416797]), ee.Geometry.Point([6.259848299, 53.36989025]), ee.Geometry.Point([5.299433382,
52.32367807]), ee.Geometry.Point([5.42455355, 52.46626589]), ee.Geometry.Point([5.450348756, 52.33571616]), ee.Geometry.Point([5.495178578, 52.32897934]),
ee.Geometry.Point([5.698668635, 51.49812562]), ee.Geometry.Point([5.76303179, 50.87566393]), ee.Geometry.Point([6.542762701, 52.45915659]), ee.Geometry.Point([6.745480845,
53.17364396]), ee.Geometry.Point([5.448647512, 51.3290279]), ee.Geometry.Point([6.918579397, 52.66469083]), ee.Geometry.Point([4.216886716, 52.05070844]),
ee.Geometry.Point([4.361276316, 51.5297889]), ee.Geometry.Point([4.412946197, 52.1348073]), ee.Geometry.Point([4.70014728, 51.58412239]), ee.Geometry.Point([4.694506692,
52.6640021]), ee.Geometry.Point([5.454212908, 51.50879859]), ee.Geometry.Point([6.631250351, 52.76037562]), ee.Geometry.Point([6.132657225, 53.06743373]),
ee.Geometry.Point([5.905884935, 51.4292485]), ee.Geometry.Point([6.437809291, 52.99488651]), ee.Geometry.Point([5.133665287, 51.42620712]), ee.Geometry.Point([5.6157736,
51.2647014]), ee.Geometry.Point([5.681225318, 51.7253989]), ee.Geometry.Point([5.709096659, 52.09333874]), ee.Geometry.Point([5.819877105, 52.07766102]),
ee.Geometry.Point([5.802210972, 52.57291835]), ee.Geometry.Point([5.816953031, 52.57199772]), ee.Geometry.Point([5.536710348, 52.00210801]), ee.Geometry.Point([5.433785778,
52.45374918]), ee.Geometry.Point([5.508482477, 52.50453629]), ee.Geometry.Point([6.984380211, 52.83576524]), ee.Geometry.Point([5.369185297, 51.37242086]),
ee.Geometry.Point([6.056184566, 52.03444665]), ee.Geometry.Point([6.985135429, 52.38389763]), ee.Geometry.Point([6.029138234, 51.30448293]), ee.Geometry.Point([6.746577818,
52.25726366]), ee.Geometry.Point([5.245860723, 51.31998121]), ee.Geometry.Point([6.376432209, 53.02975209]), ee.Geometry.Point([6.647585829, 52.90658495]),
ee.Geometry.Point([6.650505359, 52.69889091]), ee.Geometry.Point([6.395294968, 52.98362564]), ee.Geometry.Point([5.16570352, 52.19567584]), ee.Geometry.Point([5.809268991,
52.26731586]), ee.Geometry.Point([6.434070373, 52.32908373]), ee.Geometry.Point([5.753052948, 51.47037816]), ee.Geometry.Point([5.371237711, 52.03756679]),
ee.Geometry.Point([5.932603291, 51.80224011]), ee.Geometry.Point([5.791461099, 52.80172664]), ee.Geometry.Point([6.993332207, 52.37018761]), ee.Geometry.Point([5.307122981,
51.60462994]), ee.Geometry.Point([5.812224015, 52.78857197]), ee.Geometry.Point([6.20690623, 52.01102078]), ee.Geometry.Point([3.691235331, 51.54762769]),
ee.Geometry.Point([5.888137365, 50.78286992]), ee.Geometry.Point([6.131481468, 52.28972686]), ee.Geometry.Point([6.56181046, 52.7016163]), ee.Geometry.Point([6.499538255,
52.98389109]), ee.Geometry.Point([6.745822208, 52.82800388]), ee.Geometry.Point([6.01369286, 52.01908625]), ee.Geometry.Point([6.644289337, 52.77180685]),
ee.Geometry.Point([5.919596967, 51.54604126]), ee.Geometry.Point([6.811004218, 52.85580685]), ee.Geometry.Point([6.391312027, 53.02859293]), ee.Geometry.Point([6.640057178,
52.92463886]), ee.Geometry.Point([6.721034586, 51.91144791]), ee.Geometry.Point([6.237734571, 53.0746036]), ee.Geometry.Point([6.310165455, 52.34730628]),
ee.Geometry.Point([6.766088554, 52.12401273]), ee.Geometry.Point([6.69217566, 52.85434203]), ee.Geometry.Point([5.134956543, 52.24414954]), ee.Geometry.Point([5.662750923,
52.26363843]), ee.Geometry.Point([5.69934573, 51.30936005]), ee.Geometry.Point([5.840589976, 52.22213973]), ee.Geometry.Point([5.908845274, 51.20451303]),
ee.Geometry.Point([6.82581048, 52.85452575]), ee.Geometry.Point([5.093496081, 51.47291532]), ee.Geometry.Point([5.201125373, 52.17078186]), ee.Geometry.Point([5.867018284,
52.24135287]), ee.Geometry.Point([5.868024852, 51.98894012]), ee.Geometry.Point([5.983349028, 51.66104668]), ee.Geometry.Point([5.225217212, 51.90998405]),
ee.Geometry.Point([6.126791949, 52.14594583]), ee.Geometry.Point([5.619138251, 52.39722205]), ee.Geometry.Point([5.174570936, 51.63386239]), ee.Geometry.Point([4.768146098,
51.73977624]), ee.Geometry.Point([6.1429168, 51.50463655]), ee.Geometry.Point([5.700636695, 51.86665089]), ee.Geometry.Point([6.050355504, 51.5940373]),
ee.Geometry.Point([6.086253406, 52.5415025]), ee.Geometry.Point([3.494319186, 51.29505864]), ee.Geometry.Point([4.237345784, 51.40368671]), ee.Geometry.Point([4.319302794,
51.75771326]), ee.Geometry.Point([4.319839909, 51.76670724]), ee.Geometry.Point([4.541983923, 51.70369054]), ee.Geometry.Point([4.586374915, 51.8883334]),
ee.Geometry.Point([4.31529139, 51.92846794]), ee.Geometry.Point([4.409571895, 52.02605797]), ee.Geometry.Point([4.575468655, 51.65746262]), ee.Geometry.Point([5.465024707,
52.33797704]), ee.Geometry.Point([5.479707696, 52.34289176]), ee.Geometry.Point([5.703031571, 52.41491198]), ee.Geometry.Point([5.45116606, 52.32672808]),
ee.Geometry.Point([5.237136835, 52.39732056]), ee.Geometry.Point([5.399083704, 52.2664942]), ee.Geometry.Point([5.509861599, 52.33377268]), ee.Geometry.Point([4.82545796,
52.3045841]), ee.Geometry.Point([5.562658397, 52.43880746]), ee.Geometry.Point([4.691416941, 52.4289791]), ee.Geometry.Point([6.927675107, 52.7634446]),
ee.Geometry.Point([6.491483497, 52.93004372]), ee.Geometry.Point([5.811129259, 51.58332835]), ee.Geometry.Point([6.047360025, 52.04348483]), ee.Geometry.Point([6.849142525,
52.40225603]), ee.Geometry.Point([6.488579584, 52.52563056]), ee.Geometry.Point([6.359260403, 51.95135194]), ee.Geometry.Point([6.07198551, 52.0202823]),
ee.Geometry.Point([6.07643227, 52.03823312]), ee.Geometry.Point([6.901732875, 52.93980536]), ee.Geometry.Point([6.935525178, 52.23112457]), ee.Geometry.Point([5.803068675,
50.78335053]), ee.Geometry.Point([6.759332834, 53.03009475]), ee.Geometry.Point([5.979826639, 52.97878474]), ee.Geometry.Point([6.64440307, 53.21858129]),
ee.Geometry.Point([5.105704729, 52.23910433]), ee.Geometry.Point([5.571863069, 51.28547393]), ee.Geometry.Point([6.83391571, 52.29643675]), ee.Geometry.Point([6.383595204,
53.10158528]), ee.Geometry.Point([6.422768365, 52.98874324]), ee.Geometry.Point([6.041173324, 52.7155754]), ee.Geometry.Point([5.38854973, 51.37665132]),
ee.Geometry.Point([5.896298063, 52.24114129]), ee.Geometry.Point([6.032393454, 51.31345391]), ee.Geometry.Point([6.555606154, 52.55787144]), ee.Geometry.Point([6.717524901,
52.88991353]), ee.Geometry.Point([6.778875114, 52.81315101]), ee.Geometry.Point([6.374023147, 52.53547167]), ee.Geometry.Point([5.257716916, 51.40988221]),
ee.Geometry.Point([5.587773212, 51.31655086]), ee.Geometry.Point([5.893093325, 52.1512749]), ee.Geometry.Point([5.292376079, 51.43987274]), ee.Geometry.Point([6.236992038,
53.06235869]), ee.Geometry.Point([6.790236604, 52.82483282]), ee.Geometry.Point([5.637982128, 51.58170158]), ee.Geometry.Point([6.469615266, 52.54524749]),
ee.Geometry.Point([5.603947283, 51.43551024]), ee.Geometry.Point([5.262374953, 51.48548119]), ee.Geometry.Point([6.42070798, 52.17715039]), ee.Geometry.Point([5.951596075,
50.76781982]), ee.Geometry.Point([6.107399644, 52.16885419]), ee.Geometry.Point([6.712433185, 52.8809824]), ee.Geometry.Point([6.732270214, 52.88620338]),
ee.Geometry.Point([5.776689651, 52.80808597]), ee.Geometry.Point([6.714452131, 52.92589734]), ee.Geometry.Point([6.601615729, 52.99352698]), ee.Geometry.Point([6.12414631,
53.05850012]), ee.Geometry.Point([6.744385802, 53.19162991]), ee.Geometry.Point([7.072907343, 53.06181025]), ee.Geometry.Point([6.522903287, 52.59728674]),
ee.Geometry.Point([6.271043491, 53.09054519]), ee.Geometry.Point([6.714721561, 53.03374171]), ee.Geometry.Point([6.704194827, 52.94886113]), ee.Geometry.Point([6.705291477,
52.89492454]), ee.Geometry.Point([5.767433095, 51.46891313]), ee.Geometry.Point([5.747450216, 52.20858188]), ee.Geometry.Point([5.959702437, 52.43681446]),
```

```
ee.Geometry.Point([5.823076287, 52.23943384]), ee.Geometry.Point([5.873519051, 52.16868112]), ee.Geometry.Point([5.980327707, 52.0767471]), ee.Geometry.Point([5.83075751,
52.25812873]), ee.Geometry.Point([6.207821202, 53.07090047]), ee.Geometry.Point([5.416952476, 51.72026498]), ee.Geometry.Point([7.095852322, 52.96112958]),
ee.Geometry.Point([6.229395885, 51.92424043]), ee.Geometry.Point([5.761059259, 51.55125121]), ee.Geometry.Point([6.980443429, 52.29406945]), ee.Geometry.Point([5.141931194,
51.6319177]), ee.Geometry.Point([5.083969937, 51.64367536]), ee.Geometry.Point([5.827789041, 51.97950894]), ee.Geometry.Point([6.748988144, 52.95379364]),
ee.Geometry.Point([6.745909513, 52.84597826]), ee.Geometry.Point([6.393930024, 52.96566347]), ee.Geometry.Point([6.721857573, 52.85391462]), ee.Geometry.Point([6.567799762,
52.69256927])]

var i;
for (i=0; i<points_list.length; i++) {
 var curr_point = points_list[i]
 var dataset = ee.ImageCollection('COPERNICUS/S2_SR')
              .filterDate('2017-01-01', '2020-11-01')
              .filterBounds(curr_point) // don't forget the other lines with cloud mask
               // Pre-filter to get less cloudy granules.
              .filter(ee.Filter.lt('CLOUDY_PIXEL_PERCENTAGE',20))
              .map(maskS2clouds)
              .map(divideBands)
              .map(addNDVI)
              .map(
               function(image){
                return image.reduceRegions(curr_point, 'first'); // selecting pixel per point (lon, lat)
               })
              .flatten()
              .filterMetadata('B1', 'not_equals', null) // removing masked (clouded) pixels

 //Export the time series to drive
 Export.table.toDrive({
   collection: dataset, // feature collection that we got
//   description: (i+85).toString(), // filename that will be used: point_ts.csv
//   folder: 'RTM_course_114_NDVI_points', // folder in your google drive that will be created
   description: (i+12).toString(), // filename that will be used: point_ts.csv
   folder: '12_Spruce_points', // folder in your google drive that will be created
   fileFormat: 'CSV'
 });
}
```

Landsat 8

```
// cloud filter:
function maskL8sr(image) {
 // Bits 3 and 5 are cloud shadow and cloud, respectively.
 var cloudShadowBitMask = (1 << 3);
 var cloudsBitMask = (1 << 5);
 // Get the pixel QA band.
 var qa = image.select('pixel_qa');
 // Both flags should be set to zero, indicating clear conditions.
 var mask = qa.bitwiseAnd(cloudShadowBitMask).eq(0)
         .and(qa.bitwiseAnd(cloudsBitMask).eq(0));
 return image.updateMask(mask);
}

var addNDVI = function(image) {
 var ndvi = image.normalizedDifference(['B5', 'B4']).rename('NDVI');
 return image
   .addBands(ndvi);
}

var divideBands = function(image) {
 return image.select('B.*').multiply(0.0001);
}

//choose a location(s)
//var point = ee.Geometry.Point([4.61395, 52.34041])// eerste coordinaat

//all 114 points
var points_list = [ee.Geometry.Point([4.61395, 52.34041]), ee.Geometry.Point([5.79381, 52.02879]), ee.Geometry.Point([5.79522, 52.02469]), ee.Geometry.Point([5.80385, 52.28531]),
ee.Geometry.Point([5.86515, 52.17844]), ee.Geometry.Point([4.69705, 52.44832]), ee.Geometry.Point([4.97238, 52.47084]), ee.Geometry.Point([5.94128, 51.27739]),
ee.Geometry.Point([5.95525, 51.21725]), ee.Geometry.Point([5.68496, 51.30292]), ee.Geometry.Point([4.737042446, 53.05529504]), ee.Geometry.Point([5.154530615, 52.36642171]),
ee.Geometry.Point([5.6700879, 52.66399851]), ee.Geometry.Point([4.91549998, 52.79416797]), ee.Geometry.Point([6.259848299, 53.36989025]), ee.Geometry.Point([5.299433382,
52.32367807]), ee.Geometry.Point([5.42455355, 52.46626589]), ee.Geometry.Point([5.450348756, 52.33571616]), ee.Geometry.Point([5.495178578, 52.32897934]),
ee.Geometry.Point([5.698668635, 51.49812562]), ee.Geometry.Point([5.76303179, 50.87566393]), ee.Geometry.Point([6.542762701, 52.45915659]), ee.Geometry.Point([6.745480845,
53.17364396]), ee.Geometry.Point([5.448647512, 51.3290279]), ee.Geometry.Point([6.918579397, 52.66469083]), ee.Geometry.Point([4.216886716, 52.05070844]),
ee.Geometry.Point([4.361276316, 51.5297889]), ee.Geometry.Point([4.412946197, 52.1348073]), ee.Geometry.Point([4.70014728, 51.58412239]), ee.Geometry.Point([4.694506692,
52.6640021]), ee.Geometry.Point([5.454212908, 51.50879859]), ee.Geometry.Point([6.631250351, 52.76037562]), ee.Geometry.Point([6.132657225, 53.06743373]),
ee.Geometry.Point([5.905884935, 51.4292485]), ee.Geometry.Point([6.437809291, 52.99488651]), ee.Geometry.Point([5.133665287, 51.42620712]), ee.Geometry.Point([5.6157736,
51.2647014]), ee.Geometry.Point([5.681225318, 51.7253989]), ee.Geometry.Point([5.709096659, 52.09333874]), ee.Geometry.Point([5.819877105, 52.07766102]),
ee.Geometry.Point([5.802210972, 52.57291835]), ee.Geometry.Point([5.816953031, 52.57199772]), ee.Geometry.Point([5.536710348, 52.00210801]), ee.Geometry.Point([5.433785778,
52.45374918]), ee.Geometry.Point([5.508482477, 52.50453629]), ee.Geometry.Point([6.984380211, 52.83576524]), ee.Geometry.Point([5.369185297, 51.37242086]),
ee.Geometry.Point([6.056184566, 52.03444665]), ee.Geometry.Point([6.985135429, 52.38389763]), ee.Geometry.Point([6.029138234, 51.30448293]), ee.Geometry.Point([6.746577818,
52.25726366]), ee.Geometry.Point([5.245860723, 51.31998121]), ee.Geometry.Point([6.376432209, 53.02975209]), ee.Geometry.Point([6.647585829, 52.90658495]),
ee.Geometry.Point([6.650505359, 52.69889091]), ee.Geometry.Point([6.395294968, 52.98362564]), ee.Geometry.Point([5.16570352, 52.19567584]), ee.Geometry.Point([5.809268991,
52.26731586]), ee.Geometry.Point([6.434070373, 52.32908373]), ee.Geometry.Point([5.753052948, 51.47037816]), ee.Geometry.Point([5.371237711, 52.03756679]),
ee.Geometry.Point([5.932603291, 51.80224011]), ee.Geometry.Point([5.791461099, 52.80172664]), ee.Geometry.Point([6.993332207, 52.37018761]), ee.Geometry.Point([5.307122981,
51.60462994]), ee.Geometry.Point([5.812224015, 52.78857197]), ee.Geometry.Point([6.20690623, 52.01102078]), ee.Geometry.Point([3.691235331, 51.54762769]),
```

```
ee.Geometry.Point([5.888137365, 50.78286992]), ee.Geometry.Point([6.131481468, 52.28972686]), ee.Geometry.Point([6.56181046, 52.7016163]), ee.Geometry.Point([6.499538255,
52.98389109]), ee.Geometry.Point([6.745822208, 52.82800388]), ee.Geometry.Point([6.01369286, 52.01908625]), ee.Geometry.Point([6.644289337, 52.77180685]),
ee.Geometry.Point([5.919596967, 51.54604126]), ee.Geometry.Point([6.811004218, 52.85580685]), ee.Geometry.Point([6.391312027, 53.02859293]), ee.Geometry.Point([6.640057178,
52.92463886]), ee.Geometry.Point([6.721034586, 51.91144791]), ee.Geometry.Point([6.237734571, 53.0746036]), ee.Geometry.Point([6.310165455, 52.34730628]),
ee.Geometry.Point([6.766088554, 52.12401273]), ee.Geometry.Point([6.69217566, 52.85434203]), ee.Geometry.Point([5.134956543, 52.24414954]), ee.Geometry.Point([5.662750923,
52.26363843]), ee.Geometry.Point([5.69934573, 51.30936005]), ee.Geometry.Point([5.840589976, 52.22213973]), ee.Geometry.Point([5.908845274, 51.20451303]),
ee.Geometry.Point([6.82581048, 52.85452575]), ee.Geometry.Point([5.093496081, 51.47291532]), ee.Geometry.Point([5.201125373, 52.17078186]), ee.Geometry.Point([5.867018284,
52.24135287]), ee.Geometry.Point([5.868024852, 51.98894012]), ee.Geometry.Point([5.983349028, 51.66104668]), ee.Geometry.Point([5.225217212, 51.90998405]),
ee.Geometry.Point([6.126791949, 52.14594583]), ee.Geometry.Point([5.619138251, 52.39722205]), ee.Geometry.Point([5.174570936, 51.63386239]), ee.Geometry.Point([4.768146098,
51.73977624]), ee.Geometry.Point([6.1429168, 51.50463655]), ee.Geometry.Point([5.700636695, 51.86665089]), ee.Geometry.Point([6.050355504, 51.5940373]),
ee.Geometry.Point([6.086253406, 52.5415025]), ee.Geometry.Point([3.494319186, 51.29505864]), ee.Geometry.Point([4.237345784, 51.40368671]), ee.Geometry.Point([4.319302794,
51.75771326]), ee.Geometry.Point([4.319839909, 51.76670724]), ee.Geometry.Point([4.541983923, 51.70369054]), ee.Geometry.Point([4.586374915, 51.8883334]),
ee.Geometry.Point([4.31529139, 51.92846794]), ee.Geometry.Point([4.409571895, 52.02605797]), ee.Geometry.Point([4.575468655, 51.65746262]), ee.Geometry.Point([5.465024707,
52.33797704]), ee.Geometry.Point([5.479707696, 52.34289176]), ee.Geometry.Point([5.703031571, 52.41491198]), ee.Geometry.Point([5.45116606, 52.32672808]),
ee.Geometry.Point([5.237136835, 52.39732056]), ee.Geometry.Point([5.399083704, 52.2664942]), ee.Geometry.Point([5.509861599, 52.33377268]), ee.Geometry.Point([4.82545796,
52.3045841]), ee.Geometry.Point([5.562658397, 52.43880746]), ee.Geometry.Point([4.691416941, 52.4289791]), ee.Geometry.Point([6.927675107, 52.7634446]),
ee.Geometry.Point([6.491483497, 52.93004372]), ee.Geometry.Point([5.811129259, 51.58332835]), ee.Geometry.Point([6.047360025, 52.04348483]), ee.Geometry.Point([6.849142525,
52.40225603]), ee.Geometry.Point([6.488579584, 52.52563056]), ee.Geometry.Point([6.359260403, 51.95135194]), ee.Geometry.Point([6.07198551, 52.0202823]),
ee.Geometry.Point([6.07643227, 52.03823312]), ee.Geometry.Point([6.901732875, 52.93980536]), ee.Geometry.Point([6.935525178, 52.23112457]), ee.Geometry.Point([5.803068675,
50.78335053]), ee.Geometry.Point([6.759332834, 53.03009475]), ee.Geometry.Point([5.979826639, 52.97878474]), ee.Geometry.Point([6.64440307, 53.21858129]),
ee.Geometry.Point([5.105704729, 52.23910433]), ee.Geometry.Point([5.571863069, 51.28547393]), ee.Geometry.Point([6.83391571, 52.29643675]), ee.Geometry.Point([6.383595204,
53.10158528]), ee.Geometry.Point([6.422768365, 52.98874324]), ee.Geometry.Point([6.041173324, 52.7155754]), ee.Geometry.Point([5.38854973, 51.37665132]),
ee.Geometry.Point([5.896298063, 52.24114129]), ee.Geometry.Point([6.032393454, 51.31345391]), ee.Geometry.Point([6.555606154, 52.55787144]), ee.Geometry.Point([6.717524901,
52.88991353]), ee.Geometry.Point([6.778875114, 52.81315101]), ee.Geometry.Point([6.374023147, 52.53547167]), ee.Geometry.Point([5.257716916, 51.40988221]),
ee.Geometry.Point([5.587773212, 51.31655086]), ee.Geometry.Point([5.893093325, 52.1512749]), ee.Geometry.Point([5.292376079, 51.43987274]), ee.Geometry.Point([6.236992038,
53.06235869]), ee.Geometry.Point([6.790236604, 52.82483282]), ee.Geometry.Point([5.637982128, 51.58170158]), ee.Geometry.Point([6.469615266, 52.54524749]),
ee.Geometry.Point([5.603947283, 51.43551024]), ee.Geometry.Point([5.262374953, 51.48548119]), ee.Geometry.Point([6.42070798, 52.17715039]), ee.Geometry.Point([5.951596075,
50.76781982]), ee.Geometry.Point([6.107399644, 52.16885419]), ee.Geometry.Point([6.712433185, 52.8809824]), ee.Geometry.Point([6.732270214, 52.88620338]),
ee.Geometry.Point([5.776689651, 52.80808597]), ee.Geometry.Point([6.714452131, 52.92589734]), ee.Geometry.Point([6.601615729, 52.99352698]), ee.Geometry.Point([6.12414631,
53.05850012]), ee.Geometry.Point([6.744385802, 53.19162991]), ee.Geometry.Point([7.072907343, 53.06181025]), ee.Geometry.Point([6.522903287, 52.59728674]),
ee.Geometry.Point([6.271043491, 53.09054519]), ee.Geometry.Point([6.714721561, 53.03374171]), ee.Geometry.Point([6.704194827, 52.94886113]), ee.Geometry.Point([6.705291477,
52.89492454]), ee.Geometry.Point([5.767433095, 51.46891313]), ee.Geometry.Point([5.747450216, 52.20858188]), ee.Geometry.Point([5.959702437, 52.43681446]),
ee.Geometry.Point([5.823076287, 52.23943384]), ee.Geometry.Point([5.873519051, 52.16868112]), ee.Geometry.Point([5.980327707, 52.0767471]), ee.Geometry.Point([5.83075751,
52.25812873]), ee.Geometry.Point([6.207821202, 53.07090047]), ee.Geometry.Point([5.416952476, 51.72026498]), ee.Geometry.Point([7.095852322, 52.96112958]),
ee.Geometry.Point([6.229395885, 51.92424043]), ee.Geometry.Point([5.761059259, 51.55125121]), ee.Geometry.Point([6.980443429, 52.29406945]), ee.Geometry.Point([5.141931194,
51.6319177]), ee.Geometry.Point([5.083969937, 51.64367536]), ee.Geometry.Point([5.827789041, 51.97950894]), ee.Geometry.Point([6.748988144, 52.95379364]),
ee.Geometry.Point([6.745909513, 52.84597826]), ee.Geometry.Point([6.393930024, 52.96566347]), ee.Geometry.Point([6.721857573, 52.85391462]), ee.Geometry.Point([6.567799762,
52.69256927])]

var i;
for (i=0; i<points_list.length; i++) {
 var curr_point = points_list[i]
 var dataset = ee.ImageCollection('LANDSAT/LC08/C01/T1_SR')
 //              .select(['B1', 'B2', 'B3', 'B4', 'B5', 'B6', 'B7', 'B10', 'B11'])
              .filterDate('2011-01-01', '2020-11-01')
              .filterBounds(curr_point) // don't forget the other lines with cloud mask
               // Pre-filter to get less cloudy granules.
              .filter(ee.Filter.lt('CLOUD_COVER',20))
              .map(maskL8sr)
              .map(divideBands)
              .map(addNDVI)
              .map(
               function(image){
                return image.reduceRegions(curr_point, 'first'); // selecting pixel per point (lon, lat)
               })
              .flatten()
              .filterMetadata('B1', 'not_equals', null) // removing masked (clouded) pixels

 //Export the time series to drive
 Export.table.toDrive({
   collection: dataset, // feature collection that we got
   description: (i+85).toString(), // filename that will be used: point_ts.csv
   folder: 'RTM_course_114_NDVI_points_LS8', // folder in your google drive that will be created
   fileFormat: 'CSV'
 });

}
```

APPENDIX B.2: CODES FOR VALIDATION DATA RETRIEVAL FROM GEE

This is the code used for the validation time series data retrieval from Google Earth Engine as discussed in section 4.3. The code is to retrieve Sentinel-2 time series data.

The method validation GEE was exactly the same as the data retrieval code, except the code line of “var points_list = …” was replaced by the following:

```
//dead spruce points
//var points_list = [ee.Geometry.Point([6.41494, 52.73663]), ee.Geometry.Point([6.41228, 52.73559]), ee.Geometry.Point([6.40492, 52.74760]), ee.Geometry.Point([5.37659, 51.33068]),
ee.Geometry.Point([5.23570, 52.18600]), ee.Geometry.Point([5.49556, 52.01448]), ee.Geometry.Point([5.50167, 52.01885]), ee.Geometry.Point([5.88239, 52.17738]),
ee.Geometry.Point([5.89712, 51.27397]), ee.Geometry.Point([5.90463, 51.27883]), ee.Geometry.Point([5.37690, 51.33124]), ee.Geometry.Point([5.94456, 51.28639])]

//healthy spruce points
var points_list = [ee.Geometry.Point([4.64959, 52.53695]), ee.Geometry.Point([5.10802, 51.68185]), ee.Geometry.Point([5.15950, 51.66538]), ee.Geometry.Point([5.19177, 52.14681]),
ee.Geometry.Point([5.22129, 52.16165])]
```

APPENDIX B.3: CODES FOR SPI CALCULATION IN R

This is the code used to retrieve the SPI values from R. This is discussed in section 5.3.1.

```
install.packages(SPEI)

setwd("C:\\Users\\Elsa\\Documents\\1-- ITC - SE\\SPI")
df<-read.csv("KNMI_rain.csv",header=TRUE, sep=",")
spi1<-spi(df$prcp,1)
spi2<-spi(df$prcp,2)
spi3<-spi(df$prcp,3)
spi6<-spi(df$prcp,6)

spi3

plot.spei(spi3)
```

APPENDIX C.1: CORRELATION GRAPHS OF SENTINEL-2

These are the linear regression graphs from the Sentinel-2 dataset as discussed in section 6.1.

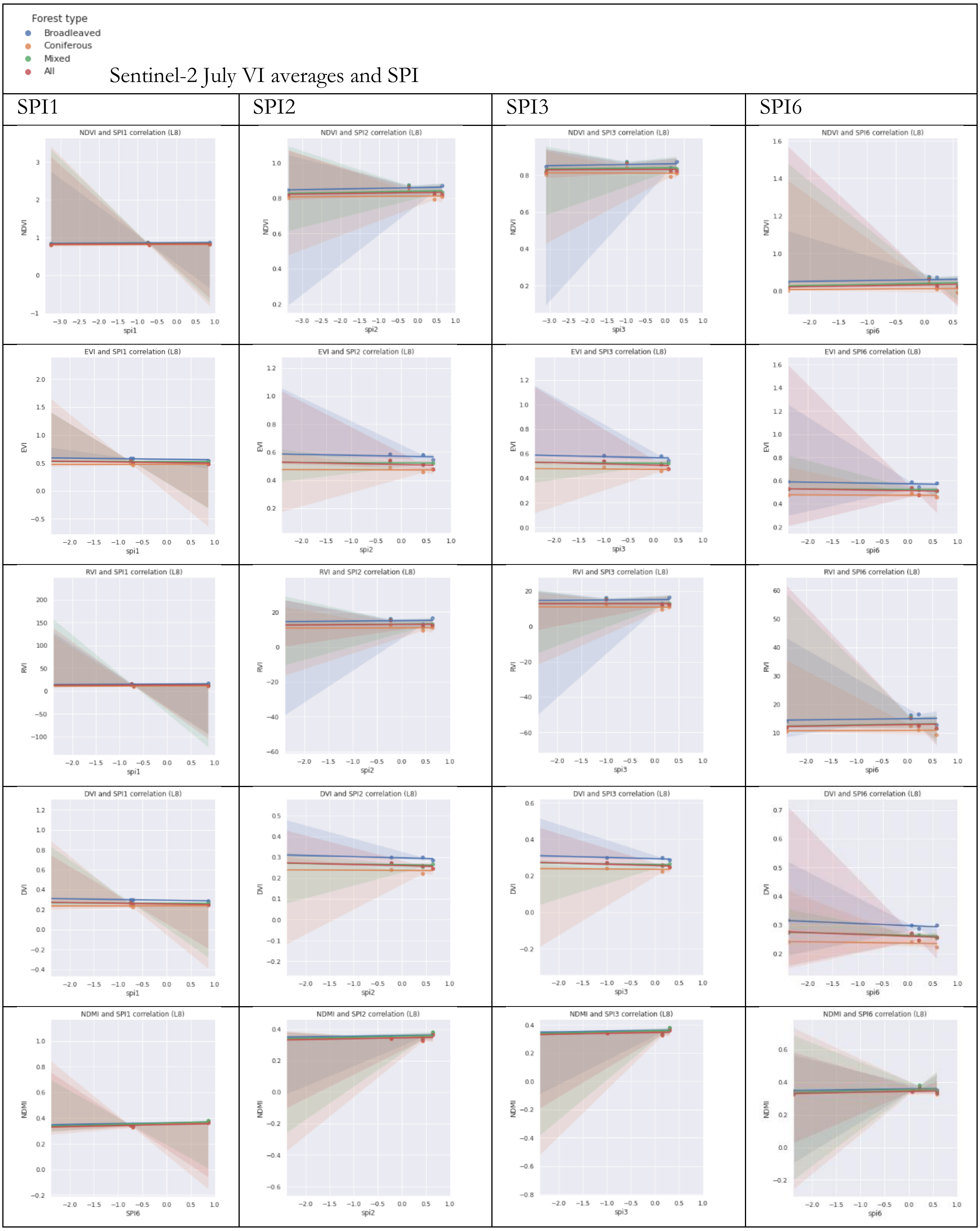

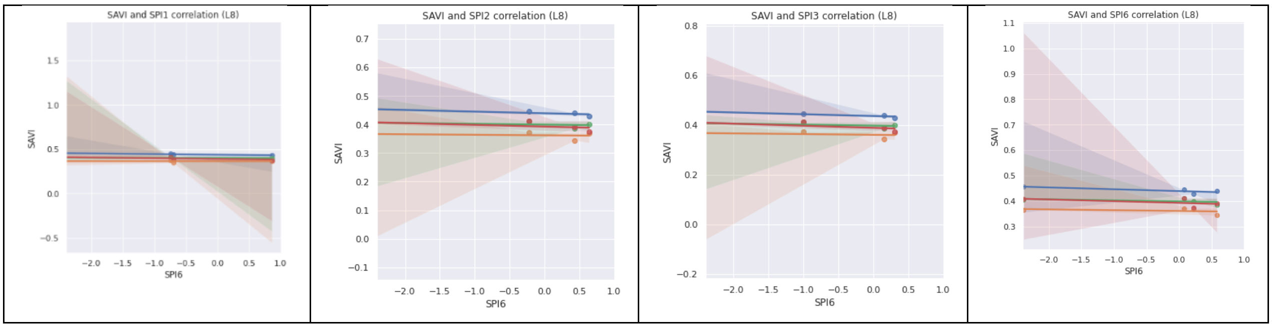
SAVI and SPI1 correlation (L8)
SAVI
SPI6
SAVI and SPI2 correlation (L8)
SAVI
SPI6
SAVI and SPI3 correlation (L8)
SAVI
SPI6
SAVI and SPI6 correlation (L8)
SAVI
SPI6

APPENDIX C.2: CORRELATION GRAPHS OF LANDSAT 8 (AND R2 TABLE)

These are the linear regression graphs from the Landsat 8 dataset and the determination coefficients (R2) as discussed in section 6.1.

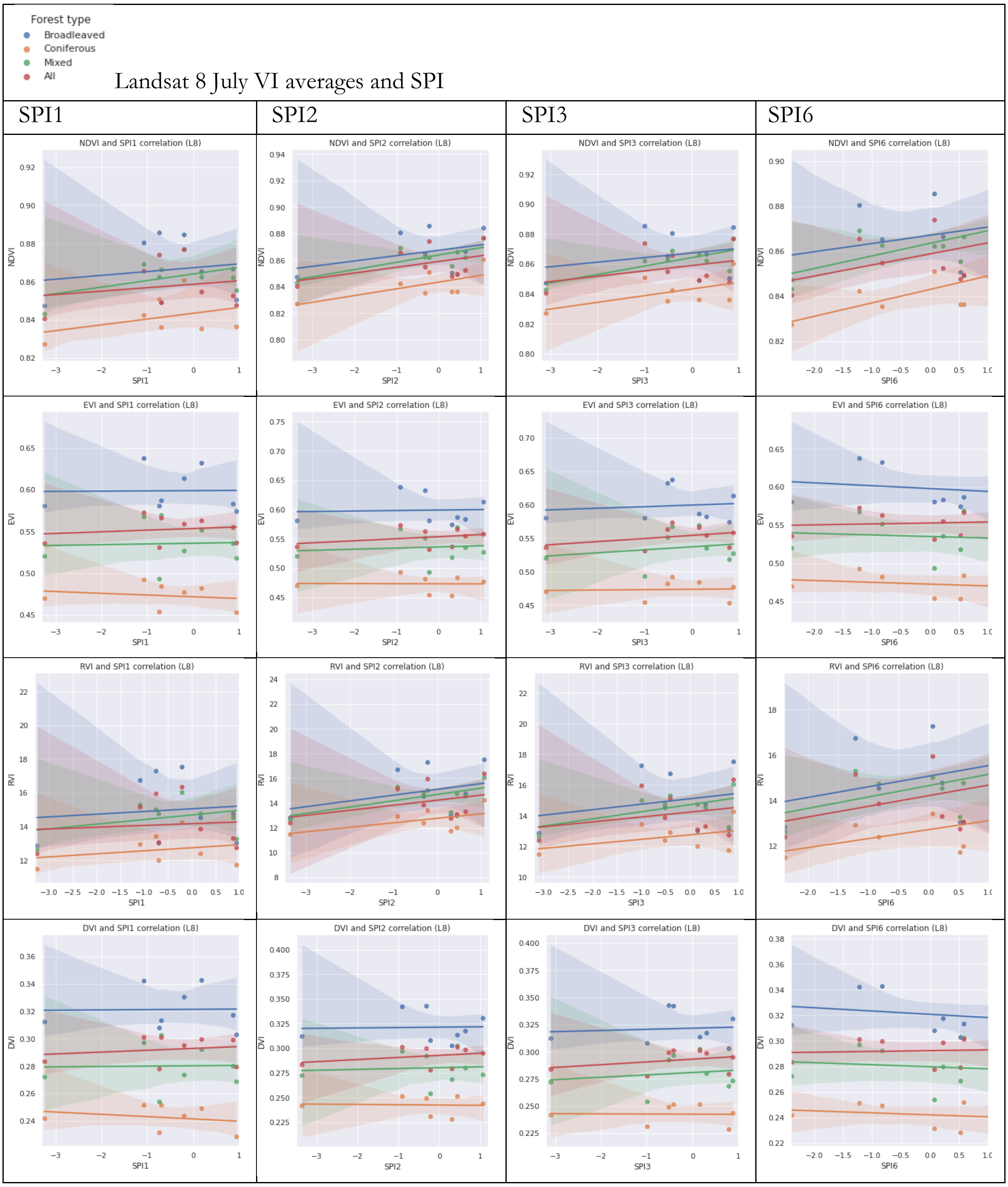

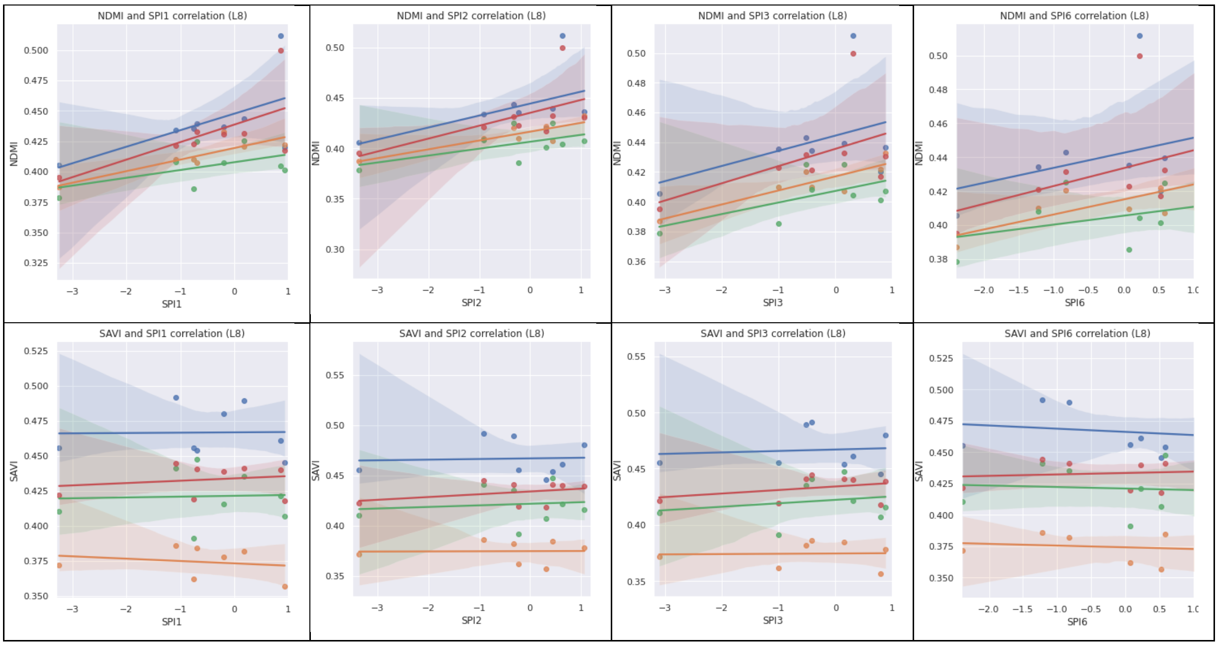

The R2 of the linear regression (Landsat 8)

Broadleaved	NDVI	EVI	RVI	DVI	NDMI	SAVI
spi1	0.027615	0.000247	0.011744	0.000335	0.33789	0.000297
spi2	0.120017	0.001863	0.107399	0.001179	0.276107	0.002407
spi3	0.059602	0.014323	0.054068	0.007891	0.176214	0.00859
spi6	0.073761	0.030929	0.079655	0.039632	0.115091	0.029105

Coniferous	NDVI	EVI	RVI	DVI	NDMI	SAVI
spi1	0.00564	0.006762	0.010652	0.007837	0.577028	0.013267
spi2	0.166753	0.017545	0.043368	0.017768	0.443526	0.032669
spi3	0.124989	0.02407	0.026479	0.012612	0.390843	0.023737
spi6	0.261503	0.007732	0.081883	0.005399	0.274046	0.000838

Mixed	NDVI	EVI	RVI	DVI	NDMI	SAVI
spi1	0.267763	0.005034	0.111923	0.002711	0.320521	0.004331
spi2	0.532417	0.03576	0.317776	0.030227	0.407377	0.038991
spi3	0.445968	0.099245	0.179055	0.07831	0.429615	0.08714
spi6	0.269584	0.000599	0.119965	0.001003	0.175512	0.000139

All	NDVI	EVI	RVI	DVI	NDMI	SAVI
spi1	0.034067	0.02726	0.008423	0.03142	0.406201	0.038893
spi2	0.209605	0.093962	0.139458	0.085573	0.343773	0.116745
spi3	0.123305	0.142159	0.073525	0.103116	0.242722	0.128905
spi6	0.202313	0.008932	0.136131	0.005319	0.173946	0.014558

APPENDIX D.1: ADDITIONAL VISUALIZATIONS OF SENTINEL-2

This is an overview of exploratory visualisations as discussed in section 6.3.

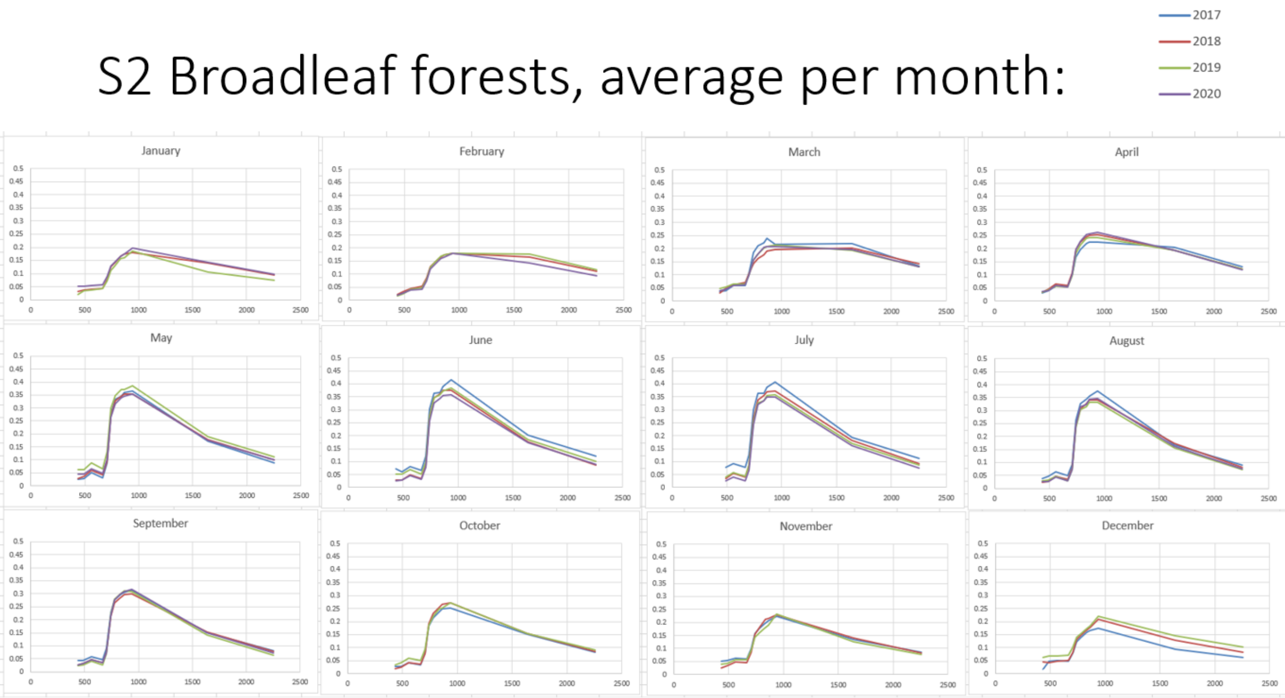

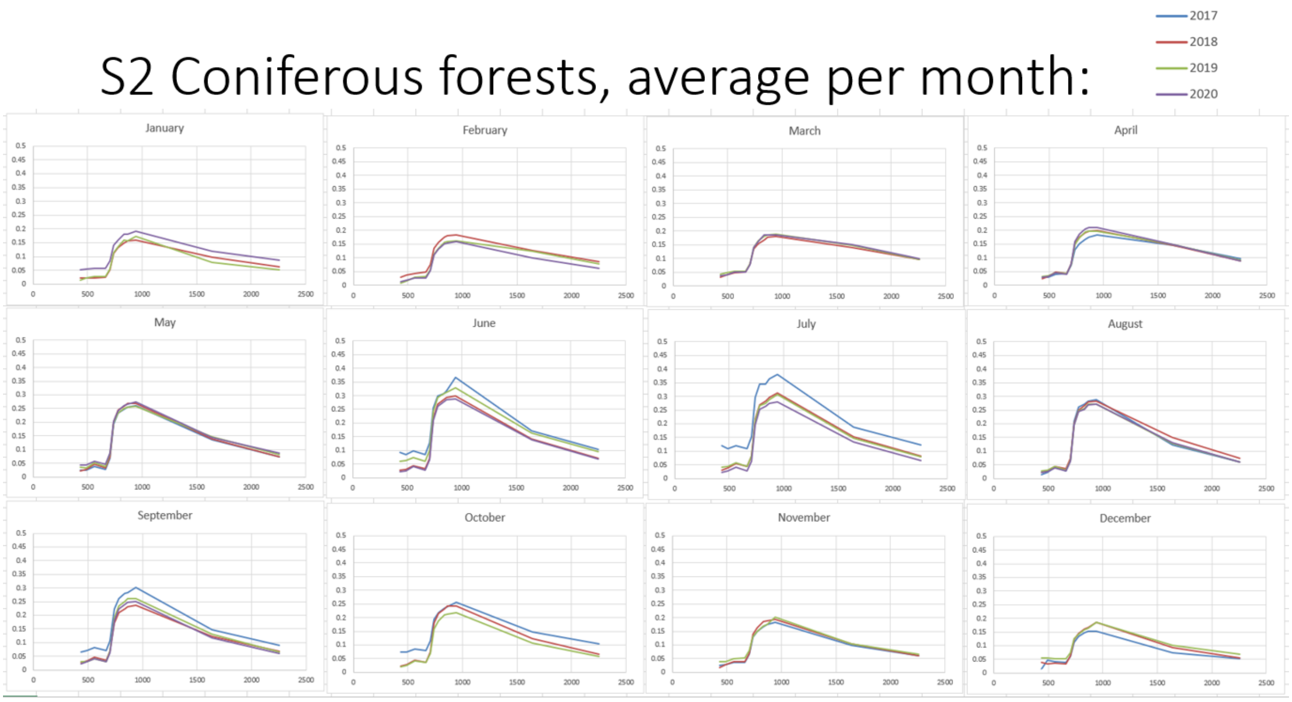

Trend over time per band, broadleaved forests:

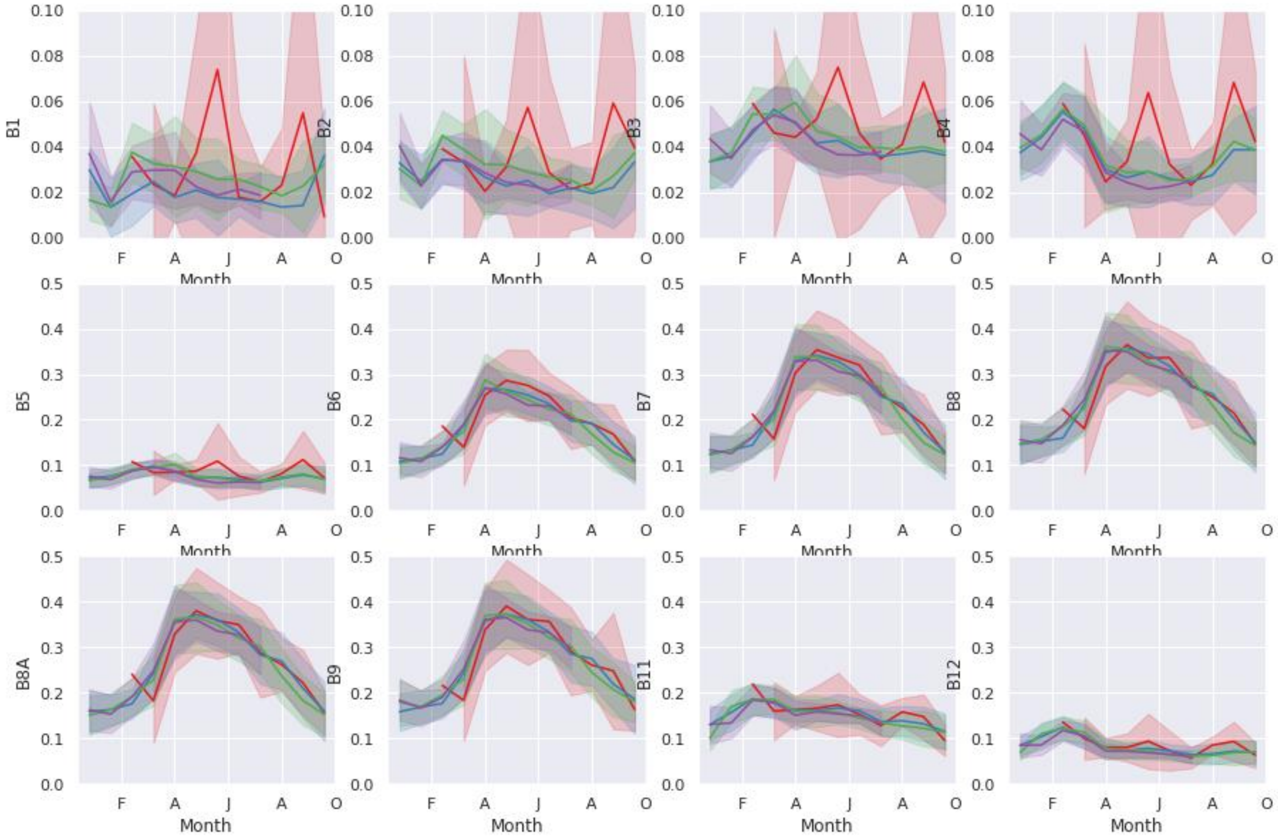

Trend over time per band, coniferous forests:

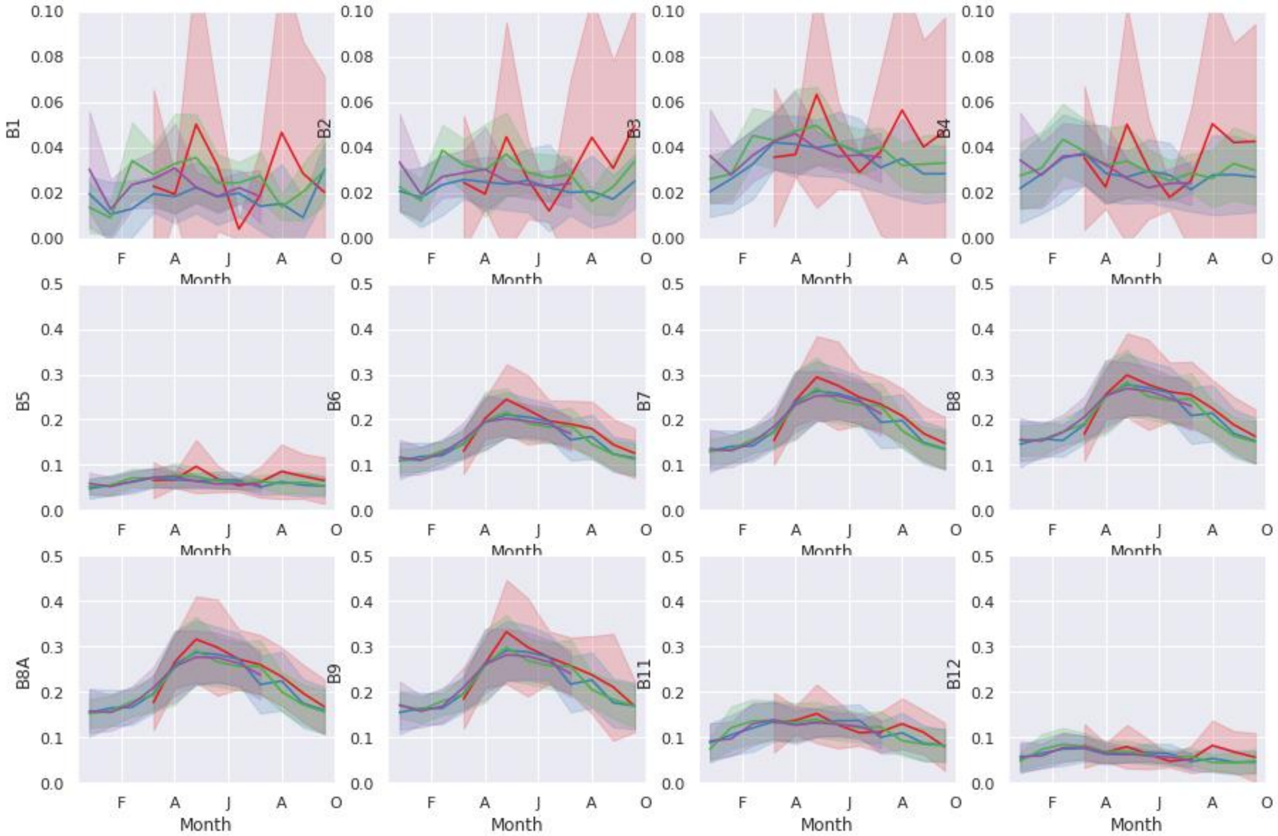

Trend over time per band, mixed forests:

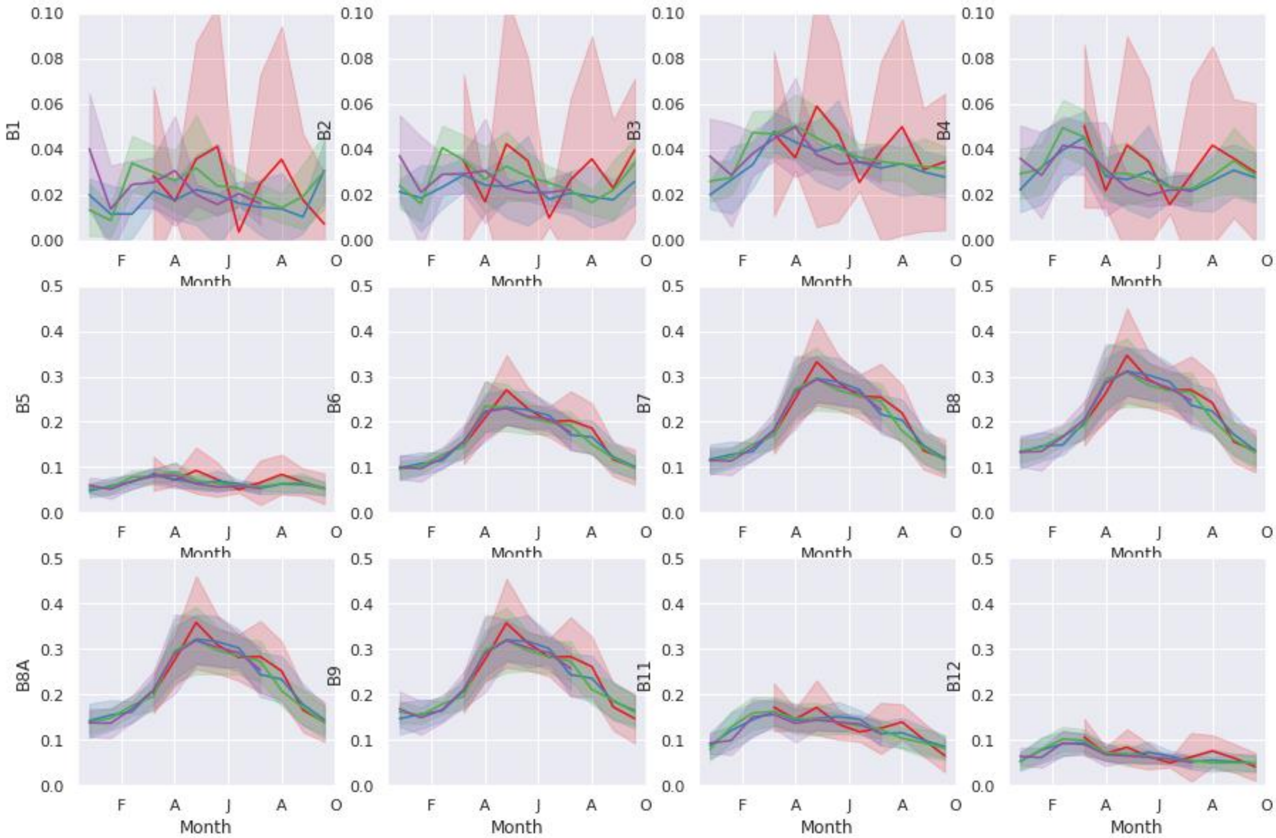

NDVI over time, per month per forest type:

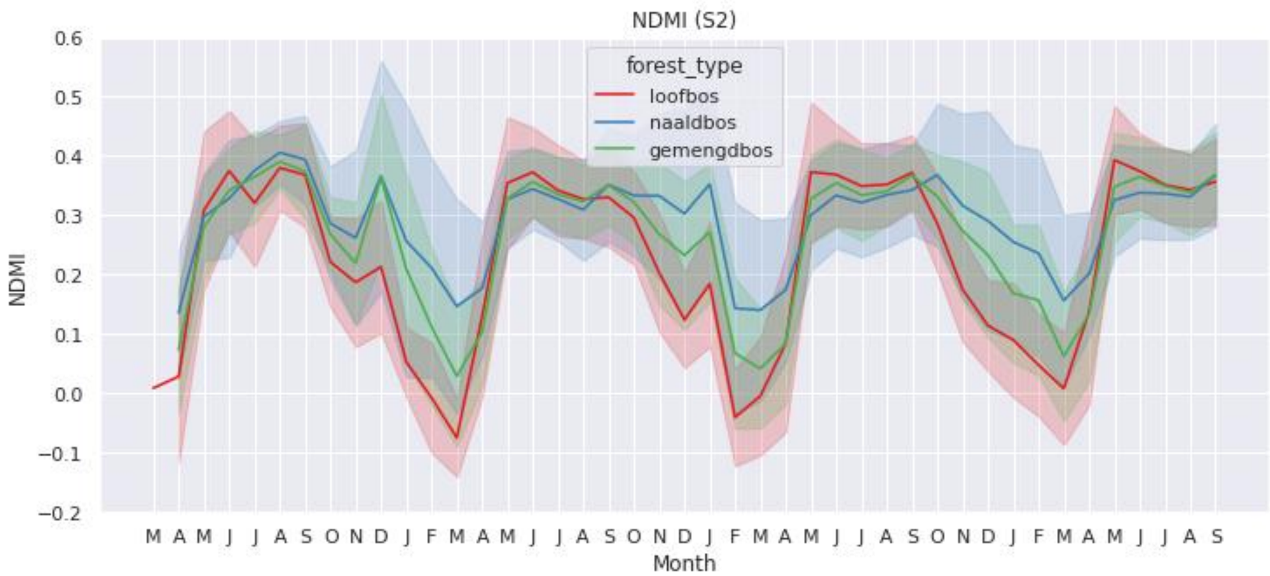

APPENDIX D.2: ADDITIONAL VISUALIZATIONS OF LANDSAT 8

This is an overview of exploratory visualisations as discussed in section 6.3.

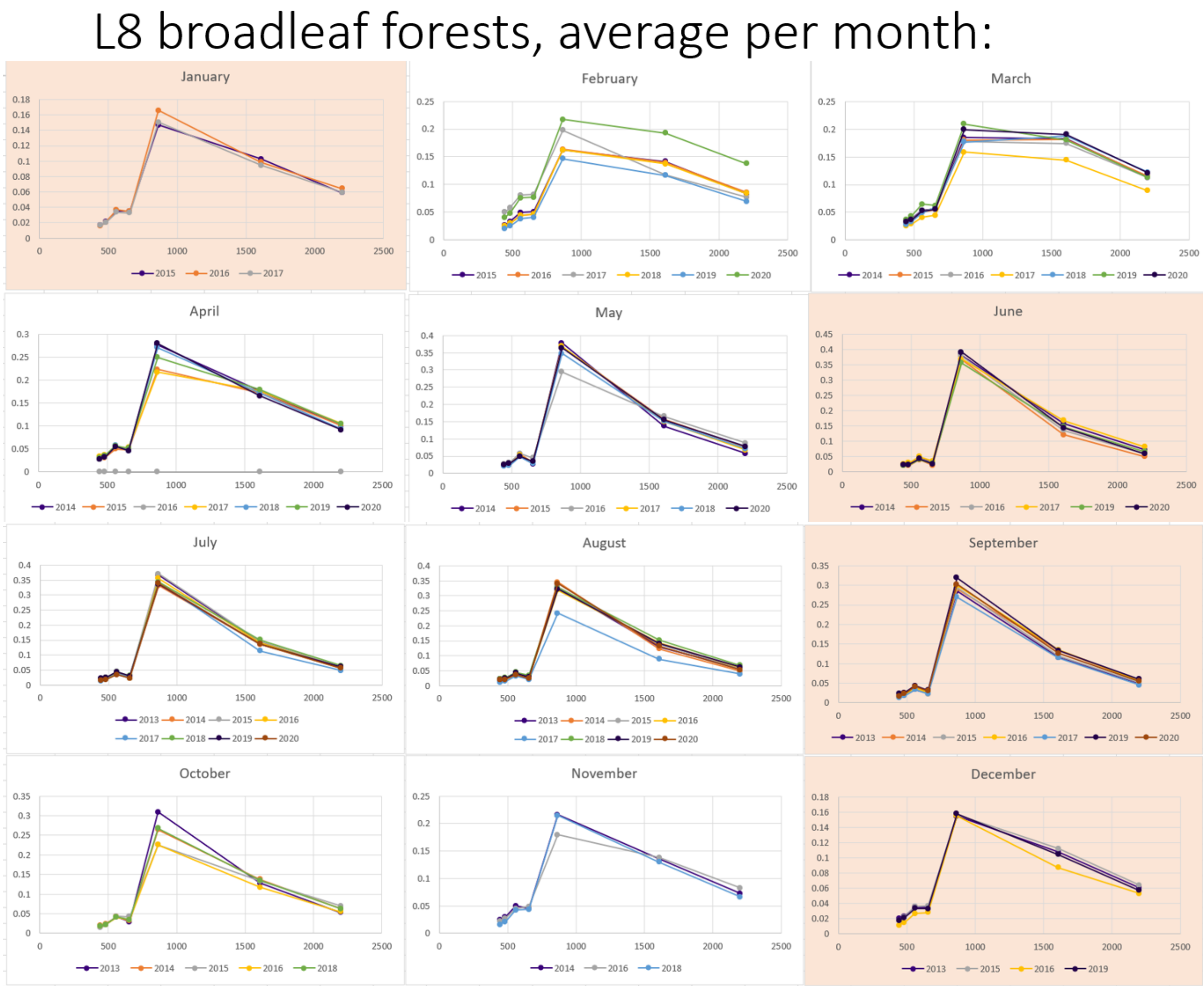

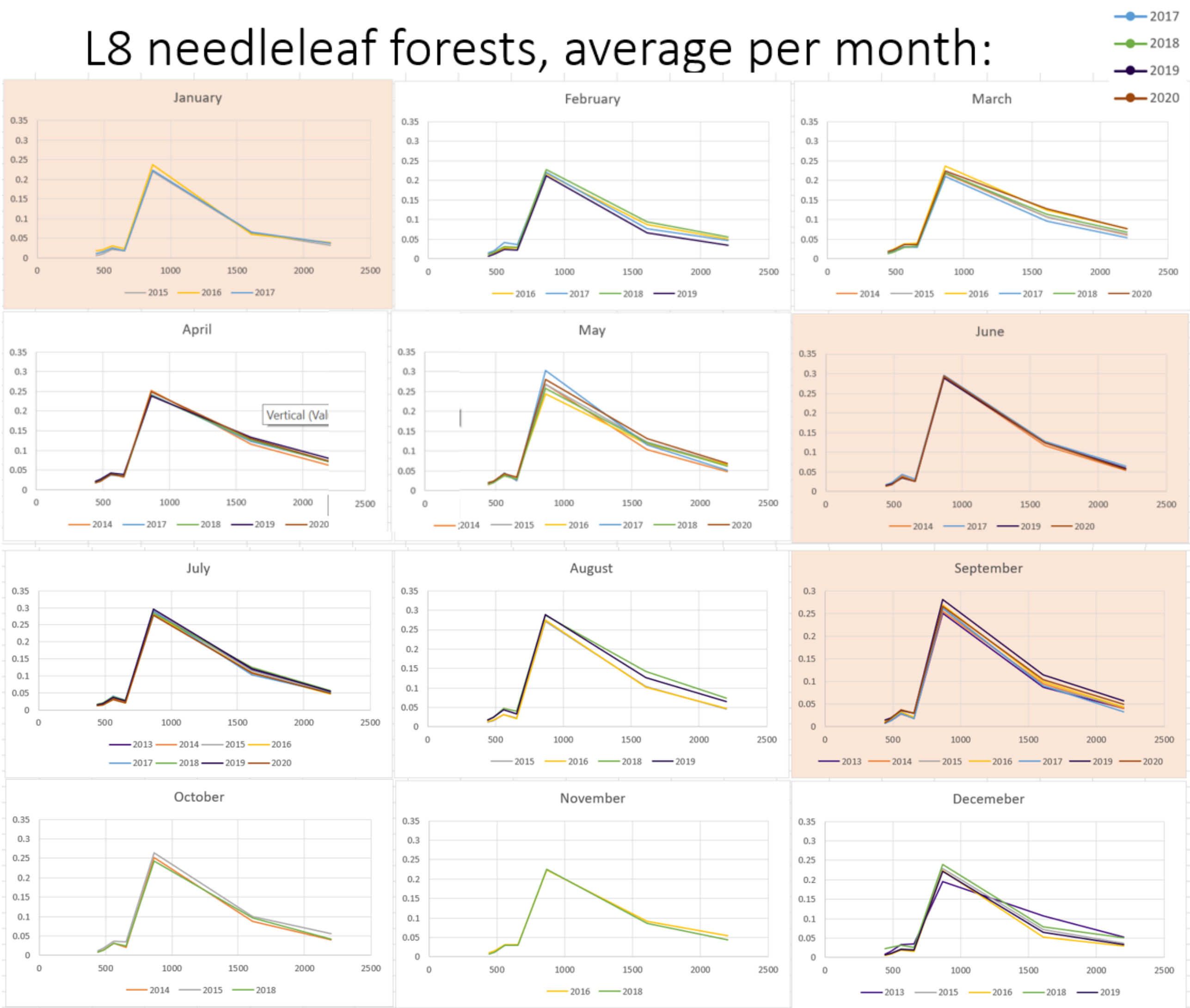

NDVI broadleaved forests, every single observation:

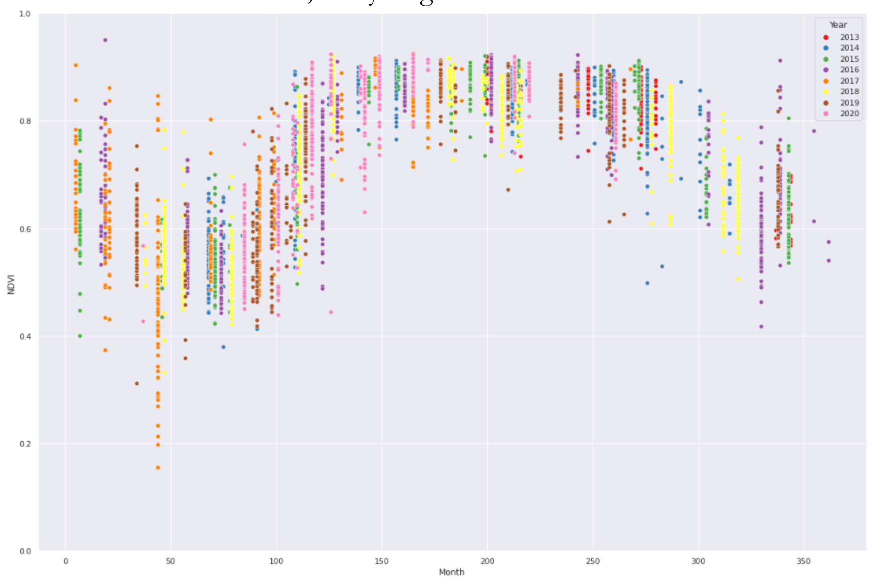

APPENDIX E: DESCRIPTIBE STATISTICS OF DATASETS

These are the descriptive statistics of the datasets used in this study as discussed in section 6.3.1.1.

Sentinel-2										
Full-year (3/2017 - 9/2020)						Summer months (2017-2020)				
	broadleaf	conifers	mixed	total			broadleaf	conifers	mixed	total
sand	3066	4099	4693	11858		**sand**	792	1136	1257	2393
clay	2961	175	1514	4650		**clay**	722	40	26	66
peat	1253	2068	844	4165		**peat**	347	572	436	1008
loess	625	0	99	724		**loess**	188	0	238	238
total	7907	6342	7150	21399		**total**	2049	1748	1957	5754

Landsat 8										
Full-year (3/2013 - 9/2020)						Summer months (2013-2020)				
	broadleaf	conifers	mixed	total			broadleaf	conifers	mixed	total
sand	1825	1574	1789	5188		**sand**	484	436	478	1398
clay	1783	101	64	1948		**clay**	434	25	16	475
peat	382	543	377	1302		**peat**	101	155	108	364
loess	267	0	234	501		**loess**	72	0	60	132
total	4257	2218	2464	8939		**total**	1091	616	662	2369

Sentinel-2				
	broadleaf	conifers	mixed	total
2017	457	379	447	1286
2018	2757	2192	2503	7452
2019	2129	1685	1906	5720
2020	2612	2086	2294	6992

Landsat 8				
	broadleaf	conifers	mixed	total
2013	206	111	129	446
2014	206	284	310	1103
2015	566	297	332	1195
2016	647	336	366	1349
2017	397	247	248	892
2018	857	469	525	1851
2019	504	229	270	1003
2020	667	341	380	1388

APPENDIX F: ANOVA RESULTS

These are the ANOVA results as discussed in various parts of section 6.3.

ANOVA of the full dataset

Landsat 8 NDMI

Box's Test of Equality of Covariance Matrices[a]

Box's M	657.466
F	1.453
df1	324
df2	12340.833
Sig.	.000

Mauchly's Test of Sphericity[a]

Measure: MEASURE_1

Within Subjects Effect	Mauchly's W	Approx. Chi-Square	df	Sig.	Epsilon[b] Greenhouse-Geisser	Huynh-Feldt	Lower-bound
year	.064	387.959	27	.000	.477	.547	.143

Multivariate Tests[a]

Effect		Value	F	Hypothesis df	Error df	Sig.	Partial Eta Squared
year	Pillai's Trace	.748	58.390[b]	7.000	138.000	.000	.748
	Wilks' Lambda	.252	58.390[b]	7.000	138.000	.000	.748
	Hotelling's Trace	2.962	58.390[b]	7.000	138.000	.000	.748
	Roy's Largest Root	2.962	58.390[b]	7.000	138.000	.000	.748
year * foresttype	Pillai's Trace	.298	3.473	14.000	278.000	.000	.149
	Wilks' Lambda	.710	3.676[b]	14.000	276.000	.000	.157
	Hotelling's Trace	.396	3.879	14.000	274.000	.000	.165
	Roy's Largest Root	.365	7.252[c]	7.000	139.000	.000	.268
year * soiltype	Pillai's Trace	.570	2.146	42.000	858.000	.000	.095
	Wilks' Lambda	.534	2.214	42.000	650.729	.000	.099
	Hotelling's Trace	.692	2.245	42.000	818.000	.000	.103
	Roy's Largest Root	.275	5.620[c]	7.000	143.000	.000	.216
year * foresttype * soiltype	Pillai's Trace	.379	.916	63.000	1008.000	.661	.054
	Wilks' Lambda	.666	.930	63.000	783.331	.630	.056
	Hotelling's Trace	.437	.946	63.000	954.000	.597	.059
	Roy's Largest Root	.242	3.877[c]	9.000	144.000	.000	.195

Tests of Within-Subjects Effects

Measure: MEASURE_1

Source		Type III Sum of Squares	df	Mean Square	F	Sig.	Partial Eta Squared
year	Sphericity Assumed	1.239	7	.177	52.899	.000	.269
	Greenhouse-Geisser	1.239	3.336	.372	52.899	.000	.269
	Huynh-Feldt	1.239	3.828	.324	52.899	.000	.269
	Lower-bound	1.239	1.000	1.239	52.899	.000	.269
year * foresttype	Sphericity Assumed	.171	14	.012	3.642	.000	.048
	Greenhouse-Geisser	.171	6.672	.026	3.642	.001	.048
	Huynh-Feldt	.171	7.655	.022	3.642	.000	.048
	Lower-bound	.171	2.000	.085	3.642	.029	.048
year * soiltype	Sphericity Assumed	.475	42	.011	3.377	.000	.123
	Greenhouse-Geisser	.475	20.015	.024	3.377	.000	.123
	Huynh-Feldt	.475	22.965	.021	3.377	.000	.123
	Lower-bound	.475	6.000	.079	3.377	.004	.123
year * foresttype * soiltype	Sphericity Assumed	.183	63	.003	.869	.756	.052
	Greenhouse-Geisser	.183	30.022	.006	.869	.669	.052
	Huynh-Feldt	.183	34.448	.005	.869	.684	.052
	Lower-bound	.183	9.000	.020	.869	.554	.052
Error(year)	Sphericity Assumed	3.374	1008	.003			
	Greenhouse-Geisser	3.374	480.350	.007			
	Huynh-Feldt	3.374	551.161	.006			
	Lower-bound	3.374	144.000	.023			

Tests of Between-Subjects Effects

Measure: MEASURE_1

Transformed Variable: Average

Source	Type III Sum of Squares	df	Mean Square	F	Sig.	Partial Eta Squared
Intercept	56.925	1	56.925	1858.736	.000	.928
foresttype	1.080	2	.540	17.635	.000	.197
soiltype	.317	6	.053	1.725	.119	.067
foresttype * soiltype	.418	9	.046	1.516	.147	.087
Error	4.410	144	.031			

Pairwise Comparisons

Measure: MEASURE_1

(I) year	(J) year	Mean Difference (I-J)	Std. Error	Sig.[c]	95% Confidence Interval for Difference[c] Lower Bound	Upper Bound
1	2	.102[*,b]	.006	.000	.090	.114
	3	.085[*,b]	.007	.000	.070	.099
	4	.108[*,b]	.009	.000	.091	.125
	5	.122[*,b]	.010	.000	.102	.142
	6	.137[*,b]	.007	.000	.122	.151
	7	.184[*,b]	.012	.000	.160	.209
	8	.109[*,b]	.007	.000	.094	.123
2	1	-.102[*,b]	.006	.000	-.114	-.090
	3	-.017[*,b]	.007	.022	-.032	-.003
	4	.006[b]	.008	.442	-.009	.021
	5	.020[*,b]	.010	.048	.000	.041
	6	.035[*,b]	.006	.000	.022	.047
	7	.083[*,b]	.011	.000	.061	.105
	8	.007[b]	.007	.313	-.007	.021
3	1	-.085[*,b]	.007	.000	-.099	-.070
	2	.017[*,b]	.007	.022	.003	.032
	4	.023[*,b]	.006	.000	.011	.036
	5	.038[*,b]	.008	.000	.022	.053
	6	.052[*,b]	.007	.000	.037	.067

Pairwise Comparisons

Measure: MEASURE_1

(I) foresttype	(J) foresttype	Mean Difference (I-J)	Std. Error	Sig.[d]	95% Confidence Interval for Difference[d] Lower Bound	Upper Bound
gemengdbos	loofbos	.020[a]	.016	.216	-.012	.051
	naaldbos	-.088[a,*,c]	.021	.000	-.129	-.046
loofbos	gemengdbos	-.020[c]	.016	.216	-.051	.012
	naaldbos	-.107[*,c]	.018	.000	-.143	-.071
naaldbos	gemengdbos	.088[a,*,c]	.021	.000	.046	.129
	loofbos	.107[a,*]	.018	.000	.071	.143

Landsat 8 NDVI

Tests of Within-Subjects Effects

Measure: MEASURE_1

Source		Type III Sum of Squares	df	Mean Square	F	Sig.	Partial Eta Squared	Noncent. Parameter	Observed Power[a]
year	Sphericity Assumed	.974	7	.139	67.817	.000	.320	474.721	1.000
	Greenhouse-Geisser	.974	3.343	.291	67.817	.000	.320	226.680	1.000
	Huynh-Feldt	.974	3.835	.254	67.817	.000	.320	260.111	1.000
	Lower-bound	.974	1.000	.974	67.817	.000	.320	67.817	1.000
year * foresttype	Sphericity Assumed	.143	14	.010	4.983	.000	.065	69.756	1.000
	Greenhouse-Geisser	.143	6.685	.021	4.983	.000	.065	33.309	.996
	Huynh-Feldt	.143	7.671	.019	4.983	.000	.065	38.221	.998
	Lower-bound	.143	2.000	.072	4.983	.008	.065	9.965	.805
year * soiltype	Sphericity Assumed	.200	42	.005	2.322	.000	.088	97.522	1.000
	Greenhouse-Geisser	.200	20.055	.010	2.322	.001	.088	46.567	.996
	Huynh-Feldt	.200	23.013	.009	2.322	.001	.088	53.435	.998
	Lower-bound	.200	6.000	.033	2.322	.036	.088	13.932	.790
year * foresttype * soiltype	Sphericity Assumed	.083	63	.001	.643	.986	.039	40.518	.881
	Greenhouse-Geisser	.083	30.083	.003	.643	.930	.039	19.347	.635
	Huynh-Feldt	.083	34.519	.002	.643	.944	.039	22.201	.684
	Lower-bound	.083	9.000	.009	.643	.759	.039	5.788	.308
Error(year)	Sphericity Assumed	2.068	1008	.002					
	Greenhouse-Geisser	2.068	481.321	.004					
	Huynh-Feldt	2.068	552.306	.004					
	Lower-bound	2.068	144.000	.014					

Pairwise Comparisons

Measure: MEASURE_1

(I) year	(J) year	Mean Difference (I-J)	Std. Error	Sig.[c]	95% Confidence Interval for Difference[c] Lower Bound	Upper Bound
1	2	.077[*,b]	.005	.000	.066	.087
	3	.074[*,b]	.006	.000	.063	.085
	4	.101[*,b]	.007	.000	.087	.115
	5	.137[*,b]	.009	.000	.119	.155
	6	.114[*,b]	.006	.000	.102	.127
	7	.151[*,b]	.010	.000	.131	.171
	8	.076[*,b]	.005	.000	.065	.086
2	1	-.077[*,b]	.005	.000	-.087	-.066
	3	-.002[b]	.006	.690	-.015	.010
	4	.024[*,b]	.006	.000	.012	.037
	5	.061[*,b]	.008	.000	.044	.077
	6	.038[*,b]	.005	.000	.028	.047
	7	.075[*,b]	.008	.000	.059	.090
	8	-.001[b]	.005	.859	-.011	.009
3	1	-.074[*,b]	.006	.000	-.085	-.063
	2	.002[b]	.006	.690	-.010	.015
	4	.027[*,b]	.005	.000	.018	.036
	5	.063[*,b]	.007	.000	.050	.076

Pairwise Comparisons

Measure: MEASURE_1

(I) foresttype	(J) foresttype	Mean Difference (I-J)	Std. Error	Sig.[d]	95% Confidence Interval for Difference[d] Lower Bound	Upper Bound
gemengdbos	loofbos	.020[a]	.011	.081	-.002	.042
	naaldbos	-.037[a,*,c]	.015	.013	-.067	-.008
loofbos	gemengdbos	-.020[c]	.011	.081	-.042	.002
	naaldbos	-.057[*,c]	.013	.000	-.082	-.031
naaldbos	gemengdbos	.037[a,*,c]	.015	.013	.008	.067
	loofbos	.057[a,*]	.013	.000	.031	.082

Sentinel-2 NDMI

Tests of Within-Subjects Effects

Measure: MEASURE_1

Source		Type III Sum of Squares	df	Mean Square	F	Sig.	Partial Eta Squared
year	Sphericity Assumed	.378	3	.126	80.223	.000	.347
	Greenhouse-Geisser	.378	1.811	.209	80.223	.000	.347
	Huynh-Feldt	.378	2.038	.186	80.223	.000	.347
	Lower-bound	.378	1.000	.378	80.223	.000	.347
year * foresttype	Sphericity Assumed	.005	6	.001	.581	.745	.008
	Greenhouse-Geisser	.005	3.622	.002	.581	.660	.008
	Huynh-Feldt	.005	4.077	.001	.581	.680	.008
	Lower-bound	.005	2.000	.003	.581	.560	.008
year * soiltype	Sphericity Assumed	.063	18	.004	2.228	.003	.081
	Greenhouse-Geisser	.063	10.867	.006	2.228	.014	.081
	Huynh-Feldt	.063	12.230	.005	2.228	.010	.081
	Lower-bound	.063	6.000	.011	2.228	.043	.081
year * foresttype * soiltype	Sphericity Assumed	.029	27	.001	.687	.882	.039
	Greenhouse-Geisser	.029	16.301	.002	.687	.810	.039
	Huynh-Feldt	.029	18.345	.002	.687	.827	.039
	Lower-bound	.029	9.000	.003	.687	.720	.039
Error(year)	Sphericity Assumed	.712	453	.002			
	Greenhouse-Geisser	.712	273.489	.003			
	Huynh-Feldt	.712	307.782	.002			
	Lower-bound	.712	151.000	.005			

Pairwise Comparisons

Measure: MEASURE_1

(I) year	(J) year	Mean Difference (I-J)	Std. Error	Sig.[c]	95% Confidence Interval for Difference[c] Lower Bound	Upper Bound
1	2	.042[*,b]	.007	.000	.029	.055
	3	.096[*,b]	.008	.000	.081	.112
	4	.065[*,b]	.008	.000	.050	.081
2	1	-.042[*,b]	.007	.000	-.055	-.029
	3	.055[*,b]	.004	.000	.046	.063
	4	.024[*,b]	.004	.000	.016	.032
3	1	-.096[*,b]	.008	.000	-.112	-.081
	2	-.055[*,b]	.004	.000	-.063	-.046
	4	-.031[*,b]	.004	.000	-.039	-.023
4	1	-.065[*,b]	.008	.000	-.081	-.050
	2	-.024[*,b]	.004	.000	-.032	-.016
	3	.031[*,b]	.004	.000	.023	.039

Pairwise Comparisons

Measure: MEASURE_1

(I) foresttype	(J) foresttype	Mean Difference (I-J)	Std. Error	Sig.[d]	95% Confidence Interval for Difference[d] Lower Bound	Upper Bound
gemengdbos	loofbos	.026[a]	.014	.056	-.001	.053
	naaldbos	-.038[a,*,c]	.017	.024	-.071	-.005
loofbos	gemengdbos	-.026[c]	.014	.056	-.053	.001
	naaldbos	-.064[*,c]	.014	.000	-.092	-.037
naaldbos	gemengdbos	.038[a,*,c]	.017	.024	.005	.071
	loofbos	.064[a,*]	.014	.000	.037	.092

Sentinel-2 NDVI

Tests of Within-Subjects Effects

Measure: MEASURE_1

Source		Type III Sum of Squares	df	Mean Square	F	Sig.	Partial Eta Squared
year	Sphericity Assumed	.180	3	.060	31.336	.000	.172
	Greenhouse-Geisser	.180	1.586	.114	31.336	.000	.172
	Huynh-Feldt	.180	1.781	.101	31.336	.000	.172
	Lower-bound	.180	1.000	.180	31.336	.000	.172
year * foresttype	Sphericity Assumed	.008	6	.001	.738	.619	.010
	Greenhouse-Geisser	.008	3.172	.003	.738	.537	.010
	Huynh-Feldt	.008	3.561	.002	.738	.552	.010
	Lower-bound	.008	2.000	.004	.738	.480	.010
year * soiltype	Sphericity Assumed	.031	18	.002	.892	.589	.034
	Greenhouse-Geisser	.031	9.516	.003	.892	.538	.034
	Huynh-Feldt	.031	10.683	.003	.892	.547	.034
	Lower-bound	.031	6.000	.005	.892	.503	.034
year * foresttype * soiltype	Sphericity Assumed	.015	27	.001	.287	1.000	.017
	Greenhouse-Geisser	.015	14.274	.001	.287	.995	.017
	Huynh-Feldt	.015	16.025	.001	.287	.997	.017
	Lower-bound	.015	9.000	.002	.287	.978	.017
Error(year)	Sphericity Assumed	.868	453	.002			
	Greenhouse-Geisser	.868	239.487	.004			
	Huynh-Feldt	.868	268.859	.003			
	Lower-bound	.868	151.000	.006			

Pairwise Comparisons

Measure: MEASURE_1

(I) year	(J) year	Mean Difference (I-J)	Std. Error	Sig.[c]	95% Confidence Interval for Difference[c] Lower Bound	Upper Bound
1	2	.009[a]	.008	.288	-.008	.026
	3	.063[a,*]	.009	.000	.045	.081
	4	.020[a,*]	.008	.016	.004	.037
2	1	-.009[a]	.008	.288	-.026	.008
	3	.054[a,*]	.004	.000	.046	.062
	4	.011[a,*]	.003	.001	.004	.018
3	1	-.063[a,*]	.009	.000	-.081	-.045
	2	-.054[a,*]	.004	.000	-.062	-.046
	4	-.043[a,*]	.004	.000	-.051	-.035
4	1	-.020[a,*]	.008	.016	-.037	-.004
	2	-.011[a,*]	.003	.001	-.018	-.004
	3	.043[a,*]	.004	.000	.035	.051

Pairwise Comparisons

Measure: MEASURE_1

(I) foresttype	(J) foresttype	Mean Difference (I-J)	Std. Error	Sig.[c]	95% Confidence Interval for Difference[c] Lower Bound	Upper Bound
gemengdbos	loofbos	.015[a]	.009	.125	-.004	.033
	naaldbos	.003[a,b]	.012	.812	-.020	.026
loofbos	gemengdbos	-.015[b]	.009	.125	-.033	.004
	naaldbos	-.012[b]	.010	.220	-.031	.007
naaldbos	gemengdbos	-.003[a,b]	.012	.812	-.026	.020
	loofbos	.012[a]	.010	.220	-.007	.031

ANOVA for the 3-month (summer) analysis

Landsat 8 NDMI

Box's Test of Equality of Covariance Matrices[a]

Box's M	198.667
F	1.460
df1	72
df2	1841.228
Sig.	.008

Tests the null hypothesis that the observed covariance matrices of the dependent variables are equal across groups.

a. Design: Intercept + foresttype + soiltype + foresttype * soiltype Within Subjects Design: year

Mauchly's Test of Sphericity[a]

Measure: MEASURE_1

Within Subjects Effect	Mauchly's W	Approx. Chi-Square	df	Sig.	Epsilon[b] Greenhouse-Geisser	Huynh-Feldt	Lower-bound
year	.101	120.042	27	.000	.595	.837	.143

Tests the null hypothesis that the error covariance matrix of the orthonormalized transformed dependent variables is proportional to an identity matrix.

Multivariate Tests[a]

Effect		Value	F	Hypothesis df	Error df	Sig.	Partial Eta Squared	Noncent. Parameter	Observed Power[d]
year	Pillai's Trace	.518	7.512[b]	7.000	49.000	.000	.518	52.584	1.000
	Wilks' Lambda	.482	7.512[b]	7.000	49.000	.000	.518	52.584	1.000
	Hotelling's Trace	1.073	7.512[b]	7.000	49.000	.000	.518	52.584	1.000
	Roy's Largest Root	1.073	7.512[b]	7.000	49.000	.000	.518	52.584	1.000
year * foresttype	Pillai's Trace	.233	.942	14.000	100.000	.518	.117	13.188	.558
	Wilks' Lambda	.776	.945[b]	14.000	98.000	.515	.119	13.226	.558
	Hotelling's Trace	.276	.947	14.000	96.000	.513	.121	13.252	.558
	Roy's Largest Root	.222	1.584[c]	7.000	50.000	.162	.182	11.090	.597
year * soiltype	Pillai's Trace	.773	1.141	42.000	324.000	.262	.129	47.931	.969
	Wilks' Lambda	.395	1.217	42.000	233.282	.184	.143	39.077	.902
	Hotelling's Trace	1.146	1.292	42.000	284.000	.118	.160	54.251	.985
	Roy's Largest Root	.740	5.710[c]	7.000	54.000	.000	.425	39.967	.998
year * foresttype * soiltype	Pillai's Trace	1.109	1.294	56.000	385.000	.086	.158	72.463	.997
	Wilks' Lambda	.224	1.538	56.000	269.184	.014	.192	64.071	.988
	Hotelling's Trace	2.195	1.853	56.000	331.000	.001	.239	103.781	1.000
	Roy's Largest Root	1.610	11.065[c]	8.000	55.000	.000	.617	88.523	1.000

Tests of Within-Subjects Effects

Measure: MEASURE_1

Source		Type III Sum of Squares	df	Mean Square	F	Sig.	Partial Eta Squared	Noncent. Parameter	Observed Power[a]
year	Sphericity Assumed	.043	7	.006	3.355	.002	.057	23.482	.961
	Greenhouse-Geisser	.043	4.166	.010	3.355	.010	.057	13.976	.853
	Huynh-Feldt	.043	5.862	.007	3.355	.003	.057	19.663	.933
	Lower-bound	.043	1.000	.043	3.355	.072	.057	3.355	.436
year * foresttype	Sphericity Assumed	.018	14	.001	.721	.753	.026	10.094	.463
	Greenhouse-Geisser	.018	8.332	.002	.721	.679	.026	6.008	.339
	Huynh-Feldt	.018	11.723	.002	.721	.727	.026	8.453	.416
	Lower-bound	.018	2.000	.009	.721	.491	.026	1.442	.166
year * soiltype	Sphericity Assumed	.064	42	.002	.828	.769	.083	34.780	.871
	Greenhouse-Geisser	.064	24.997	.003	.828	.704	.083	20.700	.700
	Huynh-Feldt	.064	35.169	.002	.828	.746	.083	29.123	.818
	Lower-bound	.064	6.000	.011	.828	.553	.083	4.969	.299
year * foresttype * soiltype	Sphericity Assumed	.143	56	.003	1.393	.040	.169	78.023	.999
	Greenhouse-Geisser	.143	33.330	.004	1.393	.084	.169	46.437	.976
	Huynh-Feldt	.143	46.892	.003	1.393	.053	.169	65.334	.996
	Lower-bound	.143	8.000	.018	1.393	.220	.169	11.146	.574
Error(year)	Sphericity Assumed	.705	385	.002					
	Greenhouse-Geisser	.705	229.140	.003					
	Huynh-Feldt	.705	322.386	.002					
	Lower-bound	.705	55.000	.013					

Tests of Between-Subjects Effects

Measure: MEASURE_1
Transformed Variable: Average

Source	Type III Sum of Squares	df	Mean Square	F	Sig.	Partial Eta Squared	Noncent. Parameter	Observed Power[a]
Intercept	48.044	1	48.044	2262.047	.000	.976	2262.047	1.000
foresttype	.040	2	.020	.949	.393	.033	1.898	.206
soiltype	.692	6	.115	5.429	.000	.372	32.571	.992
foresttype * soiltype	.195	8	.024	1.149	.346	.143	9.192	.478
Error	1.168	55	.021					

a. Computed using alpha = .05

Pairwise Comparisons

Measure: MEASURE_1

(I) year	(J) year	Mean Difference (I-J)	Std. Error	Sig.[c]	95% Confidence Interval for Difference[c] Lower Bound	Upper Bound
1	2	-.002[a]	.009	1.000	-.032	.027
	3	-.005[a]	.009	1.000	-.033	.024
	4	.007[a]	.009	1.000	-.023	.038
	5	-.008[a]	.010	1.000	-.042	.026
	6	.027[a,*]	.007	.004	.005	.049
	7	-.006[a]	.010	1.000	-.037	.026
	8	-.017[a]	.011	1.000	-.053	.018
2	1	.002[a]	.009	1.000	-.027	.032
	3	-.002[a]	.010	1.000	-.035	.030
	4	.010[a]	.010	1.000	-.022	.041
	5	-.006[a]	.013	1.000	-.048	.036
	6	.029[a]	.010	.154	-.004	.062
	7	-.003[a]	.011	1.000	-.040	.033
	8	-.015[a]	.011	1.000	-.052	.022
3	1	.005[a]	.009	1.000	-.024	.033
	2	.002[a]	.010	1.000	-.030	.035
	4	.012[a]	.008	1.000	-.014	.038
	5	[illegible]	[illegible]	[illegible]	[illegible]	[illegible]

Pairwise Comparisons

Measure: MEASURE_1

(I) foresttype	(J) foresttype	Mean Difference (I-J)	Std. Error	Sig.[c]	95% Confidence Interval for Difference[c] Lower Bound	Upper Bound
gemengdbos	loofbos	-.021[a,b]	.020	.935	-.071	.030
	naaldbos	-.025[a,b]	.023	.881	-.082	.033
loofbos	gemengdbos	.021[a,b]	.020	.935	-.030	.071
	naaldbos	-.004[a,b]	.022	1.000	-.057	.050
naaldbos	gemengdbos	.025[a,b]	.023	.881	-.033	.082
	loofbos	.004[a,b]	.022	1.000	-.050	.057

Landsat 8 NDVI

Multivariate Tests[a]

Effect		Value	F	Hypothesis df	Error df	Sig.	Partial Eta Squared	Noncent. Parameter	Observed Power[d]
year	Pillai's Trace	.734	19.309[b]	7.000	49.000	.000	.734	135.162	1.000
	Wilks' Lambda	.266	19.309[b]	7.000	49.000	.000	.734	135.162	1.000
	Hotelling's Trace	2.758	19.309[b]	7.000	49.000	.000	.734	135.162	1.000
	Roy's Largest Root	2.758	19.309[b]	7.000	49.000	.000	.734	135.162	1.000
year * foresttype	Pillai's Trace	.149	.573	14.000	100.000	.880	.074	8.024	.333
	Wilks' Lambda	.853	.579[b]	14.000	98.000	.875	.076	8.108	.336
	Hotelling's Trace	.170	.584	14.000	96.000	.871	.079	8.183	.338
	Roy's Largest Root	.159	1.135[c]	7.000	50.000	.357	.137	7.943	.437
year * soiltype	Pillai's Trace	.467	.651	42.000	324.000	.954	.078	27.332	.735
	Wilks' Lambda	.604	.630	42.000	233.282	.963	.081	20.441	.541
	Hotelling's Trace	.546	.615	42.000	284.000	.971	.083	25.846	.694
	Roy's Largest Root	.249	1.922[c]	7.000	54.000	.084	.199	13.456	.704
year * foresttype * soiltype	Pillai's Trace	.811	.901	56.000	385.000	.676	.116	50.470	.956
	Wilks' Lambda	.403	.883	56.000	269.184	.707	.122	37.283	.820
	Hotelling's Trace	1.026	.867	56.000	331.000	.738	.128	48.534	.942
	Roy's Largest Root	.456	3.137[c]	8.000	55.000	.005	.313	25.098	.941

Mauchly's Test of Sphericity[a]

Measure: MEASURE_1

Within Subjects Effect	Mauchly's W	Approx. Chi-Square	df	Sig.	Epsilon[b] Greenhouse-Geisser	Huynh-Feldt	Lower-bound
year	.046	161.826	27	.000	.506	.703	.143

Tests of Within-Subjects Effects

Measure: MEASURE_1

Source		Type III Sum of Squares	df	Mean Square	F	Sig.	Partial Eta Squared	Noncent. Parameter	Observed Power[a]
year	Sphericity Assumed	.044	7	.006	6.376	.000	.104	44.630	1.000
	Greenhouse-Geisser	.044	3.543	.012	6.376	.000	.104	22.590	.982
	Huynh-Feldt	.044	4.919	.009	6.376	.000	.104	31.361	.996
	Lower-bound	.044	1.000	.044	6.376	.014	.104	6.376	.699
year * foresttype	Sphericity Assumed	.003	14	.000	.237	.998	.009	3.319	.153
	Greenhouse-Geisser	.003	7.086	.000	.237	.976	.009	1.680	.118
	Huynh-Feldt	.003	9.838	.000	.237	.992	.009	2.332	.133
	Lower-bound	.003	2.000	.002	.237	.790	.009	.474	.085
year * soiltype	Sphericity Assumed	.017	42	.000	.420	1.000	.044	17.648	.483
	Greenhouse-Geisser	.017	21.259	.001	.420	.989	.044	8.933	.315
	Huynh-Feldt	.017	29.513	.001	.420	.997	.044	12.401	.387
	Lower-bound	.017	6.000	.003	.420	.862	.044	2.521	.161
year * foresttype * soiltype	Sphericity Assumed	.045	56	.001	.811	.830	.106	45.433	.925
	Greenhouse-Geisser	.045	28.345	.002	.811	.740	.106	22.997	.719
	Huynh-Feldt	.045	39.350	.001	.811	.783	.106	31.925	.831
	Lower-bound	.045	8.000	.006	.811	.596	.106	6.490	.337
Error(year)	Sphericity Assumed	.381	385	.001					
	Greenhouse-Geisser	.381	194.873	.002					
	Huynh-Feldt	.381	270.534	.001					
	Lower-bound	.381	55.000	.007					

a. Computed using alpha = .05

Tests of Between-Subjects Effects

Measure: MEASURE_1
Transformed Variable: Average

Source	Type III Sum of Squares	df	Mean Square	F	Sig.	Partial Eta Squared	Noncent. Parameter	Observed Power[a]
Intercept	203.299	1	203.299	18484.146	.000	.997	18484.146	1.000
foresttype	.015	2	.008	.693	.505	.025	1.386	.161
soiltype	.124	6	.021	1.872	.102	.170	11.230	.646
foresttype * soiltype	.101	8	.013	1.146	.348	.143	9.167	.477
Error	.605	55	.011					

a. Computed using alpha = .05

Pairwise Comparisons

Measure: MEASURE_1

(I) year	(J) year	Mean Difference (I-J)	Std. Error	Sig.[c]	95% Confidence Interval for Difference[c]	
					Lower Bound	Upper Bound
1	2	.015[*,b]	.007	.034	.001	.029
	3	.007[b]	.006	.195	-.004	.019
	4	-.003[b]	.006	.599	-.014	.008
	5	.012[b]	.006	.072	-.001	.025
	6	.028[*,b]	.005	.000	.019	.038
	7	.003[b]	.007	.625	-.011	.017
	8	-.016[b]	.008	.062	-.033	.001
2	1	-.015[*,b]	.007	.034	-.029	-.001
	3	-.008[b]	.009	.392	-.026	.010
	4	-.018[*,b]	.006	.002	-.030	-.007
	5	-.003[b]	.011	.756	-.024	.018
	6	.013[b]	.008	.092	-.002	.029
	7	-.012[b]	.008	.131	-.027	.004
	8	-.031[*,b]	.007	.000	-.045	-.018
3	1	-.007[b]	.006	.195	-.019	.004
	2	.008[b]	.009	.392	-.010	.026
	4	-.010[b]	.006	.097	-.023	.002
	5	.004[b]	.007	.547	-.010	.019
	6	.021[*,b]	.008	.012	.005	.037

Pairwise Comparisons

Measure: MEASURE_1

(I) foresttype	(J) foresttype	Mean Difference (I-J)	Std. Error	Sig.[c]	95% Confidence Interval for Difference[c]	
					Lower Bound	Upper Bound
gemengdbos	loofbos	-.011[a,b]	.015	.442	-.041	.018
	naaldbos	.011[a,b]	.017	.513	-.022	.044
loofbos	gemengdbos	.011[a,b]	.015	.442	-.018	.041
	naaldbos	.022[a,b]	.016	.156	-.009	.053
naaldbos	gemengdbos	-.011[a,b]	.017	.513	-.044	.022
	loofbos	-.022[a,b]	.016	.156	-.053	.009

Sentinel-2 NDMI

Multivariate Tests[a]

Effect		Value	F	Hypothesis df	Error df	Sig.	Partial Eta Squared	Noncent. Parameter	Observed Power[d]
year	Pillai's Trace	.314	14.971[b]	3.000	98.000	.000	.314	44.914	1.000
	Wilks' Lambda	.686	14.971[b]	3.000	98.000	.000	.314	44.914	1.000
	Hotelling's Trace	.458	14.971[b]	3.000	98.000	.000	.314	44.914	1.000
	Roy's Largest Root	.458	14.971[b]	3.000	98.000	.000	.314	44.914	1.000
year * foresttype	Pillai's Trace	.051	.857	6.000	198.000	.528	.025	5.143	.335
	Wilks' Lambda	.950	.854[b]	6.000	196.000	.530	.025	5.126	.334
	Hotelling's Trace	.053	.851	6.000	194.000	.532	.026	5.108	.333
	Roy's Largest Root	.045	1.501[c]	3.000	99.000	.219	.043	4.502	.386
year * soiltype	Pillai's Trace	.275	1.680	18.000	300.000	.042	.092	30.244	.943
	Wilks' Lambda	.743	1.710	18.000	277.671	.037	.094	28.927	.930
	Hotelling's Trace	.323	1.734	18.000	290.000	.033	.097	31.220	.951
	Roy's Largest Root	.231	3.849[c]	6.000	100.000	.002	.188	23.095	.958
year * foresttype * soiltype	Pillai's Trace	.223	.891	27.000	300.000	.625	.074	24.062	.777
	Wilks' Lambda	.791	.886	27.000	286.853	.632	.075	23.271	.756
	Hotelling's Trace	.246	.881	27.000	290.000	.640	.076	23.788	.769
	Roy's Largest Root	.126	1.396[c]	9.000	100.000	.200	.112	12.566	.642

Mauchly's Test of Sphericity[a]

Measure: MEASURE_1

Within Subjects Effect	Mauchly's W	Approx. Chi-Square	df	Sig.	Epsilon[b] Greenhouse-Geisser	Huynh-Feldt	Lower-bound
year	.580	53.805	5	.000	.738	.884	.333

Tests the null hypothesis that the error covariance matrix of the orthonormalized transformed dependent variables is proportional to an identity matrix.

a. Design: Intercept + foresttype + soiltype + foresttype * soiltype
Within Subjects Design: year

b. May be used to adjust the degrees of freedom for the averaged tests of significance. Corrected tests are displayed in the Tests of Within-Subjects Effects table.

Tests of Within-Subjects Effects

Measure: MEASURE_1

Source		Type III Sum of Squares	df	Mean Square	F	Sig.	Partial Eta Squared	Noncent. Parameter	Observed Power[a]
year	Sphericity Assumed	.036	3	.012	13.543	.000	.119	40.628	1.000
	Greenhouse-Geisser	.036	2.215	.016	13.543	.000	.119	29.996	.999
	Huynh-Feldt	.036	2.652	.013	13.543	.000	.119	35.920	1.000
	Lower-bound	.036	1.000	.036	13.543	.000	.119	13.543	.954
year * foresttype	Sphericity Assumed	.003	6	.000	.530	.786	.010	3.178	.213
	Greenhouse-Geisser	.003	4.430	.001	.530	.732	.010	2.346	.184
	Huynh-Feldt	.003	5.305	.001	.530	.764	.010	2.810	.200
	Lower-bound	.003	2.000	.001	.530	.590	.010	1.059	.135
year * soiltype	Sphericity Assumed	.027	18	.001	1.701	.038	.093	30.615	.946
	Greenhouse-Geisser	.027	13.290	.002	1.701	.060	.093	22.603	.881
	Huynh-Feldt	.027	15.914	.002	1.701	.047	.093	27.067	.923
	Lower-bound	.027	6.000	.004	1.701	.129	.093	10.205	.622
year * foresttype * soiltype	Sphericity Assumed	.022	27	.001	.920	.584	.076	24.827	.794
	Greenhouse-Geisser	.022	19.934	.001	.920	.563	.076	18.330	.688
	Huynh-Feldt	.022	23.871	.001	.920	.575	.076	21.950	.752
	Lower-bound	.022	9.000	.002	.920	.512	.076	8.276	.433
Error(year)	Sphericity Assumed	.263	300	.001					
	Greenhouse-Geisser	.263	221.493	.001					
	Huynh-Feldt	.263	265.237	.001					
	Lower-bound	.263	100.000	.003					

a. Computed using alpha = .05

Tests of Between-Subjects Effects

Measure: MEASURE_1
Transformed Variable: Average

Source	Type III Sum of Squares	df	Mean Square	F	Sig.	Partial Eta Squared	Noncent. Parameter	Observed Power[a]
Intercept	33.918	1	33.918	3788.025	.000	.974	3788.025	1.000
foresttype	.009	2	.004	.500	.608	.010	1.001	.130
soiltype	.417	6	.070	7.768	.000	.318	46.610	1.000
foresttype * soiltype	.112	9	.012	1.385	.205	.111	12.467	.637
Error	.895	100	.009					

a. Computed using alpha = .05

Pairwise Comparisons

Measure: MEASURE_1

(I) foresttype	(J) foresttype	Mean Difference (I-J)	Std. Error	Sig.[c]	95% Confidence Interval for Difference[c] Lower Bound	Upper Bound
gemengdbos	loofbos	-.005[a]	.013	.724	-.031	.022
	naaldbos	-.017[a,b]	.017	.317	-.049	.016
loofbos	gemengdbos	.005[b]	.013	.724	-.022	.031
	naaldbos	-.012[b]	.015	.429	-.042	.018
naaldbos	gemengdbos	.017[a,b]	.017	.317	-.016	.049
	loofbos	.012[a]	.015	.429	-.018	.042

Pairwise Comparisons

Measure: MEASURE_1

(I) year	(J) year	Mean Difference (I-J)	Std. Error	Sig.[c]	95% Confidence Interval for Difference[c] Lower Bound	Upper Bound
1	2	.031[*,b]	.006	.000	.020	.042
	3	.023[*,b]	.006	.000	.010	.035
	4	.012[b]	.006	.053	.000	.025
2	1	-.031[*,b]	.006	.000	-.042	-.020
	3	-.008[b]	.005	.083	-.017	.001
	4	-.018[*,b]	.005	.000	-.027	-.009
3	1	-.023[*,b]	.006	.000	-.035	-.010
	2	.008[b]	.005	.083	-.001	.017
	4	-.010[*,b]	.003	.003	-.017	-.004
4	1	-.012[b]	.006	.053	-.025	.000
	2	.018[*,b]	.005	.000	.009	.027
	3	.010[*,b]	.003	.003	.004	.017

Sentinel-2 NDVI

Multivariate Tests[a]

Effect		Value	F	Hypothesis df	Error df	Sig.	Partial Eta Squared	Noncent. Parameter	Observed Power[d]
year	Pillai's Trace	.563	42.101[b]	3.000	98.000	.000	.563	126.304	1.000
	Wilks' Lambda	.437	42.101[b]	3.000	98.000	.000	.563	126.304	1.000
	Hotelling's Trace	1.289	42.101[b]	3.000	98.000	.000	.563	126.304	1.000
	Roy's Largest Root	1.289	42.101[b]	3.000	98.000	.000	.563	126.304	1.000
year * foresttype	Pillai's Trace	.037	.629	6.000	198.000	.707	.019	3.775	.247
	Wilks' Lambda	.963	.625[b]	6.000	196.000	.710	.019	3.749	.246
	Hotelling's Trace	.038	.620	6.000	194.000	.714	.019	3.723	.244
	Roy's Largest Root	.031	1.007[c]	3.000	99.000	.393	.030	3.021	.267
year * soiltype	Pillai's Trace	.152	.891	18.000	300.000	.590	.051	16.035	.647
	Wilks' Lambda	.854	.887	18.000	277.671	.595	.051	15.025	.608
	Hotelling's Trace	.164	.883	18.000	290.000	.600	.052	15.887	.641
	Roy's Largest Root	.108	1.806[c]	6.000	100.000	.105	.098	10.837	.653
year * foresttype * soiltype	Pillai's Trace	.363	1.528	27.000	300.000	.049	.121	41.260	.975
	Wilks' Lambda	.676	1.525	27.000	286.853	.050	.122	40.018	.969
	Hotelling's Trace	.425	1.520	27.000	290.000	.051	.124	41.037	.974
	Roy's Largest Root	.230	2.558[c]	9.000	100.000	.011	.187	23.020	.922

Mauchly's Test of Sphericity[a]

Measure: MEASURE_1

Within Subjects Effect	Mauchly's W	Approx. Chi-Square	df	Sig.	Epsilon[b] Greenhouse-Geisser	Huynh-Feldt	Lower-bound
year	.190	163.804	5	.000	.498	.590	.333

Tests of Within-Subjects Effects

Measure: MEASURE_1

Source		Type III Sum of Squares	df	Mean Square	F	Sig.	Partial Eta Squared	Noncent. Parameter	Observed Power[a]
year	Sphericity Assumed	.048	3	.016	9.072	.000	.083	27.217	.996
	Greenhouse-Geisser	.048	1.495	.032	9.072	.001	.083	13.567	.935
	Huynh-Feldt	.048	1.771	.027	9.072	.000	.083	16.068	.960
	Lower-bound	.048	1.000	.048	9.072	.003	.083	9.072	.847
year * foresttype	Sphericity Assumed	.007	6	.001	.616	.717	.012	3.698	.245
	Greenhouse-Geisser	.007	2.991	.002	.616	.605	.012	1.843	.176
	Huynh-Feldt	.007	3.542	.002	.616	.632	.012	2.183	.190
	Lower-bound	.007	2.000	.003	.616	.542	.012	1.233	.150
year * soiltype	Sphericity Assumed	.030	18	.002	.960	.506	.054	17.284	.690
	Greenhouse-Geisser	.030	8.973	.003	.960	.475	.054	8.616	.464
	Huynh-Feldt	.030	10.627	.003	.960	.483	.054	10.204	.513
	Lower-bound	.030	6.000	.005	.960	.456	.054	5.761	.364
year * foresttype * soiltype	Sphericity Assumed	.080	27	.003	1.677	.021	.131	45.275	.986
	Greenhouse-Geisser	.080	13.459	.006	1.677	.069	.131	22.569	.868
	Huynh-Feldt	.080	15.940	.005	1.677	.055	.131	26.729	.911
	Lower-bound	.080	9.000	.009	1.677	.104	.131	15.092	.740
Error(year)	Sphericity Assumed	.528	300	.002					
	Greenhouse-Geisser	.528	149.544	.004					
	Huynh-Feldt	.528	177.110	.003					
	Lower-bound	.528	100.000	.005					

a. Computed using alpha = .05

Pairwise Comparisons

Measure: MEASURE_1

(I) foresttype	(J) foresttype	Mean Difference (I-J)	Std. Error	Sig.[c]	95% Confidence Interval for Difference[c]	
					Lower Bound	Upper Bound
gemengdbos	loofbos	.000[a]	.010	.978	-.021	.020
	naaldbos	.016[a,b]	.013	.224	-.010	.041
loofbos	gemengdbos	.000[b]	.010	.978	-.020	.021
	naaldbos	.016[b]	.012	.173	-.007	.039
naaldbos	gemengdbos	-.016[a,b]	.013	.224	-.041	.010
	loofbos	-.016[a]	.012	.173	-.039	.007

Pairwise Comparisons

Measure: MEASURE_1

(I) year	(J) year	Mean Difference (I-J)	Std. Error	Sig.[c]	95% Confidence Interval for Difference[c]	
					Lower Bound	Upper Bound
1	2	.006[a]	.009	.496	-.012	.025
	3	.014[a]	.010	.152	-.005	.034
	4	-.023[a,*]	.010	.022	-.042	-.003
2	1	-.006[a]	.009	.496	-.025	.012
	3	.008[a]	.005	.086	-.001	.017
	4	-.029[a,*]	.004	.000	-.037	-.021
3	1	-.014[a]	.010	.152	-.034	.005
	2	-.008[a]	.005	.086	-.017	.001
	4	-.037[a,*]	.004	.000	-.044	-.030
4	1	.023[a,*]	.010	.022	.003	.042
	2	.029[a,*]	.004	.000	.021	.037
	3	.037[a,*]	.004	.000	.030	.044

ANOVA for the soil-types analysis (broadleaved forests only)

Landsat 8 NDMI

Box's Test of Equality of Covariance Matrices[a]

Box's M	213.161
F	1.324
df1	108
df2	4550.569
Sig.	.015

Mauchly's Test of Sphericity[a]

Measure: MEASURE_1

Within Subjects Effect	Mauchly's W	Approx. Chi-Square	df	Sig.	Epsilon[b]		
					Greenhouse-Geisser	Huynh-Feldt	Lower-bound
year	.053	168.424	27	.000	.449	.524	.143

Tests the null hypothesis that the error covariance matrix of the orthonormalized transformed dependent variables is proportional to an identity matrix.

Multivariate Tests[a]

Effect		Value	F	Hypothesis df	Error df	Sig.	Partial Eta Squared	Noncent. Parameter	Observed Power[d]
year	Pillai's Trace	.929	100.557[b]	7.000	54.000	.000	.929	703.899	1.000
	Wilks' Lambda	.071	100.557[b]	7.000	54.000	.000	.929	703.899	1.000
	Hotelling's Trace	13.035	100.557[b]	7.000	54.000	.000	.929	703.899	1.000
	Roy's Largest Root	13.035	100.557[b]	7.000	54.000	.000	.929	703.899	1.000
year * soiltype	Pillai's Trace	1.026	1.738	42.000	354.000	.004	.171	73.002	.999
	Wilks' Lambda	.300	1.788	42.000	256.735	.004	.182	57.026	.989
	Hotelling's Trace	1.437	1.791	42.000	314.000	.003	.193	75.214	.999
	Roy's Largest Root	.654	5.515[c]	7.000	59.000	.000	.396	38.603	.997

Tests of Within-Subjects Effects

Measure: MEASURE_1

Source		Type III Sum of Squares	df	Mean Square	F	Sig.	Partial Eta Squared	Noncent. Parameter	Observed Power[a]
year	Sphericity Assumed	1.488	7	.213	60.183	.000	.501	421.284	1.000
	Greenhouse-Geisser	1.488	3.140	.474	60.183	.000	.501	188.982	1.000
	Huynh-Feldt	1.488	3.665	.406	60.183	.000	.501	220.567	1.000
	Lower-bound	1.488	1.000	1.488	60.183	.000	.501	60.183	1.000
year * soiltype	Sphericity Assumed	.385	42	.009	2.596	.000	.206	109.047	1.000
	Greenhouse-Geisser	.385	18.841	.020	2.596	.001	.206	48.917	.997
	Huynh-Feldt	.385	21.989	.018	2.596	.000	.206	57.092	.999
	Lower-bound	.385	6.000	.064	2.596	.026	.206	15.578	.814
Error(year)	Sphericity Assumed	1.484	420	.004					
	Greenhouse-Geisser	1.484	188.406	.008					
	Huynh-Feldt	1.484	219.895	.007					
	Lower-bound	1.484	60.000	.025					

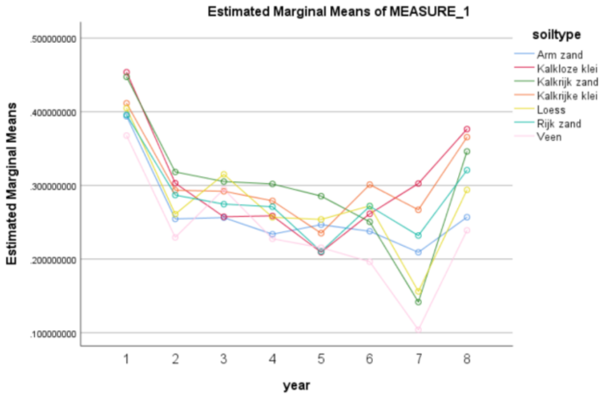

Pairwise Comparisons

Measure: MEASURE_1

(I) soiltype	(J) soiltype	Mean Difference (I-J)	Std. Error	Sig.[b]	95% Confidence Interval for Difference[b] Lower Bound	Upper Bound
Clay	Loess	.027	.020	.180	-.013	.068
	Peat	.070*	.017	.000	.036	.104
	Sand	.029*	.011	.012	.007	.052
Loess	Clay	-.027	.020	.180	-.068	.013
	Peat	.042	.024	.076	-.005	.089
	Sand	.002	.020	.929	-.038	.042
Peat	Clay	-.070*	.017	.000	-.104	-.036
	Loess	-.042	.024	.076	-.089	.005
	Sand	-.041*	.016	.016	-.073	-.008
Sand	Clay	-.029*	.011	.012	-.052	-.007
	Loess	-.002	.020	.929	-.042	.038
	Peat	.041*	.016	.016	.008	.073

Landsat 8 NDVI

Tests of Within-Subjects Effects

Measure: MEASURE_1

Source		Type III Sum of Squares	df	Mean Square	F	Sig.	Partial Eta Squared	Noncent. Parameter	Observed Power[a]
year	Sphericity Assumed	1.002	7	.143	73.027	.000	.537	511.188	1.000
	Greenhouse-Geisser	1.002	3.459	.290	73.027	.000	.537	252.622	1.000
	Huynh-Feldt	1.002	3.859	.260	73.027	.000	.537	281.817	1.000
	Lower-bound	1.002	1.000	1.002	73.027	.000	.537	73.027	1.000
year * soiltype	Sphericity Assumed	.125	21	.006	3.028	.000	.126	63.593	1.000
	Greenhouse-Geisser	.125	10.378	.012	3.028	.001	.126	31.427	.983
	Huynh-Feldt	.125	11.577	.011	3.028	.001	.126	35.059	.990
	Lower-bound	.125	3.000	.042	3.028	.036	.126	9.085	.686
Error(year)	Sphericity Assumed	.864	441	.002					
	Greenhouse-Geisser	.864	217.936	.004					
	Huynh-Feldt	.864	243.123	.004					
	Lower-bound	.864	63.000	.014					

Pairwise Comparisons

Measure: MEASURE_1

(I) soiltype	(J) soiltype	Mean Difference (I-J)	Std. Error	Sig.[a]	95% Confidence Interval for Difference[a] Lower Bound	Upper Bound
Clay	Loess	-.006	.014	.679	-.033	.021
	Peat	.014	.011	.229	-.009	.036
	Sand	.002	.008	.836	-.014	.017
Loess	Clay	.006	.014	.679	-.021	.033
	Peat	.019	.016	.224	-.012	.051
	Sand	.007	.013	.590	-.019	.034
Peat	Clay	-.014	.011	.229	-.036	.009
	Loess	-.019	.016	.224	-.051	.012
	Sand	-.012	.011	.274	-.034	.010
Sand	Clay	-.002	.008	.836	-.017	.014
	Loess	-.007	.013	.590	-.034	.019
	Peat	.012	.011	.274	-.010	.034

Sentinel-2 NDMI

Tests of Within-Subjects Effects

Measure: MEASURE_1

Source		Type III Sum of Squares	df	Mean Square	F	Sig.	Partial Eta Squared	Noncent. Parameter	Observed Power[a]
year	Sphericity Assumed	.221	3	.074	43.299	.000	.386	129.898	1.000
	Greenhouse-Geisser	.221	1.758	.126	43.299	.000	.386	76.121	1.000
	Huynh-Feldt	.221	1.879	.118	43.299	.000	.386	81.351	1.000
	Lower-bound	.221	1.000	.221	43.299	.000	.386	43.299	1.000
year * soiltype	Sphericity Assumed	.025	9	.003	1.649	.103	.067	14.842	.753
	Greenhouse-Geisser	.025	5.274	.005	1.649	.149	.067	8.697	.573
	Huynh-Feldt	.025	5.636	.004	1.649	.143	.067	9.295	.594
	Lower-bound	.025	3.000	.008	1.649	.186	.067	4.947	.414
Error(year)	Sphericity Assumed	.353	207	.002					
	Greenhouse-Geisser	.353	121.303	.003					
	Huynh-Feldt	.353	129.638	.003					
	Lower-bound	.353	69.000	.005					

a. Computed using alpha = .05

Pairwise Comparisons

Measure: MEASURE_1

(I) soiltype	(J) soiltype	Mean Difference (I-J)	Std. Error	Sig.[b]	95% Confidence Interval for Difference[b] Lower Bound	Upper Bound
Clay	Loess	.037	.019	.056	-.001	.074
	Peat	.089*	.015	.000	.058	.120
	Sand	.055*	.010	.000	.035	.075
Loess	Clay	-.037	.019	.056	-.074	.001
	Peat	.052*	.022	.022	.008	.096
	Sand	.019	.019	.326	-.019	.056
Peat	Clay	-.089*	.015	.000	-.120	-.058
	Loess	-.052*	.022	.022	-.096	-.008
	Sand	-.034*	.015	.034	-.064	-.003
Sand	Clay	-.055*	.010	.000	-.075	-.035
	Loess	-.019	.019	.326	-.056	.019
	Peat	.034*	.015	.034	.003	.064

<u>Sentinel-2 NDVI</u>

Tests of Within-Subjects Effects

Measure: MEASURE_1

Source		Type III Sum of Squares	df	Mean Square	F	Sig.	Partial Eta Squared	Noncent. Parameter	Observed Power[a]
year	Sphericity Assumed	.164	3	.055	29.179	.000	.297	87.536	1.000
	Greenhouse-Geisser	.164	1.764	.093	29.179	.000	.297	51.471	1.000
	Huynh-Feldt	.164	1.885	.087	29.179	.000	.297	55.016	1.000
	Lower-bound	.164	1.000	.164	29.179	.000	.297	29.179	1.000
year * soiltype	Sphericity Assumed	.011	9	.001	.675	.731	.029	6.079	.329
	Greenhouse-Geisser	.011	5.292	.002	.675	.651	.029	3.574	.245
	Huynh-Feldt	.011	5.656	.002	.675	.661	.029	3.820	.253
	Lower-bound	.011	3.000	.004	.675	.570	.029	2.026	.185
Error(year)	Sphericity Assumed	.388	207	.002					
	Greenhouse-Geisser	.388	121.716	.003					
	Huynh-Feldt	.388	130.098	.003					
	Lower-bound	.388	69.000	.006					

a. Computed using alpha = .05

Pairwise Comparisons

Measure: MEASURE_1

(I) soiltype	(J) soiltype	Mean Difference (I-J)	Std. Error	Sig.[b]	95% Confidence Interval for Difference[b] Lower Bound	Upper Bound
Clay	Loess	-.009	.016	.593	-.041	.024
	Peat	.040*	.013	.004	.013	.066
	Sand	.016	.009	.077	-.002	.033
Loess	Clay	.009	.016	.593	-.024	.041
	Peat	.048*	.019	.013	.010	.087
	Sand	.024	.016	.139	-.008	.057
Peat	Clay	-.040*	.013	.004	-.066	-.013
	Loess	-.048*	.019	.013	-.087	-.010
	Sand	-.024	.013	.074	-.051	.002
Sand	Clay	-.016	.009	.077	-.033	.002
	Loess	-.024	.016	.139	-.057	.008
	Peat	.024	.013	.074	-.002	.051